Fall 12-20-2018

Comparison of Switched Reluctance Motor and Double Stator Switched Reluctance Motor

Nirdesh Neupane
University of New Orleans, nneupane@uno.edu

Comparison of Switched Reluctance Motor and Double Stator Switched Reluctance Motor

A Thesis

Submitted to the Graduate Faculty of the
University of New Orleans
in partial fulfillment of the
requirements for the degree of

Master of Science
in
Engineering
Electrical Engineering

by

Nirdesh Neupane

B.Tech. Dehradun Institute of Technology, 2014

December, 2018

Acknowledgements

I would like to extend my sincere gratitude to my thesis advisor Dr. Ebrahim Amiri for all his support, guidance and encouragement. Without his help this research was nowhere possible.

I would like to thank my parents, my parents in laws, my beloved wife Asmita, brothers Sandesh and Aayush, and my sister Prakriti for all the continuous support, motivation and always believing me.

Lastly, I would like to extend my appreciation to my friends Bikrant, Rochak, Jyoti and Mahesh for all the encouragement, help, support and giving me extra push whenever I needed.

Contents

List of Figures

List of Tables

Abstract

This thesis is concerned with the design and analysis of Switched Reluctance Motor (SRM) and its improved structure Double Stator Switched Reluctance Motor (DSSRM). Three configurations of SRM viz. Inner Stator, Outer stator and Double Stator are designed and simulated in ANSYS Maxwell Suite. Design parameters are chosen by aiming optimum performance of motor after literature review and analytical study of the motor. SRM is not a line start machine, so power converter circuit is required to excite the motor. Without proper switching of current, desired torque is not obtained in SRM. The converter circuit and switching unit is built in Maxwell Circuit Editor Tools. Both magnetostatics and transient analysis is performed to investigate motion torque, torque ripple, normal force and radial force. A good comprehensive comparison of three different types of SRMs based on their torque profile and force densities is presented. Simulation performed verified better performance of DSSRM.

Keywords: SRM, DSSRM, Motor Drives, Electric Vehicle, Magnetostatics Analysis, Transient Analysis, Motional Torque, ANSYS

Chapter 1

Introduction

1.1 Background of SRM

Nonrenewable energy sources like fossil fuels and natural gas are the biggest source of pollution [1]. These sources are more expensive and will vanish in 100-200 years [1]. So, everyone is focusing on alternating sources of energy [1]. Vehicles are one of the most that consumes these sources [1]. This is the reason why everyone is into Electric Vehicle [1]. Electric vehicle run by converting electrical energy to mechanical energy [1]. Electric Motor are used to convert electrical energy to mechanical energy [1]. Electrical energy from battery is converted to mechanical energy by producing torque that moves shaft [1]. Shaft is connected to wheel of the vehicle [1]. This is how Electrical Vehicle works.

Variable Speed Drives are one of the most research areas in Machine Drives and Power Electronics Technology [2]. Advancement in semiconductor switches and devices, microcontrollers and other electronic devices has resulted in the economical, faster, reliable and influential power electronics technology [3]. This improvement in power electronics has resulted in energy saving approaches in many industrial and residential applications [4].

Most important factors to consider in research activities in advanced traction are high efficiency, high torque and power density, quick dynamic response, low cost, less noise, rugged and robust [5]. In recent years huge amount of research and investigation has been done in electric motors for traction applications [6]. Permanent Magnet Synchronous Motors and brushless DC motors are found to be extensively used as electric motor in traction applications [2]. Due to the high price of permanent magnet, price fluctuations and rare availability Electric Vehicle makers are now more

inclined towards magnet less electric motors [3]. Research interest has grown towards motors without permanent magnet [6].

1.2 History of SRM

Developments of Switched Reluctance Motors dates to 19th Century [7]. The minimum reluctance principle based Switched Reluctance Motors came into existence since the discovery of electromagnetism [7]. Switched Reluctance Motor was supposed to be built in 1838 by W.H. Taylor who had patent for electromagnetic engines [8]. During that time SRM was known as electromagnetic engines [8]. Controlling the machines was much difficult so SRM was not widely used until late 1960's when control of the SRM becomes easier due to advancement in semiconductor devices [8]. Finite Element Analysis and use of ICs and microcontroller in signal processing aided the development of control of SRM [9].

In 1980 Lawrenson et al laid general foundation for the practical design of Switched Reluctance Motors [10]. Lawrence et al demonstrated SRM are capable of high level of performance, can be controlled in simple ways, are simple in structure and cheap to manufacture [10]. Lawrence et all showed absence of field winding does advantage to machine by lowering cost and eliminating commutator without affecting machine performance [10]. Lawrence et al also introduced design parameters values of pole numbers and pole arcs, frequency and form of flux variations for high efficiency of machines [10]. To conclude, this paper explained satisfactory working performance of variable speed Switched Reluctance Motor with compared to daily used induction motor. This paper reopened the door for research and development in Switched Reluctance Motor.

1.3 Research objectives

The main objective of this research is to compare design structure and performance characteristics of single stator conventional switched reluctance motors and double stator switched reluctance motor.

Sub objectives of the research are as follows:

1. To study single stator switched reluctance motors and determine the complications associated with their negligible industrial applications.
2. To study double stator switched reluctance motors, their development progress and significant improvement in design.
3. To compare transient and magnetostatics analysis of Inner Stator SRM, Outer Stator SRM and Double Stator (Inner and Outer stator combined) SRM in terms of maximum moving torque, average moving torque and torque ripple.
4. To perform Finite Element Analysis (FEA) Test for Magnetostatics and Transient Analysis to evaluate SRMs performance.
5. To modify design of original SRM and DSSRM with the aim to improve motor performance.
6. To modify rotor of original DSSRM and compare the motor performance of original DSSRM and modified rotor DSSRM.

Chapter 2

Literature Review

2.1 SRM

2.1.1 Design Structure

In [11] Ibrahim et Al describes necessary design parameters of SRM. Authors discussed about motor specification, output torque, motor dimensions, pole numbers, air gap length [11]. The authors also mentioned constraints in calculation of stator and rotor pole angles, relation between stack length and rotor outer radius, and rotor outer radius and stator outer radius relationship [11]. The authors concluded design by doing Finite Element Analysis investigating flux density, shaft torque, phase currents and inductance with respect to time [11]. The authors completed the paper with parametric study by changing design parameters such as number of turns of phase windings, resistance of phase windings, and materials [11]. During the study driving circuit parameters remained unchanged.

In [12] Besharati et al designed high speed SRM capable of running at 60000 rpm with output power of 60kW. Authors demonstrated potential of SRM in automotive traction applications which demand high speed and high power [12]. At high speed, radial and tangential force increases due to increase in centripetal force [12]. This result in high mechanical stress on rotor leading to increase in vibrations and frequency of the motor affecting acoustic noise of the motor [12]. The authors dealt with this high mechanical stress by introducing flywheel type design rotor [12]. This design uses bolts to hold laminations together assisting in transfer of torque to shaft only through end plates of rotor instead of using whole shaft to feed the machine [12]. Authors of this paper

concluded by discussing importance of proper cooling system to avoid losses during high speed applications [12].

Author TJE Miller in his paper [13] presented new equations to describe practical design and development of Switched Reluctance Motor Drives. Author points out design calculation of Switched Reluctance Motor is much sophisticated and needs computer numerical methods even for basic design computation [13]. Author also points out drive system of induction motor is also complex as compared to switched reluctance motor drives but the reason behind fewer practical drive system of SRM is inadequate knowledge of design architecture and working of SRM controllers to many designers [13]. Author mentions these are the possible complications in employing the design theory from research papers to real motor [13]. Author concludes the paper by stating practical development of Switched Reluctance Motor drive is a process involving in-depth calculation of electromagnetic and mechatronics design, proper laboratory testing and notable tooling [13].

2.1.2 Torque Ripple

One of the major disadvantage of SRM is torque ripple [14]. Acoustics noise and vibrations are results of torque ripple [14]. Nonlinear nature of SRM, current switching and phase commutation are the major causes of torque ripple [15]. When rotor and stator overlap, inductance of the motor does not vary linearly if magnetic saturation effect is considered [14]. Though constant current is supplied by controlling each phase, it does not necessarily produce constant torque due to this nonlinearity [14]. During each phase a controlled current should be supplied to the machine by switching the semiconductor device [15]. This results in torque ripple at switching interval due to switching loss associated with the semiconductor switches [15]. Torque ripple produced during current switching interval depends on switching frequency of semiconductor switches and other

operating conditions [15]. Another reason for torque ripple is phase commutation [15]. Switched reluctance motors has double salient structure [14]. Torque is produced in each phase by magnetic reluctance properties as it does not have smooth rotating magnetic field [15]. So, torque ripple is produced during such phase commutation from one to another [15].

In [16] Lee et al discuss torque ripple is because of fringing flux which is produced before overlapping of stator and rotor poles. This flux results in nonlinear current giving rise to torque variation [16]. Author was successful to reduce torque ripple by 4.4% compared to previous design by presenting new rotor with notch in forward rotating direction [16]. In [13] Miller explains torque is produced in SRM by the amplification of cogging torque. The variation of energy in motor due to interaction of rotor and stator poles during open circuit is cogging torque [13]. It is defined as the rate of change of magneto static energy with respect to angle of rotation and is given by [13]

$$T_{cog} = \frac{\partial W}{\partial \theta} \tag{1}$$

Where W= Magnetostatics Energy $\theta =$ Rotation Angle [Reduction of cogging torque by various structure of rotor PM in brushless DC Motors]

Cogging torque can be controlled by current wave shaping at low speed [13]. However, at high speed this is not possible due to current saturation [13].

2.1.3 Design Improvement

Many research has been done to mitigate problems of torque ripple [16-21]. Two methods extensively used to reduce torque ripple in switched reluctance motors are

1) Method which involves improvement in magnetic design of rotor and stator pole structure of SRM [16-18].
2) Method involving design of drive and control circuit of SRM [19-21].

Most of the methods involving design improvement of drive and control circuit are based on current control technique [19-21]. In [21] authors have changed slops of source current in commutation region to reduce torque ripple. Group of researchers in [20] have proposed a new control technique based on pre- computed current profile which minimizes peak magnetic flux during high speed operations reducing both torque ripple and source current ripple. In [22] authors present new algorithms and use of digital Integrated Circuits in control of SRM. Marija et al used Floquet transformation to represent SRM equations in rotating reference frame and propose time varying control of SRM which generates desired torque on dynamic operating conditions with reduced torque ripple [22].

Group of researchers have used Torque Sharing Function (TSF) method [23-25] to minimize torque ripple. TSF is one of the torque control methods which converts overall torque of the motor to a unity torque [23]. It is a well-known fact that most of the ripples in SRM are produced during the overlap period of two phases [23]. Torque sharing function monitors the instantaneous torque generated by each phase by wave shaping the phase current [23]. This wave shaping minimizes pulsating torque occurring in overlapping period [23]. Torque sharing function regulates individual phase current by sharing reference torque between incoming and outgoing phases at the commutation region [23]. One of the method to achieve ripple free torque is explained in [23]. Husain et al presents improved PWM current control method to minimize torque pulsations in overlapping region by defining a contour function to be followed by individual phases such that summation of individual torques is constant and equals to required torque [23].

In [24] A.-C Pop and coworkers compares three types of TSFs viz. Cosine sharing function, exponential sharing functions and piecewise cubic sharing functions to improve efficiency of

SRM. Authors optimized three different types of TSFs minimizing ripple related loss by 50%, expanding torque speed region by 30% and increasing overall efficiency by 10% [24].

Though TSFs producing unity torque are dominant in motoring applications, they give rise to phase current error [25]. Phase current errors occurs when current could not track reference value due to high inductance during commutation [25]. So, group of researchers [25] proposed non- unity torque sharing function. Hye Ung Shin et al successfully minimized torque ripple to 22% by inserting ripple components into reference torque [25]. These preinserted ripple components neutralize actual torque ripples produced during the commutation period [25].

Some research [26-28] extended TSF by combing Artificial Neural Network (ANN) to minimize torque ripple. Due to its simple model and less memory requirement, ANN inherits low cost and high accuracy [26-28]. ANN is used to predict anticipated current for specified torque by using rotor position information [26-28]. In [26] network is trained with neurons using Levenberg Marquardt Algorithm. FEM test is performed to get magnetic characteristics, which is then organized to train network [26]. The torque obtained using this control method using ANN consist of ripples less than 10% [26]. Group of researchers have introduced new control technique SHRFNN [29] by combining Supervisory Control, Recurrent Fuzzy Neural Network (RFNN) and Compensated Control to minimize torque ripple. Supervisory control job is to stabilize the states around predefined boundary region where as RFNN control and compensated control are associated with smoothing and reducing excessive chattering control effort produced by supervisory control [29]. One of the good advantage of this control method is its adaptive nature which make it independent of the motor predefined characteristics and adjust to any dynamic behavior [29]. Provided experimental data verified the effectiveness of SHRFNN control method however the paper lack actual data that shows numerical value of torque ripple minimization [29].

Another novel SRM instantaneous torque control strategy based on online fuzzy neural network [28] is proposed to lessen torque ripples. TSF is modeled using adaptive neural fuzzy inference system to calculate phase torque value [28]. Current profile is then generated using Adaptive Neural Fuzzy Interference System (ANFIS) [28]. ANFIS parameters are controlled by online-supervised learning which aids in the design of adaptive sliding mode current controller which in turn track required phase current [28]. This control method minimizes torque ripple however closed loop control scheme is not included in this work.

Some researchers have used holistic approaches combining both magnetic design improvement and control circuit design to tackle torque ripple [30-31]. [30] has used iterative process in Finite Element Analysis to modify voltage and inductance profile and using torque ripple as a correction term in succeeding step of iterative process. Though simulation results showed improvement in voltage and inductance profile, the Finite Element methods did not match the experimental results [30]. Gaurang et al [31] successfully reduced torque ripple by 37.31% by optimization of both machine design and control design simultaneously. For machine design improvement authors varied rotor pole arc and depth of multiple teeth per rotor pole [31]. Regarding control improvement authors proposed novel stator excitation pattern where each phase is excited for one step with positive and negative excitations in one rotor pole pitch [31].

From the above literature review it can be inferred that most of the electromagnetic force produced in conventional switched reluctance motors does not take part in desired electromagnetic energy conversion [32]. Most of the electromagnetic force generated by SRM is not in the direction of motion [32]. Only small amount of produced force is in motional direction which result in low energy conversion efficiency [32]. This is the reason SRM generate low motional torque but high torque ripple, vibrations and acoustic noise [32].

2.2 DSSRM

Mohammadali Abbasian et al [32] introduced switched reluctance motor with double stator which results more force in the direction of motion. This Double Stator Switched Reluctance Motor (DSSRM) works in the same principle conventional SRM runs [32]. One exterior and one interior stator configuration directs magnetic flux lines to pass in the direction of motion producing higher amount of useful force in normal direction and less amount of unwanted force in radial direction [32]. Maxwell stress tensor (MST) method is used to calculate electromagnetic force and "MagNet" is used for Finite Element Analysis (FEA) test to study force generation process [32]. Experimental prototype is developed to match FEA calculation which verify the successful working of proposed design [32].

[33] presents comparison between SRM and DSSRM structures and force density with same machines parameters like power output, yoke thickness and outer diameter. Using FEM, velocity, acceleration and maximum deformation is computed for both machines and found to be lower in DSSRM by the factor of 9,6 and 7 respectively [33]. Finally, the paper is concluded by proving the fact DSSRM produces low vibration and less radial force [33]. However, current chopping and end winding leakage is not considered in the electromagnetic analysis [34].

[34] computed acoustic noise and vibration of DSSRM by using Multiphysics analysis considering effects of current chopping and end winding leakage inductance. Hassanpour and coworkers [34] computed electromagnetic flux using 3D FEM and phase current using hysteresis current control. The force density obtained by 2D electromagnetic FEM is used to compute vibration in the outer stator of DSSRM [34]. Acoustic power is then obtained using acoustic BEM [34]. Comparison shows lower acoustic noise power in DSSRM than SRM by 26 dBA at speed below 2000 rpm and 12.5 dBA at 2000 rpm [34]. It is also shown DSSRM experience 12 times (below 2000rpm) or 19

times (at 2000rpm) lesser acceleration than conventional SRM which is much better result than [33].

DSSRM is in the process of development [33]. Countable number of research [33, 35-37] has been focused on vibrational and acoustic noise analysis of SRM and most of the analysis are magnetostatics analysis. Only few research [5] [38] has been done in transient analysis and torque ripple behavior of DSSRM. In this thesis, Transient analysis of DSSRM is performed and comparison of motional torque and torque ripple is demonstrated between DSSRM, Outer Stator SRM and Inner Stator SRM. Magnetostatics analysis is also done to examine force density. Rotor is then modified to study any improvement in torque characteristics.

Chapter 3

Principle and Operation of SRM

In this chapter principles and operations of SRM is explained.

3.1 Overview of SRM

SRM is free of permanent magnets (PM) [9]. Construction of SRM is extremely simple [9]. It has doubly salient structure as both rotor and stator have saliency [7]. Number of poles in stator and rotor are different [9]. Most importantly, winding is present only in stator whereas rotor is simply laminated structure [7]. Only stator windings need to be excited for the operation [7]. So, SRM is also known as singly excited machines [7]. Due to simple geometry associated with it and absence of PM, SRM inherits properties like low manufacturing and maintenance costs, rugged structure and high reliability [7]. Windings of stator pole is connected in series to its diametrically opposite stator pole windings to form one phase [7]. Cross section view of 3 phase SRM with 6 stator poles and 4 rotor poles with winding diagram of Phase A is shown in Figure 1 below [7].

Switched Reluctance Motors operates in minimum reluctance principle [7]. When one of the phase is excited, current passes through two of the stator poles producing magnetic flux path around stator, rotor and airgap between rotor and stator [7]. As magnetic reluctance is inversely proportional to magnetic flux, the excited stator poles have minimum reluctance [7]. Rotor pole close to the corresponding excited stator pole is attracted towards the position of minimum reluctance [7]. This process of alignment of two rotor poles with two diametrically opposite excited stator poles generates torque in switched reluctance machines [7]. At the same time remaining set of rotor poles is out of alignment with unexcited set of stator poles [7]. Now another pair of unaligned stator poles is energized to align second pair of rotor poles and the process continues

[7]. Thus, continuous torque is generated in SRM by consecutive excitation of individual phase [7]. Torque generated in the process does not depend on direction of current flow but depends on sequence of exciting stator poles and position of rotor [10]. Due to these reasons unidirectional current is used which simplifies control circuit to drive SRM [10].

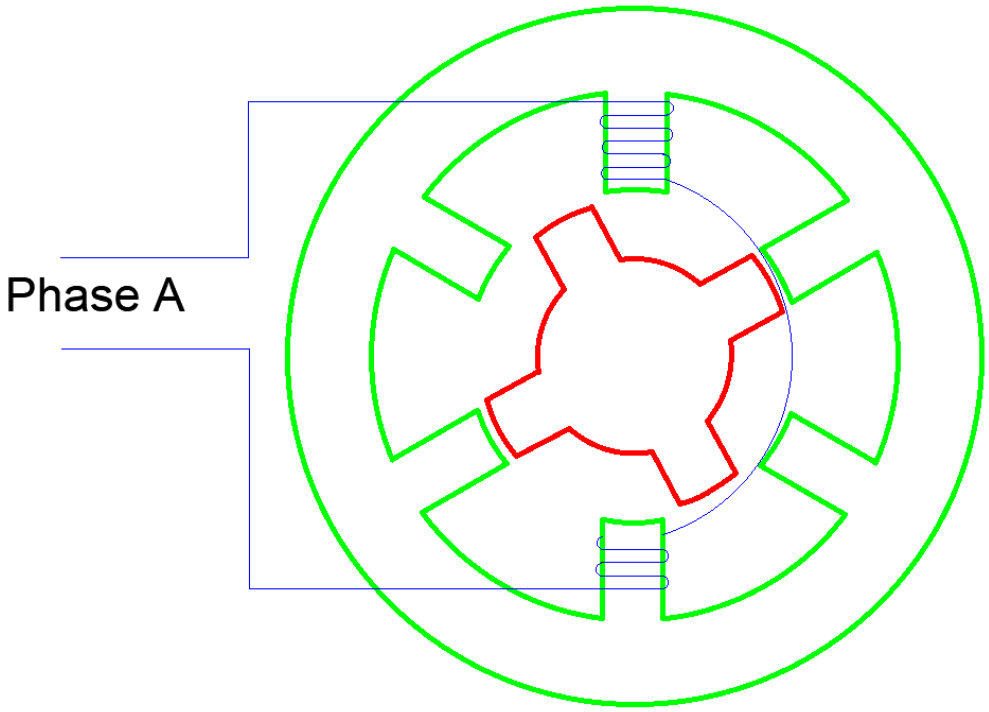

Figure 1: Cross Section view of SRM with Phase A [7]

Relation of Inductance and Magnetic Reluctance

Torque generated in Switched Reluctance Machine is the function of inductance [39]. Thus, SRM operation can be best explained with the help of inductance [39].

In Magnetic circuits, Magnetomotive force (F) is given by [39]

$$F = \emptyset R \tag{2}$$

Where $\emptyset$ is Equivalent Flux and R is Magnetic Reluctance.

And $\emptyset$ is given by [39]

$$\emptyset = \frac{\lambda}{N} \quad (3)$$

Where $\lambda\ (= L.i)$ is flux linkage, N is number of turns, L is inductance and i is current.

From equations (2) and (3) we can write [39],

$$F = \frac{\lambda}{N} R \quad (4)$$

$$Ni = \frac{\lambda}{N} R \quad (5)$$

$$N^2 = \frac{\lambda}{i} R \quad (6)$$

$$N^2 = LR \quad (7)$$

$$L = \frac{N^2}{R} \quad (8)$$

Thus, it can be said Phase Inductance of the coil is inversely proportional to magnetic reluctance [39].

At any given time, there are three relative position between stator and rotor poles [40].

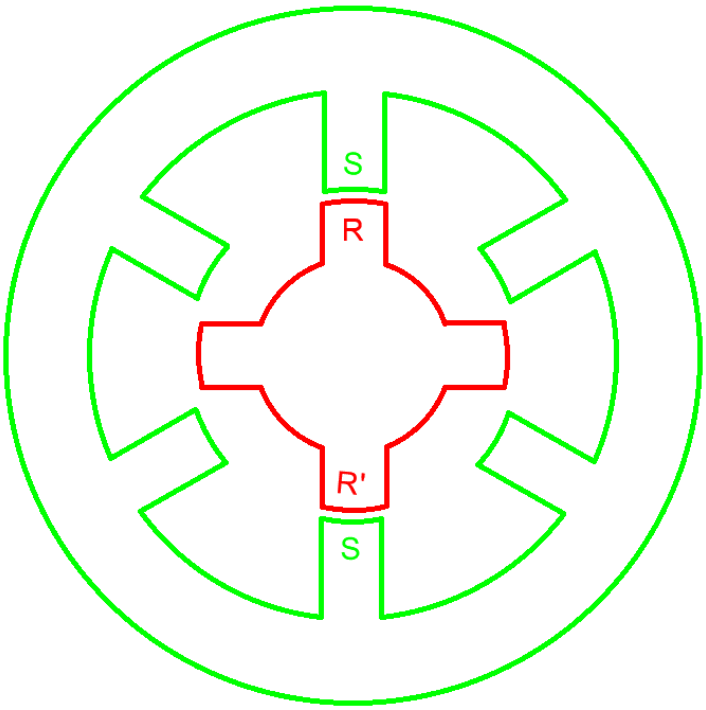

Figure 2: Aligned Position [40]

1. When rotor poles exactly align itself with stator poles at any phase, then the position is called aligned position [40]. In Figure 2 rotor poles RR' perfectly align with stator poles SS'[40]. During this interval of time, phase inductance of the coil is maximum and magnetic reluctance is minimum [40].

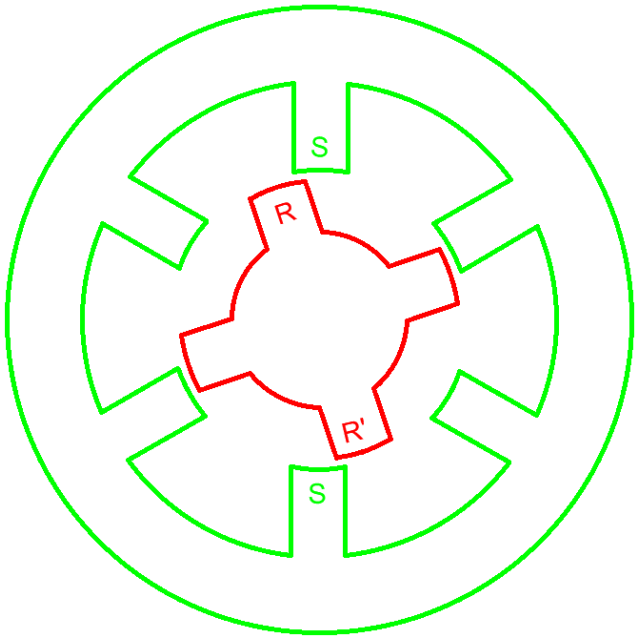

Figure 3: Unaligned Position [40]

2. When rotor poles do not exactly align itself with stator poles at any phase the position is called unaligned position [40]. In figure 3 rotor poles RR' do not align perfectly with stator poles SS'[40]. During such interval of time when rotor pole is moving away from aligned position, phase inductance of the coil gradually decreases while magnetic reluctance starts increasing [40].

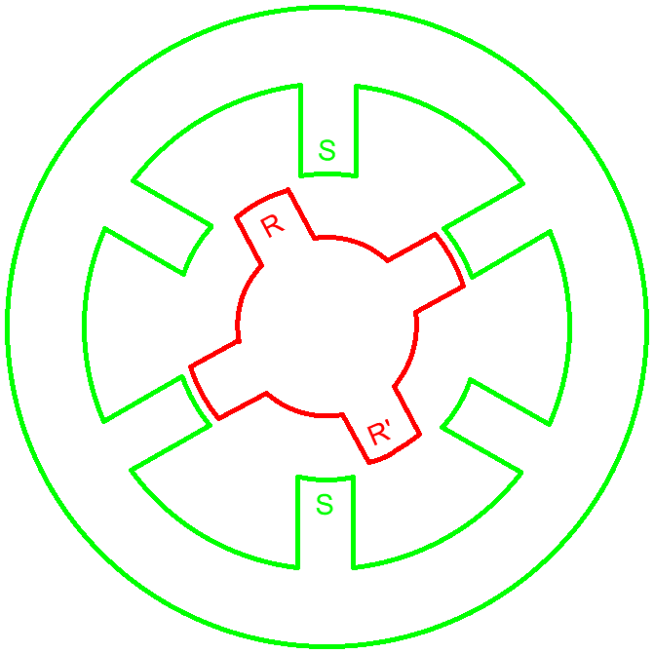

Figure 4: Misaligned Position [40]

3. When rotor pole is between two stator poles, the position is called misaligned position [40] as shown in figure 4. Rotor poles RR' is misaligned with respect to stator poles SS' [40]. During this interval of time, phase inductance of the coil becomes minimum and magnetic reluctance gets its maximum value [40].

3.2 Mathematical Model and Equivalent Circuit of SRM

SRM can be modeled analytically using three differential equation viz. Voltage Equation, Electromagnetic Torque Equation and motion equation [41]. Instantaneous voltage across the terminals of a single-phase winding of SRM is given by Faraday's Law [41]

$$v = iR + \frac{d\phi}{dt} \tag{9}$$

Where v is terminal voltage, R is phase resistance, i is phase current and ϕ is flux linkage.

Due to double saliency in SRM and magnetic saturation effects, flux linkage ϕ varies as a function of rotor position θ and phase current i [41].

$$\phi = \phi(\theta, i) \tag{10}$$

On differentiating, Terminal voltage can be calculated from equation (9) and (10) as [41]

$$v = iR + \frac{\partial\phi(\theta,i)}{\partial i}.\frac{di}{dt} + \frac{\partial\phi(\theta,i)}{\partial\theta}.\frac{d\theta}{dt} \tag{11}$$

Where $\frac{\partial\phi(\theta,i)}{\partial i} = L(\theta, i)$=instatnaeous inductance [41]

$\frac{\partial\phi(\theta,i)}{\partial\theta} = e$= Instantaneous Back EMF [41]

$\frac{d\theta}{dt} = \omega$= angular velocity [41]

Neglecting magnetic saturation, inductance does not depend on current but depends only on rotor position so relationship between flux and current can be written as [41]

$$\phi = L(\theta).i \tag{12}$$

And $L(\theta) = \frac{\phi}{i}$

Equation (11) can be rewritten as [41]

$$v = iR + L(\theta).\frac{di}{dt} + i\omega.\frac{dL(\theta)}{d\theta} \tag{13}$$

Where first, second and third term of right hand side of equation (13) are equivalent to resistive voltage drop, inductive voltage drop and back emf or induced emf respectively [41]. Equation (13) relates transfer of electrical energy to magnetic field in SRM [41].

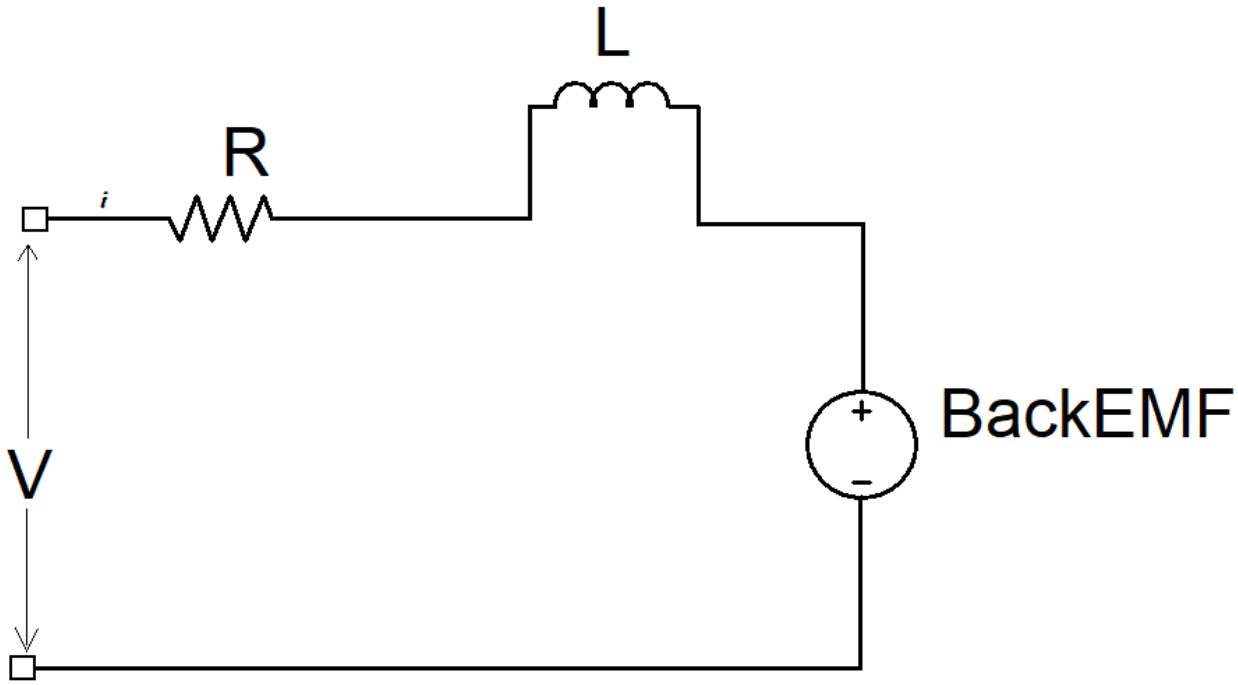

Figure 5: Equivalent Circuit of Single Phase SRM [41]

Multiplying both sides of equation (13) by i yields [41]

$$P = vi = i^2R + iL(\theta).\frac{di}{dt} + i^2\omega.\frac{dL(\theta)}{d\theta} \tag{14}$$

P represents instantaneous electrical power delivered to the SR motor [41].

3.3 Electromechanical Energy Conversion (EEC)

To make electromechanical energy conversion more understandable, nonlinear analysis based on magnetization curve is presented here [42]. Saturation of the magnetic circuit is considered during the analysis [42]. Magnetization curve is a plot of flux linkage ϕ versus current i for fixed rotor position θ [42]. EEC can be explained with the help of stored magnetic field energy W and co-energy W' [42]. Co-energy is non-physical quantity and is useful in derivation of torque expressions in electromagnetic circuits [42].

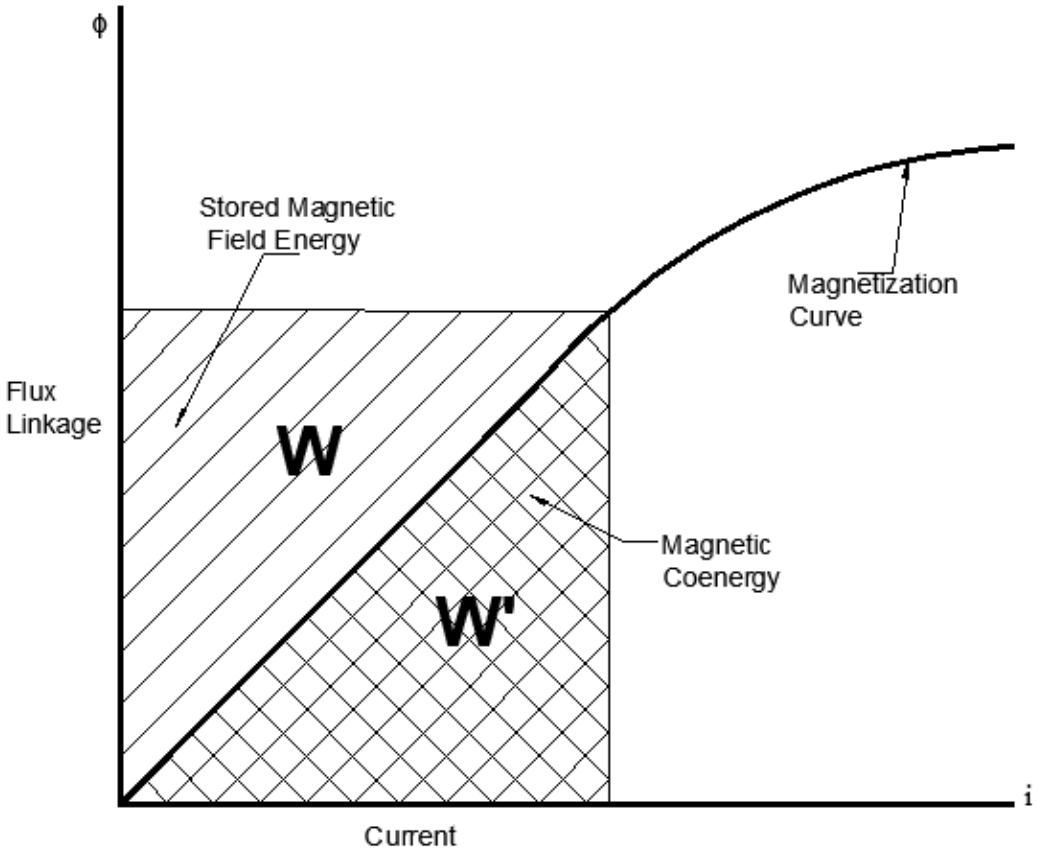

Figure 6: Ideal Magnetization curve [42]

Stored magnetic field energy W can be expressed as [39] [42]

$$W = \int i.d\phi \tag{15}$$

Area below magnetization curve is co-energy and can be expressed as [39] [42]

$$W' = \int \phi . di \tag{16}$$

Ignoring dissipation of energy from coil resistance and at constant current, SRM's electrical input energy is equal to sum of stored magnetic field energy W and co-energy W' converted to mechanical energy and can be expressed as [39] [42]

$$W + W' = i . \phi \tag{17}$$

During the energy conversion process, lost magnetic field energy can be recovered by using proper converter configuration [42]. In magnetic linear circuit, magnetization curve is straight line so, stored magnetic field energy and co-energy are equal as shown in Figure 6 [42].

But under magnetic saturation, most of the input energy is towards co-energy [42]. Magnetization curve is no more a straight line and stored magnetic field energy is not equal to co-energy as shown in Figure 7 [42].

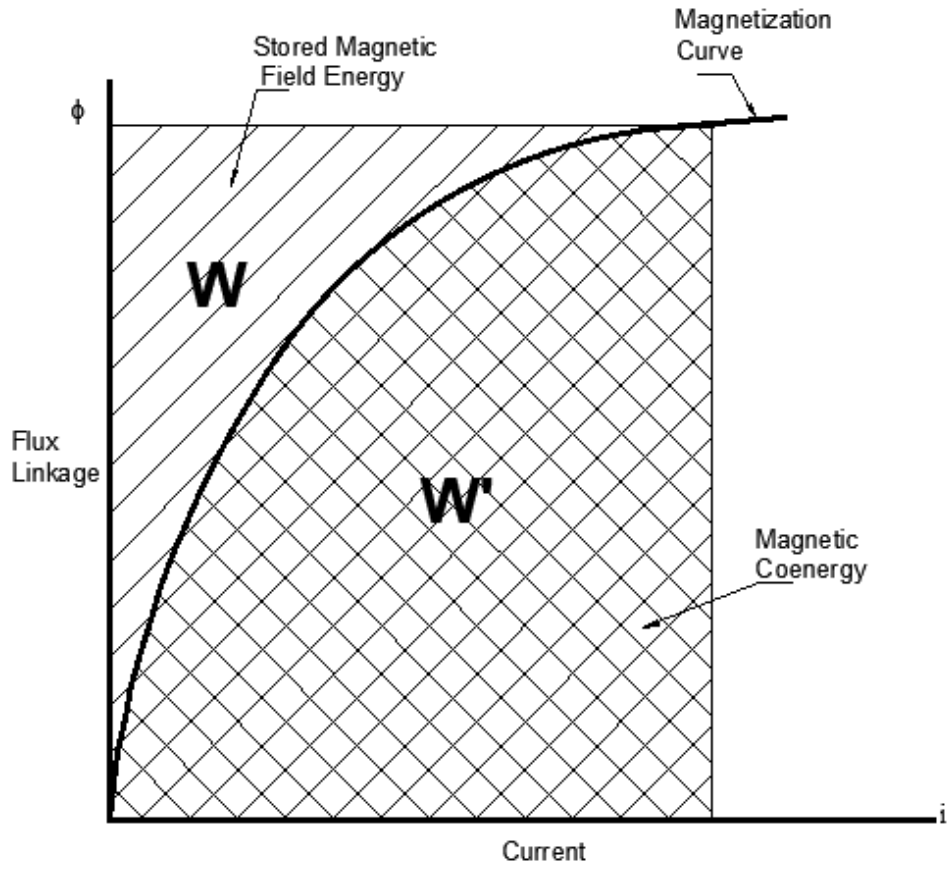

Figure 7: Magnetization Curve under magnetic saturation [42]

From above it is observed magnetic field co-energy is higher than stored magnetic energy [42]. Magnetic saturation is one of the drawback of electrical machines [39]. In [43] Byrne discuss decrease of this magnetic saturation in reluctance machines during overlap of stator and rotor which almost doubles tangential force.

3.4 Torque Equation

It is often desirable to represent torque in terms of current rather than flux and similarly torque in terms of co-energy rather than energy [41]. Electromagnetic Torque in magnetic nonlinear system is calculated in terms of co-energy W' as [41-42]

$$T(\theta, i) = \frac{\partial W'(\theta, i)}{\partial \theta} \tag{18}$$

Where θ is angular position of rotor and i is current flowing through the coil.

Co-energy depends on θ and instantaneous value of current [41].

At any value of θ, W' is the area below the magnetization curve and can be expressed as [41-42]

$$W' = \int_0^i \phi(\theta, i) di \tag{19}$$

Now Combining From (18) and (19) [41-42]

$$W' = \int_0^i L(\theta).\, i\, di \tag{20}$$

$$W' = \frac{i^2}{2} L(\theta) \tag{21}$$

$$T = \frac{i^2}{2} * \frac{dL}{d\theta} \tag{22}$$

Where L is the value of self-inductance. Equation (22) is general Torque Equation [41-42].

Motion Torque T is given by [41]

$$T = J\frac{\partial \omega}{\partial t} + D\omega + T_L \tag{23}$$

Where J = Rotor Inertia, D = Damping Coefficient and T_L = Load Torque

3.5 Torque Speed Characteristics of SRM

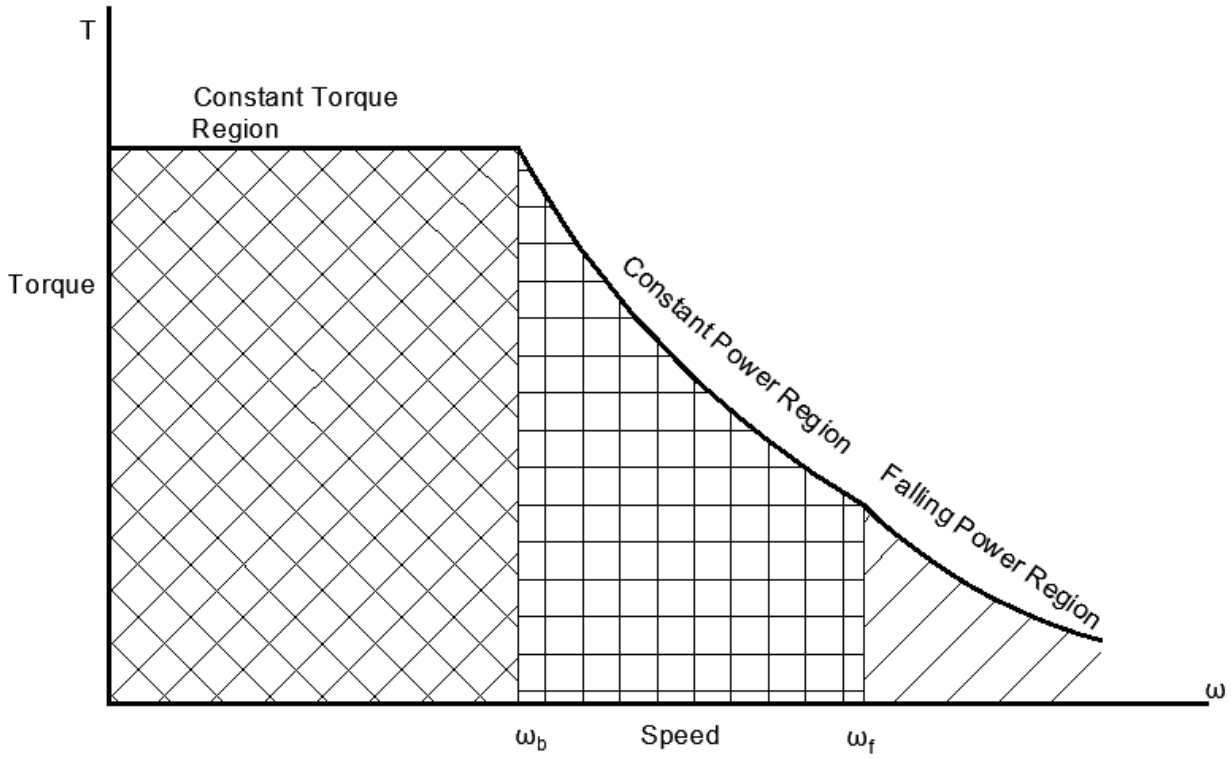

Figure 8: Torque Speed Characteristics Plot [41]

Control mechanism of SRM is based on torque-speed characteristics of the motor [42]. Based on different speed ranges, operation of SRM is divided into three regions viz. Constant torque, constant power and falling power region [41]. Base speed ω_b is the maximum speed at which maximum current can be supplied to the motor at rated voltage to achieve rated torque [41]. At low speed (below ω_b) generated voltage is higher than back emf, so desired level of current can be set and constant torque is achieved [41]. When the speed becomes higher than base speed, back emf also becomes higher and conduction angle is increased to reach desired current level [41]. This increase in conduction angle results in constant power production [41]. At the same time torque starts falling and is not constant anymore [41]. If conduction angle is further increased, turn off angle of current cycle coincide with turn on angle of next cycle [41]. Flux level won't return to zero at the end of each pulse [41]. With further increase in speed beyond ω_f, conduction angle

can no longer be increased [41]. So, torque falls off more rapidly and constant power is not achieved and the region is falling power region [41].

3.6 Switching of Phases in SRM

For the operation of SRM only one stator phase should be active at a time [44]. Another phase should be activated at the end of each pulse to generate continuous torque in SRM [44]. Correct way of switching of phases is shown in Figure 9 below [44]:

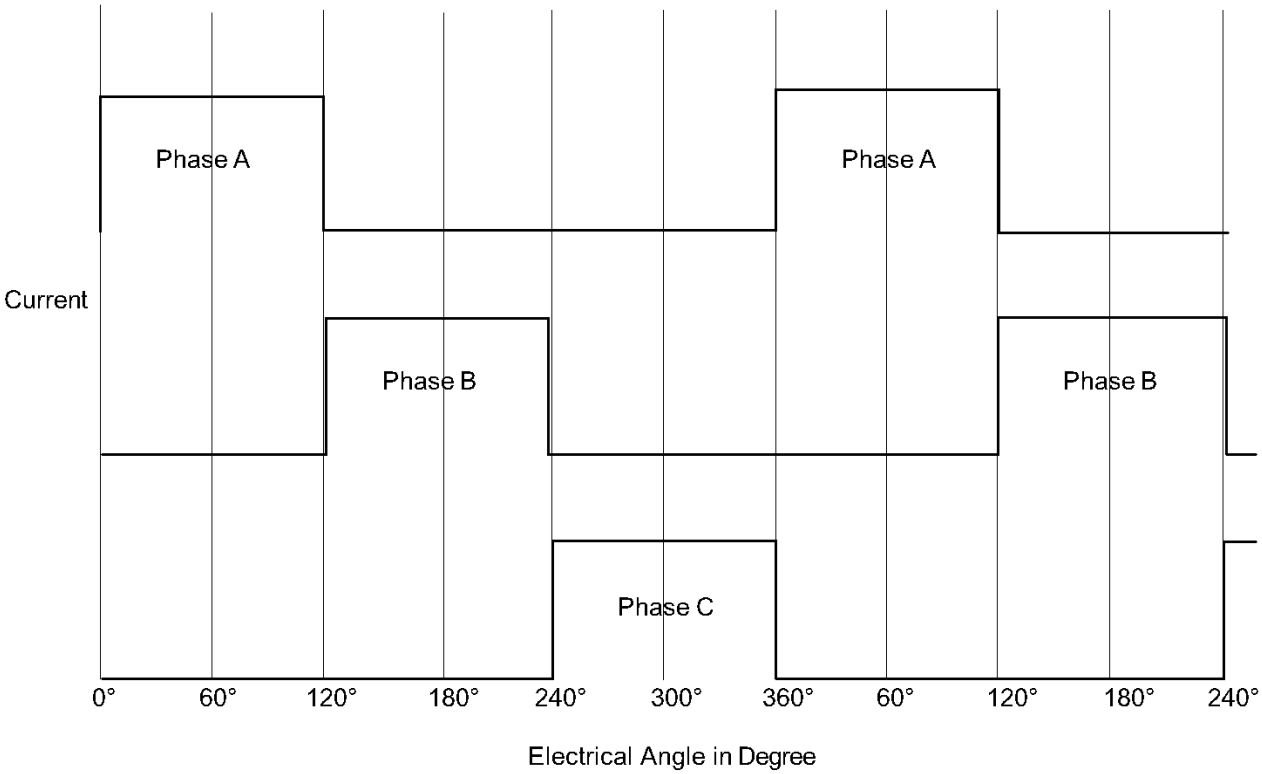

Figure 9: Switching of Phases [44]

Switching of phases in proper sequence is very important phenomenon in SRM to ensure current flow in each opposite pair of stator poles at a time during the period of one pulse according to rotor position [44]. Converter circuit is employed to activate and switch stator phase according to the rotor position information [39]. From Torque Equation **,** we know torque generated in SRM does not depend on the direction of current [39]. So, unidirectional current carrying converter suits SRM

[39]. However, non-sinusoidal alternating current can also be used but due to high hysteresis loss associated with it, unidirectional current is the ultimate choice [39]. Hence, independent operation of individual phases and supply of unidirectional current are the necessary conditions that must be satisfied by converters for satisfactory operation of SRM [39].

3.7 Converters

Converters for SRM are mainly divided into two categories viz. Hard Switching Converters and Soft Switching Converters [45]. Both types of converters are briefly introduced below.

1) Hard Switching Converters: In hard switching types of converters, switching occurs at input voltage level [45]. This reason makes it more prone to switching loss making it less efficient. One of the good advantage of these types of converters is low cost as they do not require resonant capacitors and inductors [45]. Examples include Classic Bridge converters, (n+1) switch converter, Bifiliar Winding converter and C-dump converters [45].
2) Soft Switching Converters: In soft switching types of converters, switching occurs at zero current or zero voltage [45]. As there is no switching loss associated with it, efficiency of these types of converters is high [45]. However, they are more expensive than their counterparts as they require resonant capacitors and inductors for zero crossings of currents and voltages [45]. Examples includes New series resonant converter and Quasi resonant converter [45].

Selection of these different types of converter in SRM is based on the applications of the motor [7]. For applications where, accurate control of torque is not required hard switching types of converters are used [7]. Some applications demanding accurate control of torque and high efficiency make use of soft switching converters [7].

Among these different converters topology, Classic bridge converter is most flexible [46] and most versatile [33] [45] and are often used as switching circuit in SRM. This converter is also known as Asymmetric bridge converter and consist of two switches and two diodes per phase [34] [46]. So, there are 2N switches and 2N diodes for N phase SRM [46]. Each stator's phase winding is connected to the classic converter and each phase can be controlled independently [46]. While supplying current to one phase winding, another phase winding can be demagnetized simultaneously to ensure return of flux linkage to zero at the end of each pulse [46]. This high control flexibility of Classic converters makes them popular among SRM technologies [46]. Circuit diagram of three phase classic converter is shown in the Figure 10 below [46].

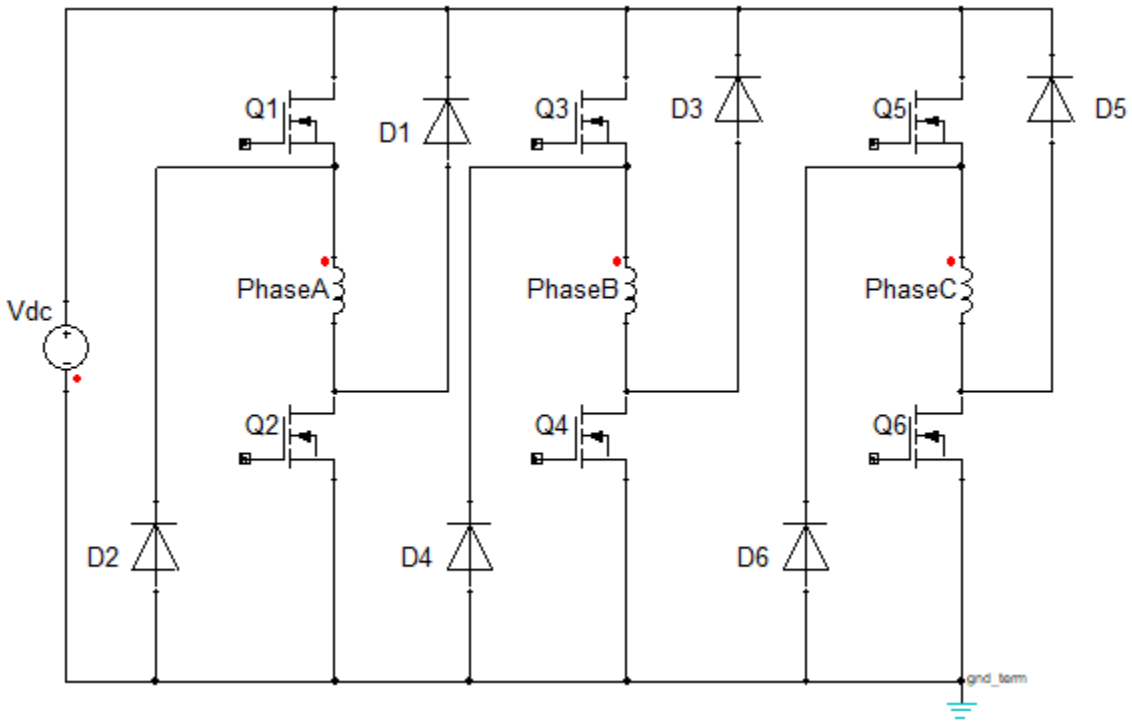

Figure 10: Classic Converter [46]

There are three modes of operation in asymmetric bridge converters viz. Magnetization, Freewheeling and Demagnetization mode [46].

1) **Magnetization or Conduction Mode:** Both the upper (Q1) and lower(Q2) semiconductor switches are turned ON together [46]. Stator winding is connected to the DC supply voltage (V_{DC}). Phases are magnetized by the flow of current [46]. Voltage across the phase winding (v) is equal to supply voltage i.e. $v = V_{DC}$ [46].
2) **Freewheeling Mode:** When current reaches the reference value, one of the switches is turned OFF such that when Q1 is OFF, D2 is ON and Q2 if OFF, D1 is ON [46]. Phase current flows in a continuous path and voltage across phase winding is zero i.e. $v = 0$ [46].
3) **Demagnetization or Commutation Mode:** Both switching devices Q1 and Q2 are turned off and both diodes are forward biased [46]. Current flows through the diodes transferring trapped magnetic energy is from phase winding back to the DC source [46]. Rate of demagnetization is high and voltage across phase winding is negative of supply voltage i.e. $v = -V_{DC}$ [46]. During commutation period, demagnetization of one phase and magnetization of another phase in sequence is done simultaneously to reduce torque ripple [46].

Chapter 4

Double Stators Switched Reluctance Motor (DSSRM)

4.1 Overview

Double stator switched reluctance motor (DSSRM) is a new type of variable reluctance machine and consist of two stators and one rotor [32]. DSSRM were first introduced in 2010 [32]. Power density in DSSRM is relatively high compared to conventional SRM [32]. The machine is designed in such a way that maximum force is produced in the direction of motion reducing the force on non-motional direction [32]. Due to this more torque is produced in DSSRM with subsequently less vibration, toque ripple and acoustic noise [32]. In this chapter configuration and principle of DSSRM is discussed.

4.2 Structure and principle

Two stators are fixed in exterior and interior part of the machine [32]. Permanent magnet less rotor lie in between the two stators as shown in Figure 11 [32]. Rotor and stators are made up of laminated ferromagnetic materials [5]**.** It is singly excited machine as winding is present only on stators and make use of concentrated type of windings [5] [32]. Both stators have same pole and winding configuration [5] [32] as shown in Figure 12. That means two diametrically opposite poles of outer stator and two diametrically opposite poles of inner stator are excited at the same time [5] [32]. Coils are placed in such a way that flux path is short during the motor operation [5] [32]. Stators are stationary whereas rotor is extended in one side for connection to the load through shaft [5] [32].

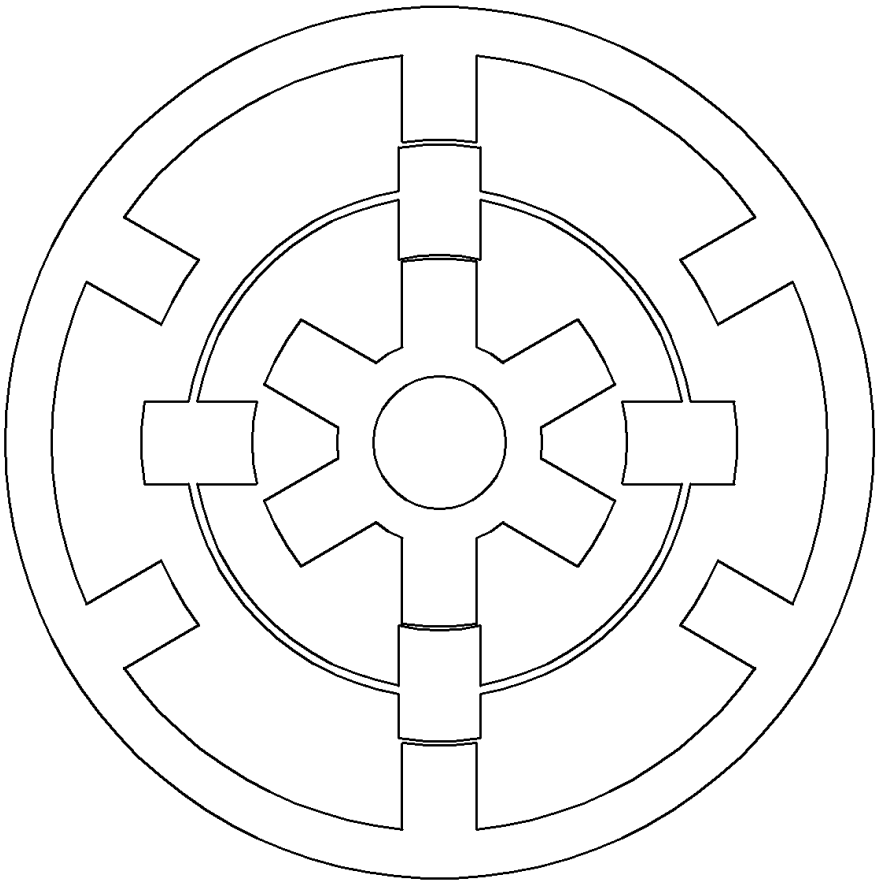

Figure 11: Cross section view of DSSRM [32]

DSSRM works in the similar minimum reluctance principle conventional SRM works [5] [32]. When one of the phase is excited, current passes through four diametrically opposite outer and inner stator poles [5] [32]. As energized stator poles have minimum reluctance, nearby rotor poles try to align with excited stator poles and torque is generated [5] [32]. In case of DSSRM, rotor achieves shortest flux path in the air maximizing normal force and simultaneously minimizing radial force [5] [32]. Normal force act in the direction of motion while radial force act in non-motional direction [5] [32]. Continuous torque is generated by activating inner and outer stator phases in a particular sequence [5] [32].

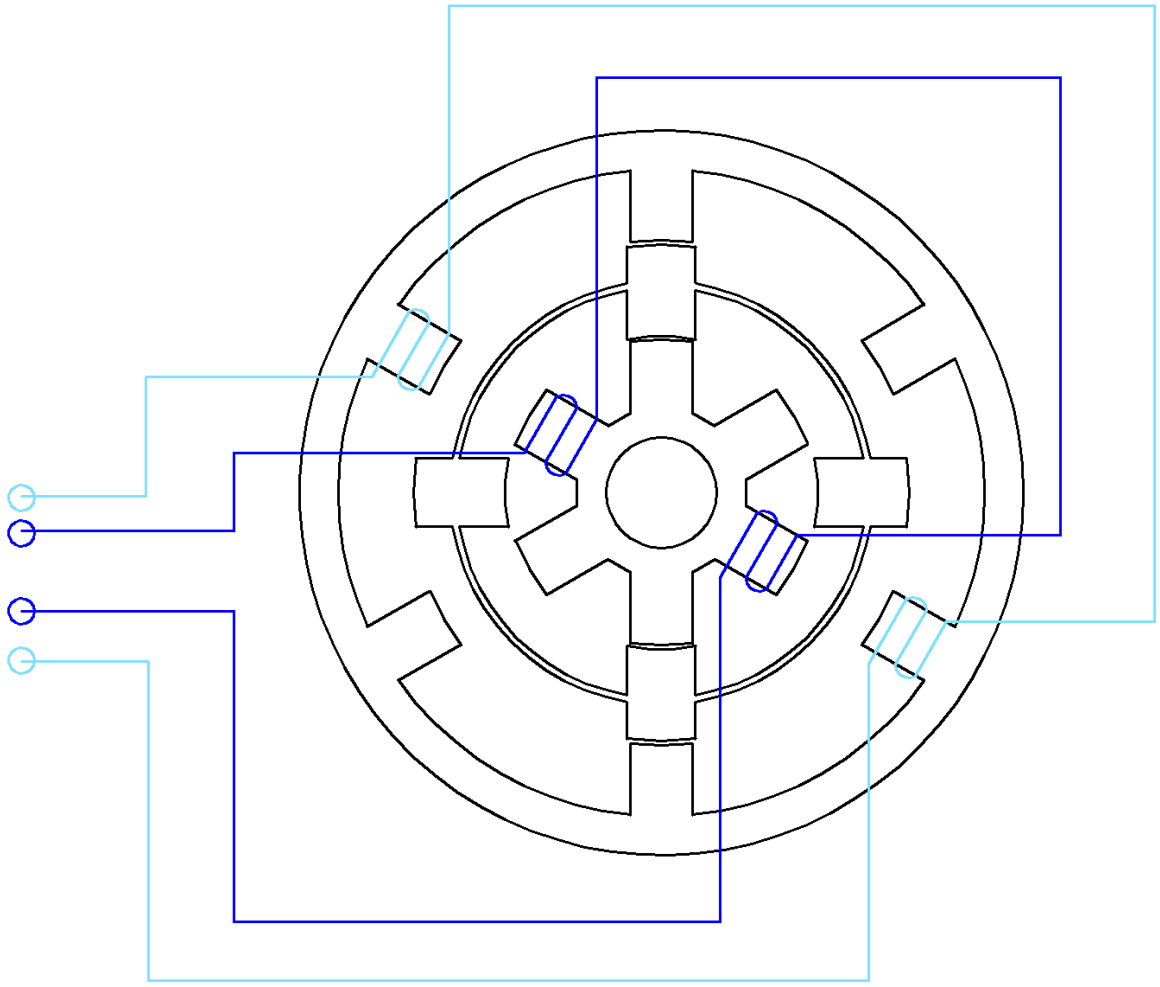

Figure 12: Phase A Winding configuration in DSSRM [32]

4.3 Magnetic Force Analysis and Electromechanical Energy Conversion of DSSRM

Magnetic force production is maximum where reluctance variation is highest [32]. In SRM it occurs along the edges of the rotor [32]. Computation of amplitude of force component is based on the same principle [32]. Maximum force component is produced where energy change in the given direction is highest [32]. Electromagnetic force in electrical machine is the product of interaction between normal and tangential components of the flux density [32]. Normal and tangential components of force density is expressed as [32]

$$f_{normal} = \frac{1}{2\mu_o}.(B_{normal}^2 - B_{tangential}^2) \quad (24)$$

$$f_{tangential} = \frac{1}{2\mu_o} . \left(B_{normal} . B_{tangential}\right) \quad (25)$$

Where f_{normal} and $f_{tangential}$ is normal and tangential component of force density, B_{normal} and $B_{tangential}$ are normal and tangential components of flux density and μ_o is absolute permeability [32].

In the air side of interface, $B_{tangential}$ is much smaller than B_{normal} [32]. So, tangential force component along air side of interface is approximately zero [32]. Normal force component in air side of interface between ferromagnetic material and air is high [32]. Thus, it can be inferred that normal force component directed towards the air are produced on the surface of ferromagnetic material [32]. If this force act in the motional direction electromechanical conversion efficiency (ECE) increases, production of torque increases and vibration, acoustic noise and torque ripple decreases [32]. ECE is given by [32]

$$ECE = \frac{F_{Motional}}{F_{Motional} + F_{Radial}} * 100\% \quad (26)$$

In conventional SRM force in the direction of motion is smaller so only small portion of magnetic field energy is converted to mechanical work [33]. But double stator configuration in DSSRM make magnetic flux lines to pass in the desired direction by creating novel flux path [33]. Due to this, normal force in the direction of motion is higher and more torque is produced [33]. Radial force along non- motional direction averages to zero [33]. Thus, in DSSRM higher portion of magnetic field energy is converted to mechanical work increasing electromechanical conversion efficiency [33].

Chapter 5

ANSYS Maxwell

5.1 Familiarization

ANSYS is engineering design and simulation software developed by an American Public Company Ansys Inc [47-48]. Ansys software is used in product design and create simulation to conduct Finite Element Analysis(FEA) test, thermal and vibrational analysis test and other electromagnetic analysis test [47-48]. ANSYS Maxwell is a high-performance software package which implement FEA to solve electrostatic, magnetostatics, eddy current and transient problems [47-48]. Maxwell is used to simulate finite distribution of mass through Finite Element Methods. ANSYS Maxwell solves these electric and electromagnetic field problems in motors, transformers, actuators and other electric machines by solving Maxwell's Equations in a finite region of space with suitable boundary conditions and other user defined initial conditions to obtain unique solution [47-48].

First geometry is defined depending on the problem and defined geometry is divided into many fundamental elements [47-48]. The assembly of such fundamental elements is called finite element mesh of the model [47-48]. Differential equations related to electromagnetic phenomenon are solved for each of these fundamental elements using Maxwell's equations [47-48].

James Clerk Maxwell, a Scottish scientist combined Ampere's Law, Faraday's Law, Gauss Law to create four equations to form fundamental of classic electromagnetism [49]. Using mathematical formulation given by him, principles governing electromagnetic system can be defined [49]. These mathematical equations define electric and magnetic forces involved in electromechanical

conversion process [49]. These four Maxwell equations [49-50] that define electromagnetic field are briefly discussed below:

1) **Gauss Law for electricity** [49-50]

$$\nabla . D = \rho \tag{27}$$

Where ∇ = Divergence operator, D = Electric flux density and ρ = Charge density

Equation (27) is the first Maxwell's Equation and is known as Gauss law [49-50]. According to this law electric charge acts as sources or sinks for electric fields [49-50]. The equation interprets divergence of electric flux density over any region is equal to total amount of charge in that region [49-50].

2) **Gauss Law for Magnetism** [49-50]

$$\nabla . B = 0 \tag{28}$$

Where B = Magnetic field

Equation (28) is the second Maxwell's Equation and is known Gauss Law for Magnetism [49-50].

According to this law, magnetic monopoles does not exist in the universe [49-50]. The equation interprets divergence of magnetic field is zero through any region [49-50].

3) **Faraday's Law of induction** [49-50]

$$\nabla \times E = -\frac{\partial B}{\partial t} \tag{29}$$

Where E = Electric field

Equation (29) is the third Maxwell's equation and is known as Faraday's Law [49-50]. According to this law, change in magnetic flux within a closed loop of wire produces voltage across the wire [49-50].

4) Ampere's Law [49-50]

$$\nabla \times H = \frac{\partial D}{\partial t} + J \tag{30}$$

Where H = Magnetic field strength and J = Current density

Equation (30) is the fourth Maxwell's equation and is known as Ampere's law [49-50]. According to this law, electric current flowing through the wire produces magnetic field that circles the wire [49-50].

5.2 ANSYS RMxprt

Rotating Machine expert (RMxprt) is a template- based design tool of ANSYS which is used to compute rotational machine performance [47]. RMxprt automatically set up complete Maxwell 2D/3D project and includes geometry, boundary conditions, mesh and materials [47]. RMxprt utilize analytical and magnetic circuit equations to predict dynamic and transient behavior of the machine [47].

In our work, a conventional SRM is first designed in RMxprt by entering all the design parameters. Suitable design parameters are determined after investigating literature review of SRM. 2-Dimensional Computer Aided Design (2D CAD) is then extracted from RMxprt. In the process switching circuit is also obtained for conventional SRM. The 2D design of conventional SRM is then modified to obtain DSSRM. Novel boundary conditions and mesh operations is defined for DSSRM. Winding configuration and excitation parameters are same for both stators of DSSRM and is identical to conventional SRM before modification [5]. Switching circuit to drive DSSRM

is not changed in the process. Same switching circuit is used to excite both stators of DSSRM [5]. Transient analysis is performed to study motional torque, current behavior, flux behavior and torque ripple of DSSRM. Magnetostatics analysis is also performed to study normal and tangential force characteristics in DSSRM.

2-D design of DSSRM is modified to obtain 2 conventional SRM design viz. Outer Stator SRM and Inner Stator SRM. A good comparison between DSSRM, Inner stator SRM and Outer Stator SRM then follows. At last design of rotor is also modified to see if it affects performance on three different designs of SRM.

5.3 Design Process

Design Process for conventional SRM in RMxprt is described below. Steps are summarized in the following flowchart [47]:

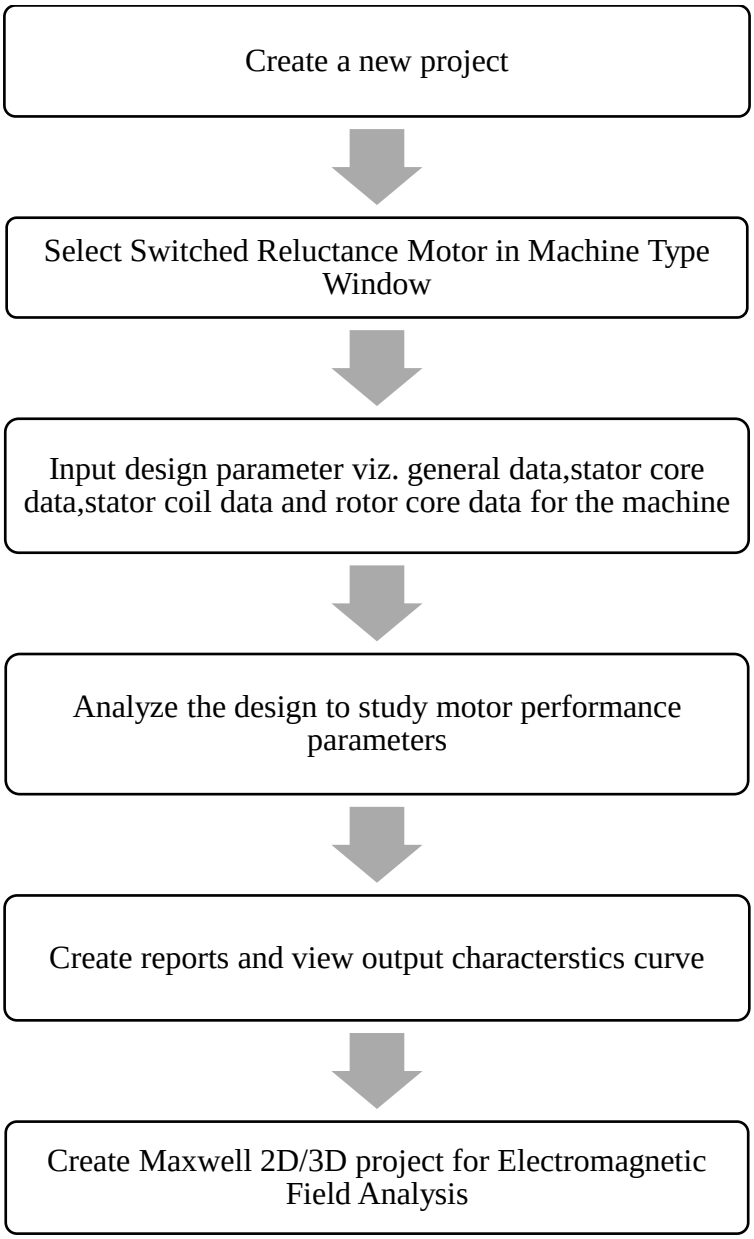

Figure 13: Flowchart diagram of Design process [47]

5.3.1 Machine Type Window

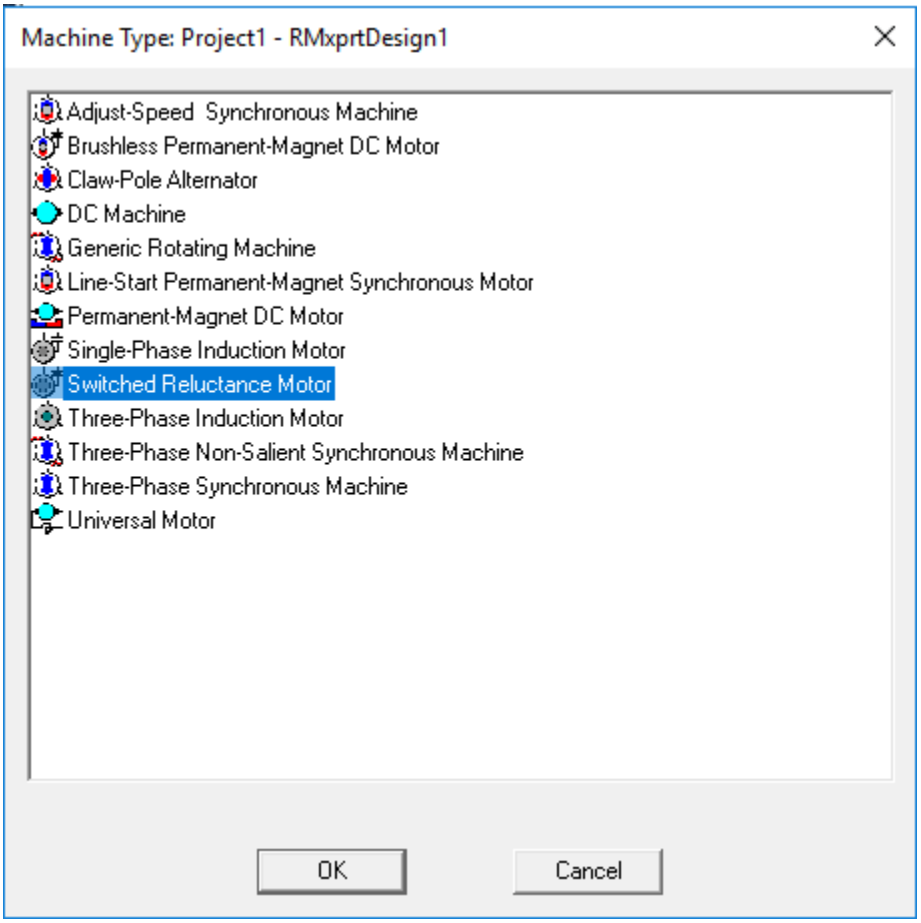

Figure 14: Machine Type Window

13 types of rotating machines that can be designed and simulated using RMxprt is listed in Machine Type window. To design conventional SRM, Switched Reluctance Motor is selected. All necessary dimensions, electrical and mechanical properties are included in the template. In the design of SRM, RMxprt assumes SRM operates with shaft position feedback to synchronize the commutation of phase currents with rotor position [47].

5.3.2 Project Screen

After selecting Switched Reluctance Motor from Machine Type window, we can see Project screen as shown in Figure 15 where we design the machine.

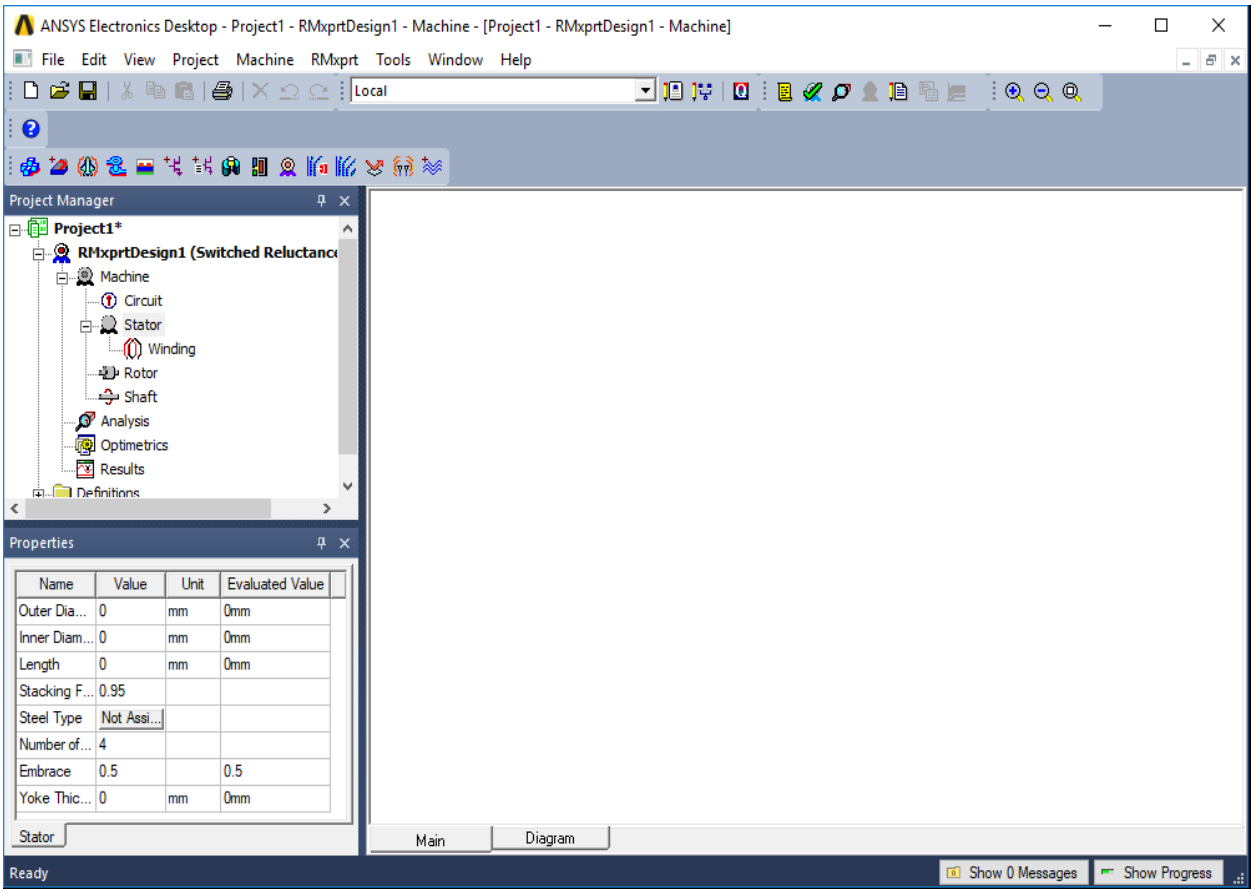

Figure 15: Project Screen

5.3.3 Project Manager Window

All the design parameters are entered using Project Manager window as shown in Figure 16 by selecting each the design parameter of the machine.

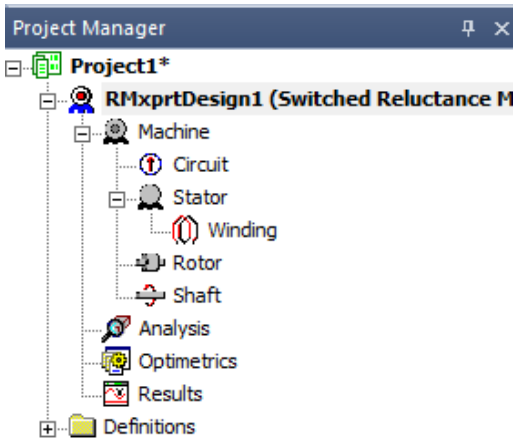

Figure 16: Project Manager

5.3.4 Machine Properties Window

Machine parameters like reference speed, loss, type of SRM control and type of drive circuit is entered in machine properties window which is shown in Figure 17.

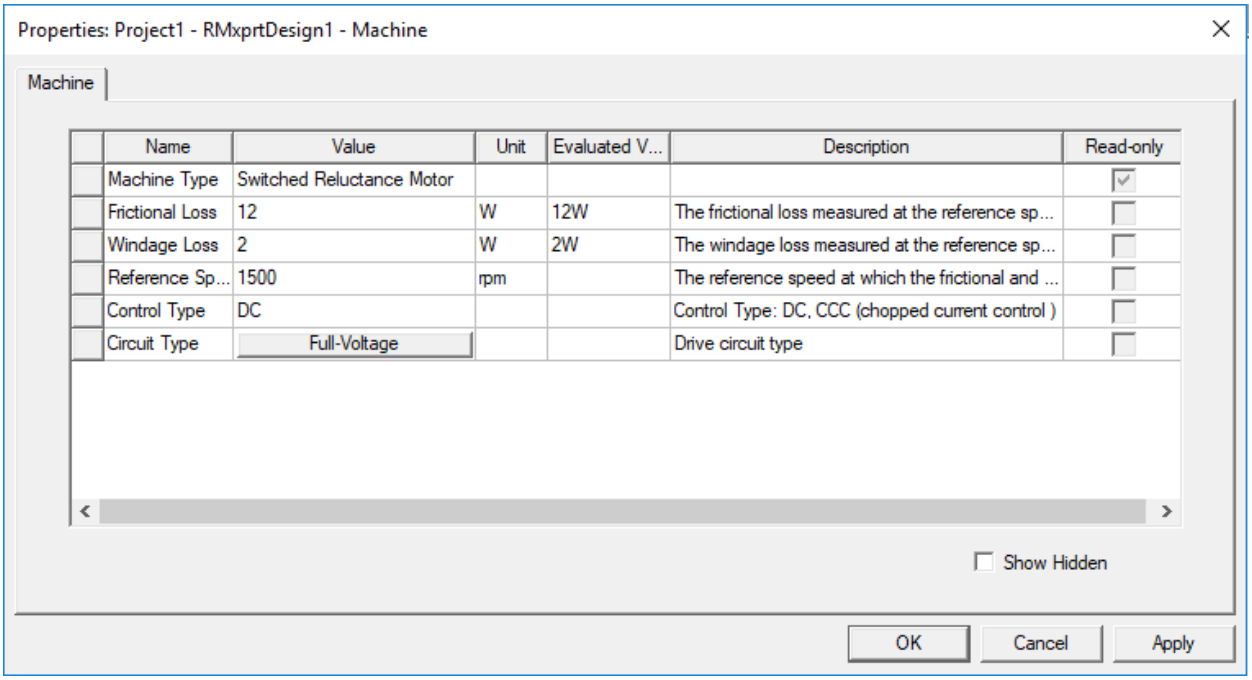

Figure 17: Machine Properties Window

Reference speed is the given speed at which losses are measured [47]. Two types of control are supported in RMxprt viz. DC and CCC (Chopped Current Control). In DC control strategy each phase is activated at turn on angle and deactivated at turn off angle [47]. In CCC, minimum and maximum current should be entered so that current fall between these specified values [47]. Semiconductor switches are turned on or off depending whether current is less than or greater than the specified current [47]. In RMxprt template for SRM, three types of circuit are supported which are full-voltage, half-voltage and coupled-coil which are shown in the following figure. All these circuits are based on industry standard [47]. For our design, choice of circuit type does not affect performance. Full Voltage (if none is selected by default full voltage circuit is selected) circuit is used in our design.

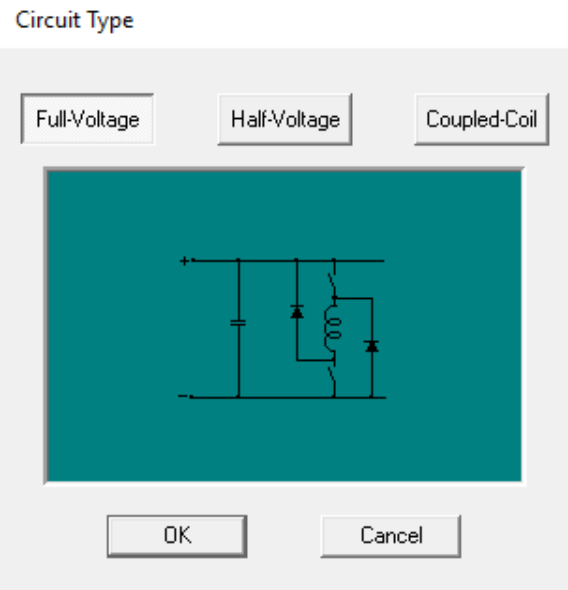

Figure 18 : Full-Voltage Circuit Type

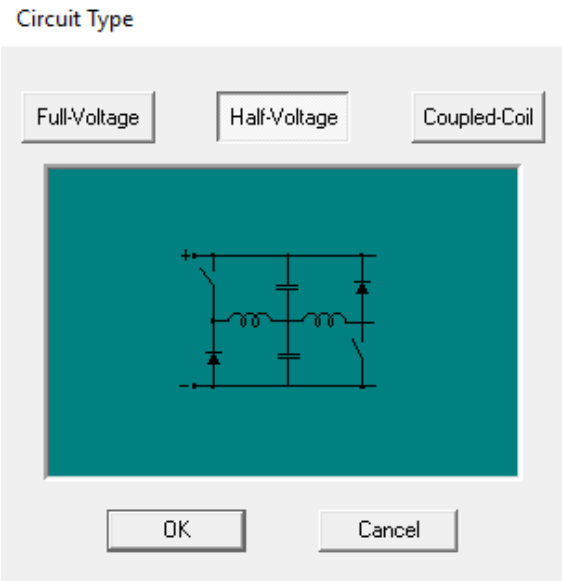

Figure 19: Half-Voltage Circuit Type

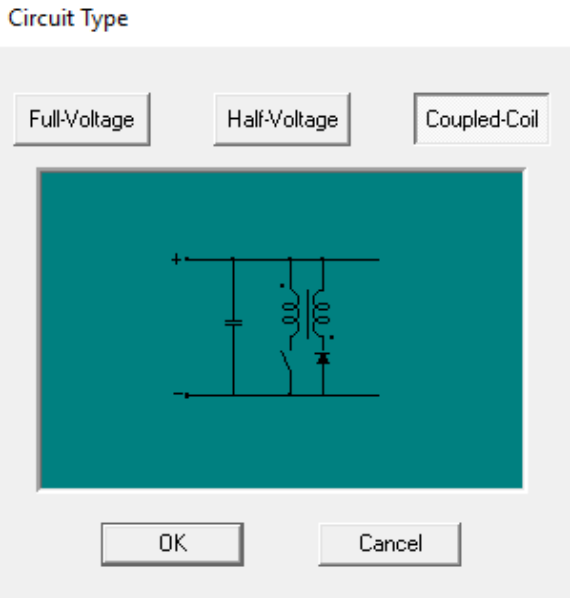

Figure 20: Coupled-Coil Circuit Type

5.3.5 Circuit Properties Window

Circuit data such as Lead angle of trigger, Trigger Pulse Width, Transistor drop and Diode drop are inserted in circuit properties window as shown in Figure 21.

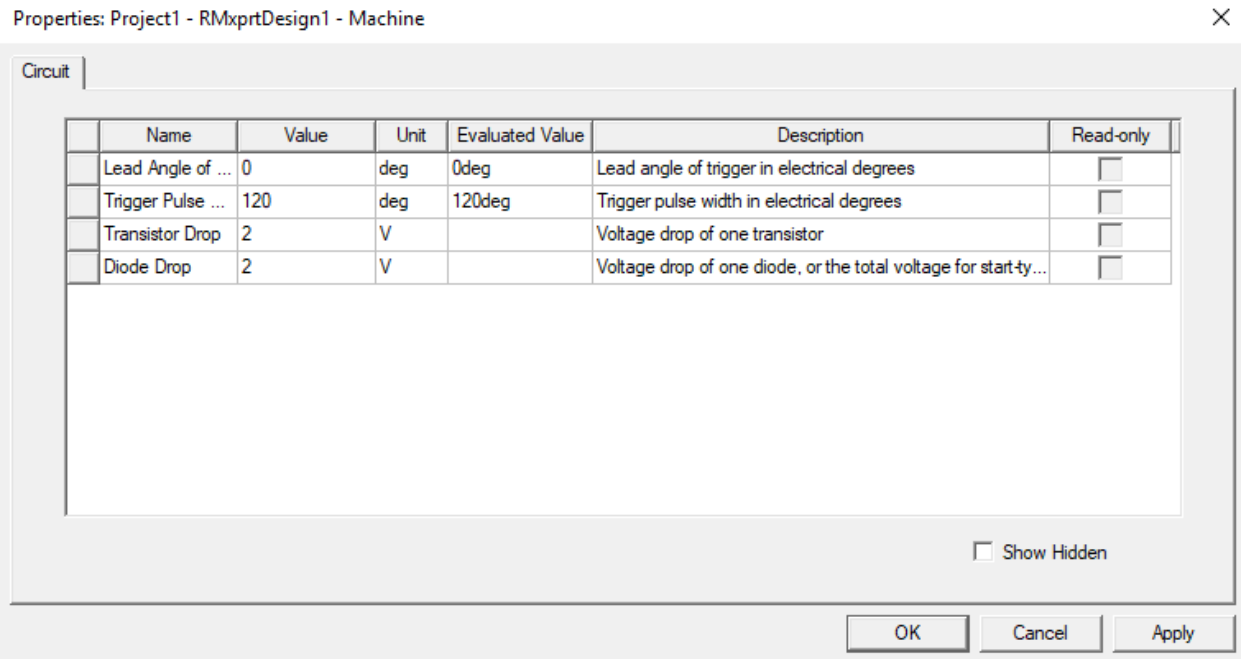

Figure 21: Circuit Properties Window

Lead angle is entered 0 so that each phase is triggered when its axis is aligned with the center of rotor slot [47]. Trigger Pulse Width is the period in electrical degree from turn ON to turn OFF of the transistor [47] and is entered 120 deg. Voltage drop on all transistors over one conduction path and anti-parallel diodes over one discharge path is entered [47].

5.3.6 Stator Properties window

Design parameters of stator such as number of poles, outer and inner diameters, core length, material and yoke thickness are entered in Stator window as shown in Figure 22.

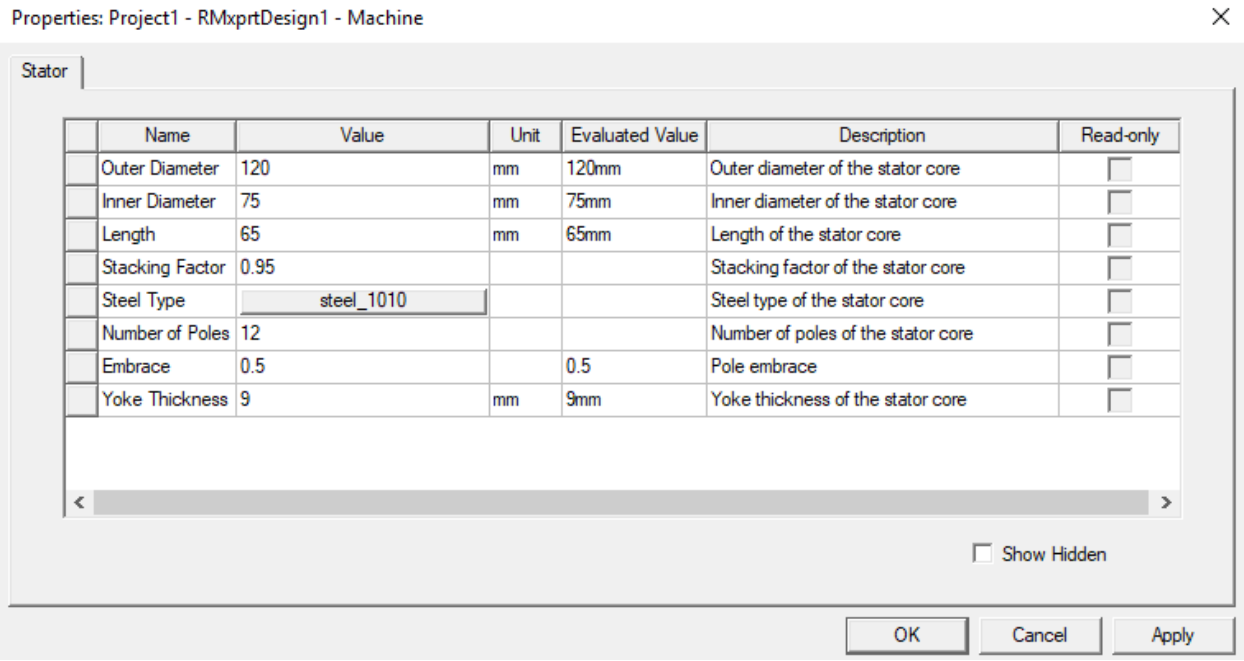

Figure 22: Stator Properties Window

Embrace is the ratio of actual pole arc to the maximum pole angle and value lies between 0 and 1 [47]. Yoke thickness is the thickness of stator core and stator length is effective magnetic length of the core [47]. Stator core is made up of Steel_1010 and has the properties as shown in Figure 23 [47].

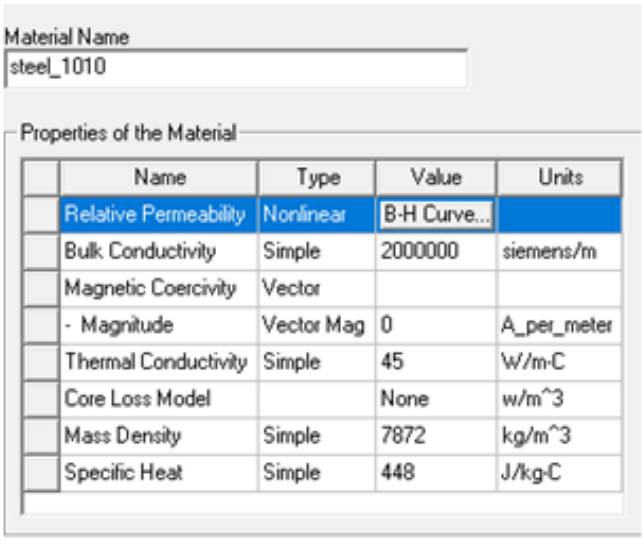

Figure 23: Steel_1010 Properties [47]

5.3.7 Stator Winding Properties Window

Excitation for the phase is provided by stator coils [47]. Coil parameters such as number of turns, size of wire and insulation thickness are entered in Winding window as shown in Figure 24. Value of some coil parameters like size of wire, wire wrap thickness and number of coil is provided by RMxprt itself if 0 is entered as the value [47].

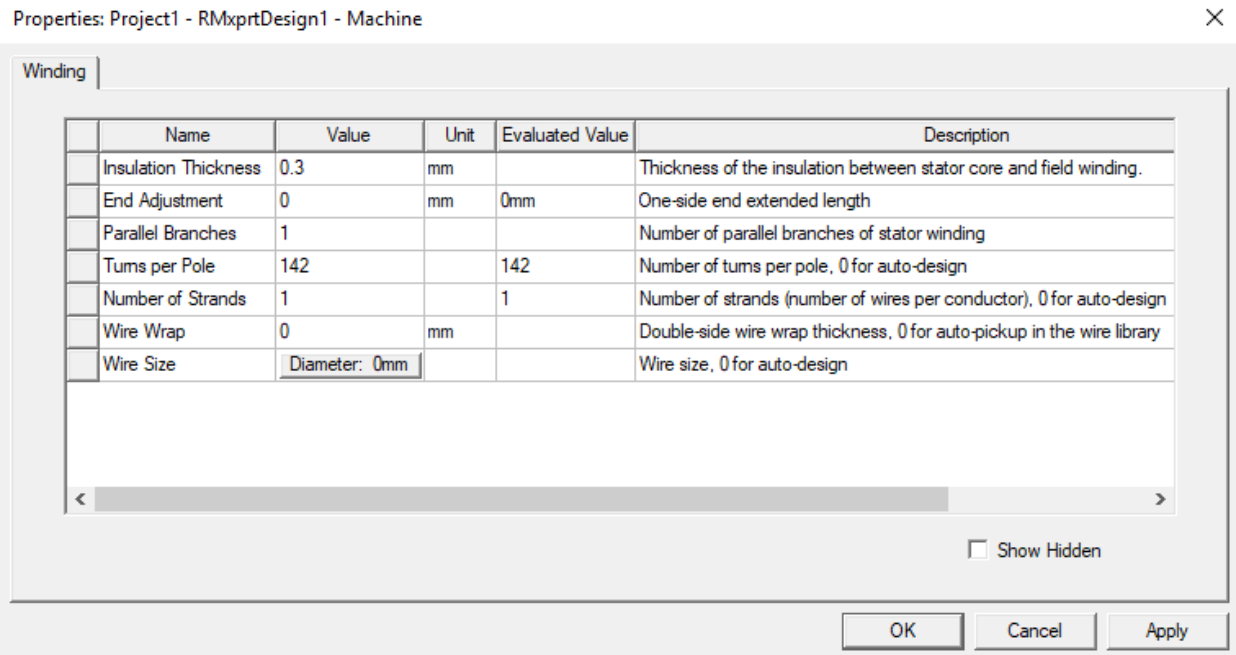

Figure 24: Stator Winding Properties Window

5.3.8 Rotor Properties Window

Rotor properties window appears as shown in following Figure 25.

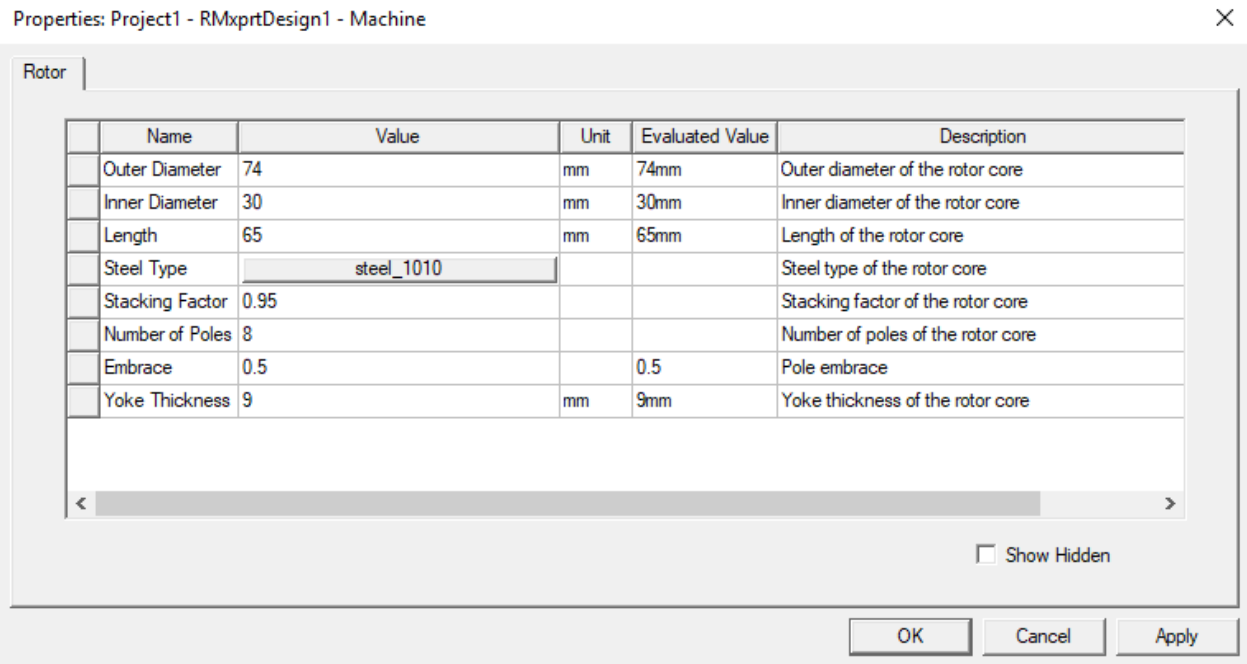

Figure 25: Rotor Properties Window

General rotor design parameters like number of poles, outer and inner diameter, length and materials are entered in this section. RMxprt can only design SRM which have number of rotor poles lesser than stator poles [47].

5.3.9 Shaft properties window

In shaft properties window as shown in Figure 26 there is option for whether to design shaft of magnetic material or not. Size of shaft can be changed by changing inner diameter of rotor.

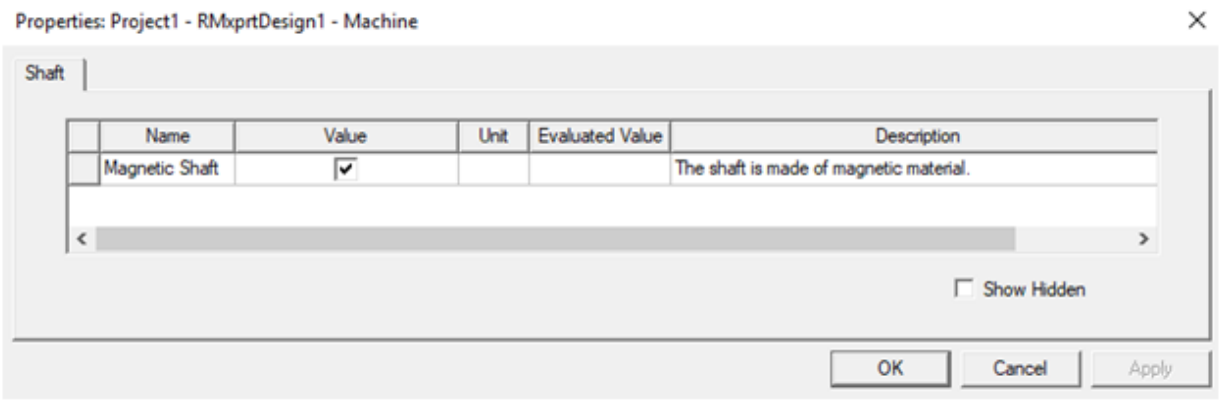

Figure 26: Shaft Properties Window

Designed SRM motor structure with 12 stator poles and 8 rotor poles is shown in Figure 27 below:

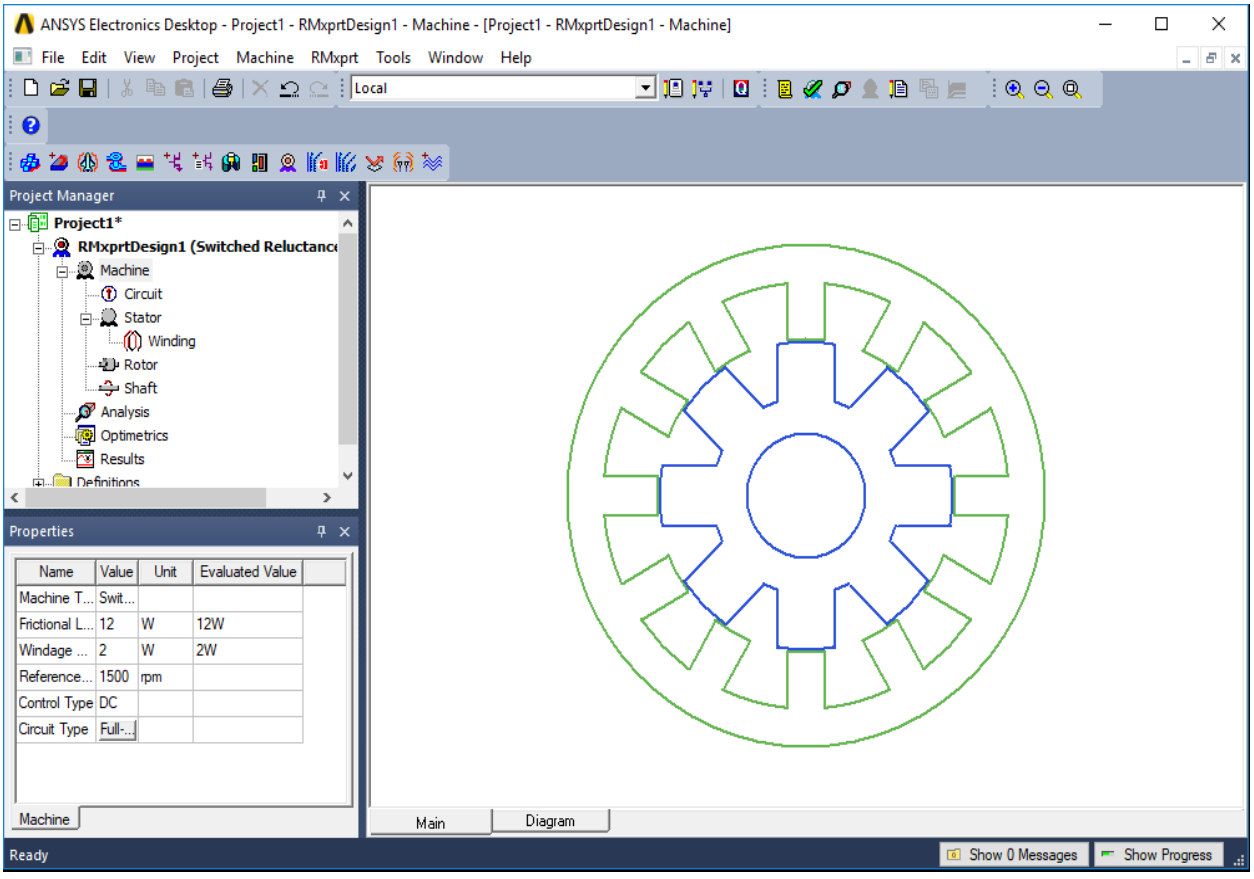

Figure 27: Designed SRM in RMxprt

5.3.10 Solution setup window

To analyze motor performance parameters solution setup is required. Type of load, rated output power, rated voltage, rated speed and operating temperature are defined in Solution data window as shown in Figure 28.

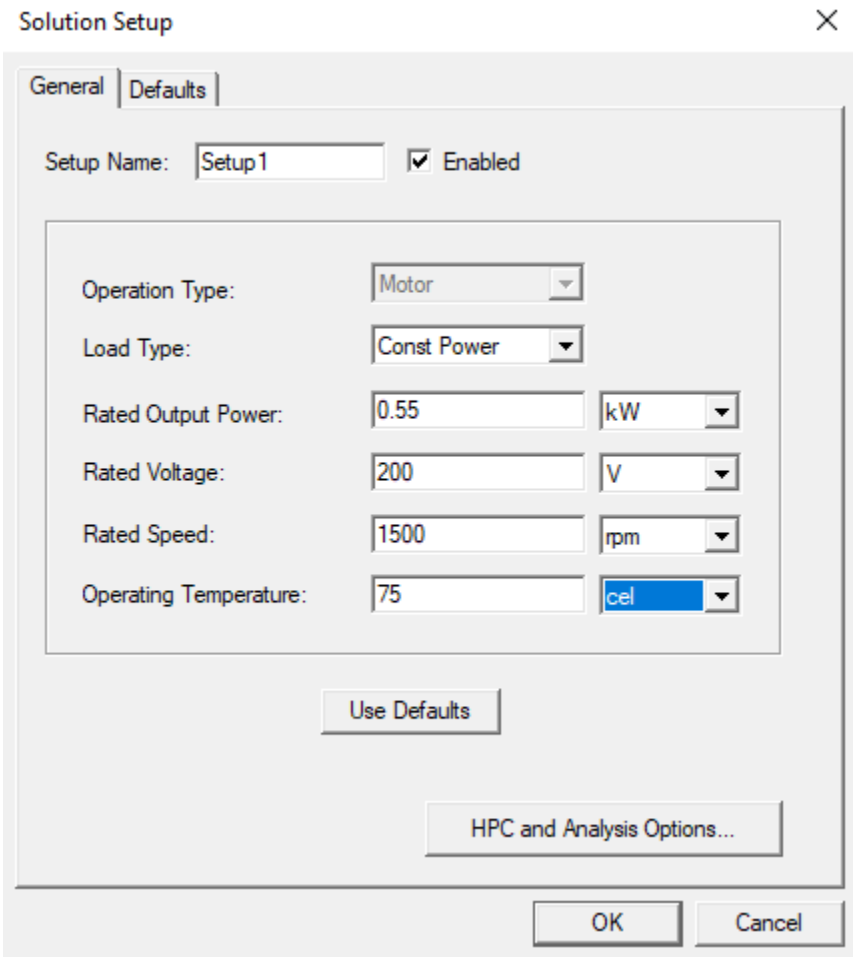

Figure 28: Solution Setup Window

Five different types of load are supported viz. Constant Speed, Constant Power, Constant Torque, Linear Torque and Fan type load [47]. Constant power load is used in our design where output power remains constant in the motor. Rated output power is the output power developed at the shaft [47]. Rated voltage is RMS line to line voltage and rated speed is the required output speed of the motor [47].

Simulation is then performed to investigate performance parameters of our designed SRM.

5.3.11 Design Output Window

RMxprt computes motor performance parameters at the rated output power [47] and all the computed output data is shown in Design output window. All the data entered are also available in this section. In the following figures start operation data and material consumption data calculated by RMxprt are shown.

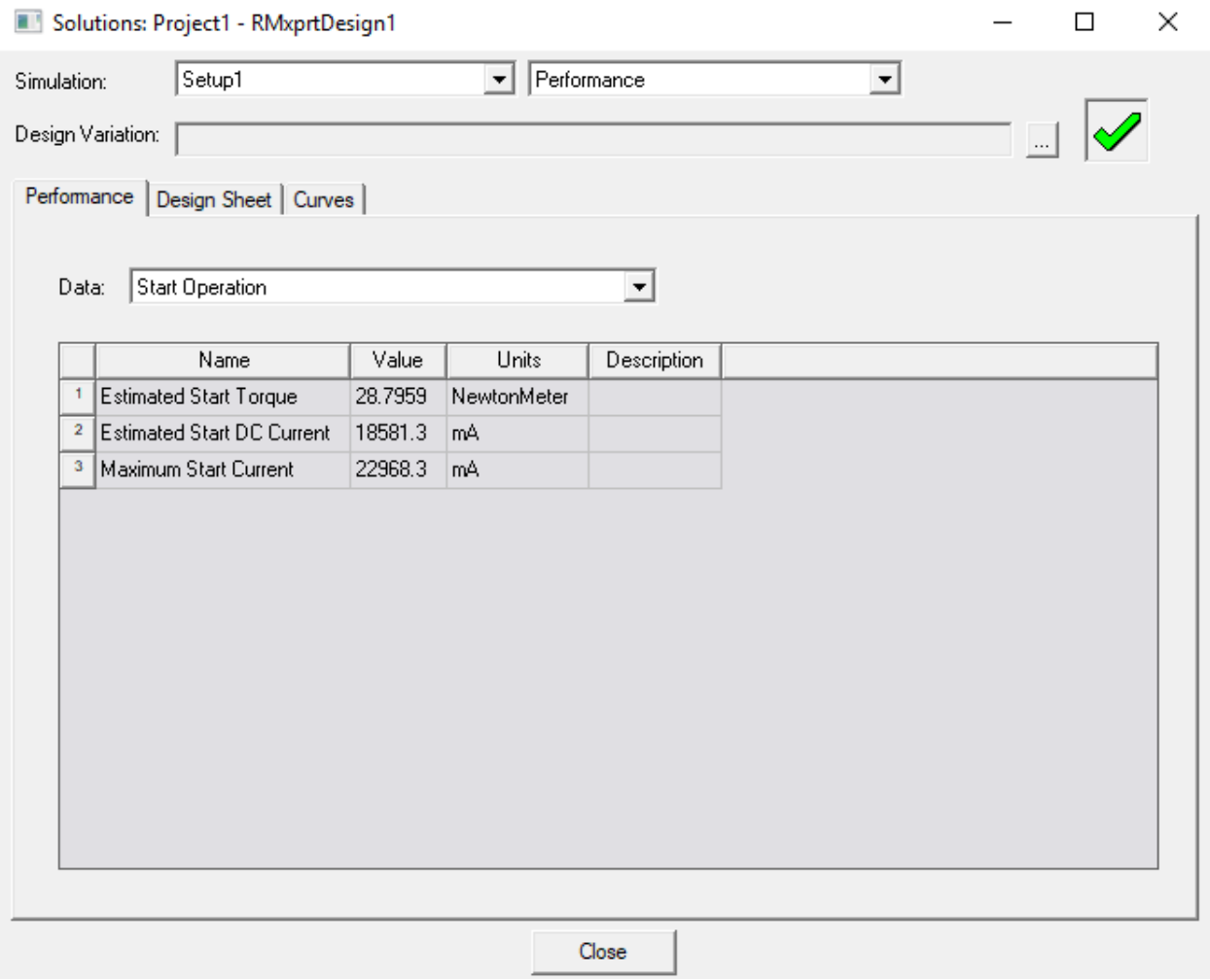

Figure 29: Solution showing Start Operation Data

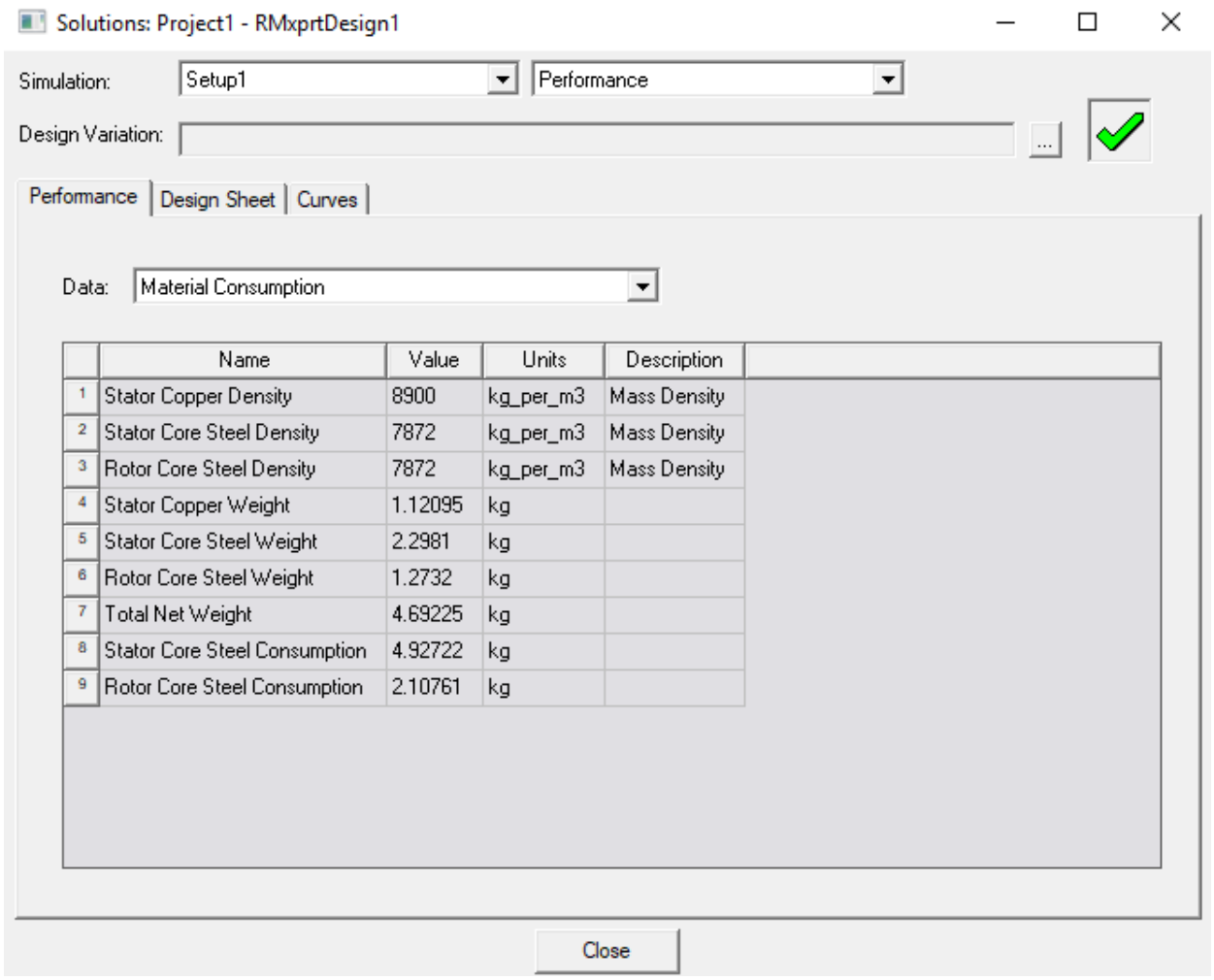

	Name	Value	Units	Description
1	Stator Copper Density	8900	kg_per_m3	Mass Density
2	Stator Core Steel Density	7872	kg_per_m3	Mass Density
3	Rotor Core Steel Density	7872	kg_per_m3	Mass Density
4	Stator Copper Weight	1.12095	kg	
5	Stator Core Steel Weight	2.2981	kg	
6	Rotor Core Steel Weight	1.2732	kg	
7	Total Net Weight	4.69225	kg	
8	Stator Core Steel Consumption	4.92722	kg	
9	Rotor Core Steel Consumption	2.10761	kg	

Figure 30: Solution showing Material Consumption Data

Performance curves for the designed SRM can also be plotted. Flux linkage vs Current at Various positions and output torque vs speed are shown in figure below.

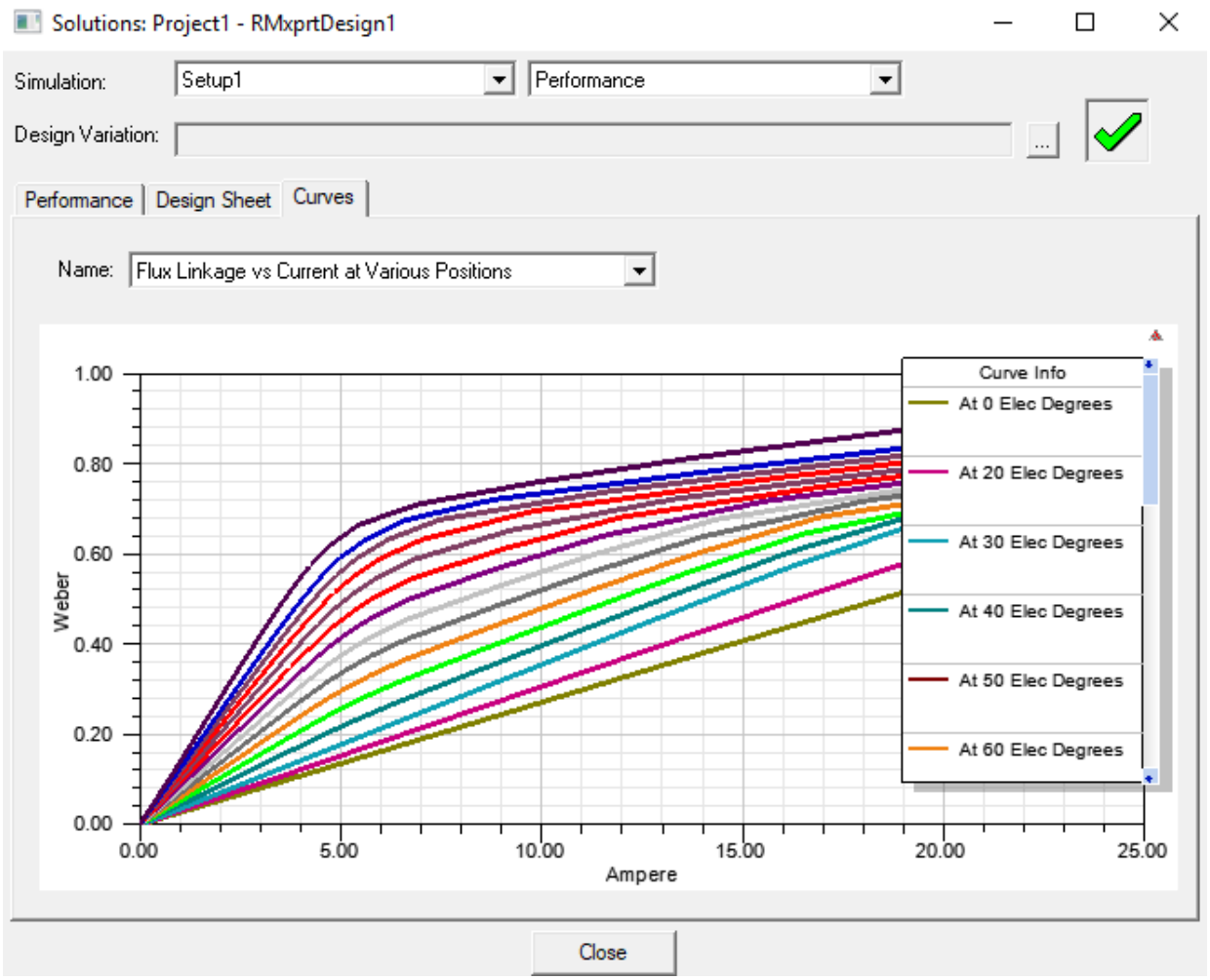

Figure 31: Solution Showing Flux Linkage Vs Current at Various Positions

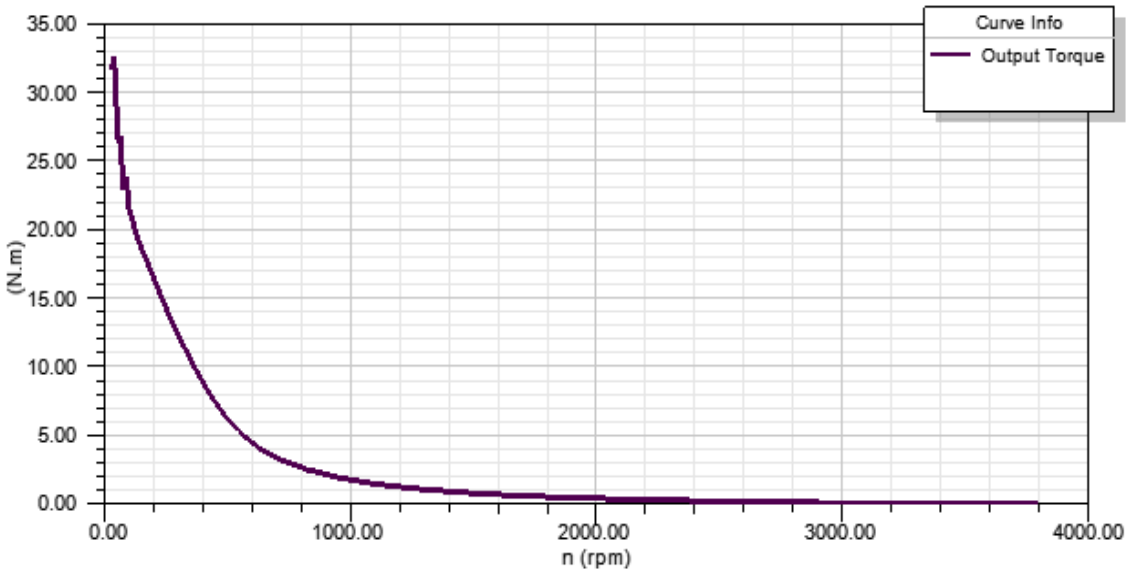

Figure 32: Torque vs Speed Characteristics

5.4 2-D Design of Conventional SRM in Maxwell

Once motor performance characteristics are analyzed, Maxwell 2D design of SRM is created from RMxprt model. Operations like meshing, current excitation, defining boundary conditions and modelling of switching circuit are done in Maxwell 2D model to perform Magnetostatics and Transient analysis [48].

Switching circuit is modelled automatically in the process of extraction of 2D design from RMxprt [48]. This switching circuit is used for phase excitation. However, circuit editor tool Simplorer can also be used to design switching circuit and integrate within the machine. In our design, automatically generated model of switching circuit as shown in Figure 33 is used [47].

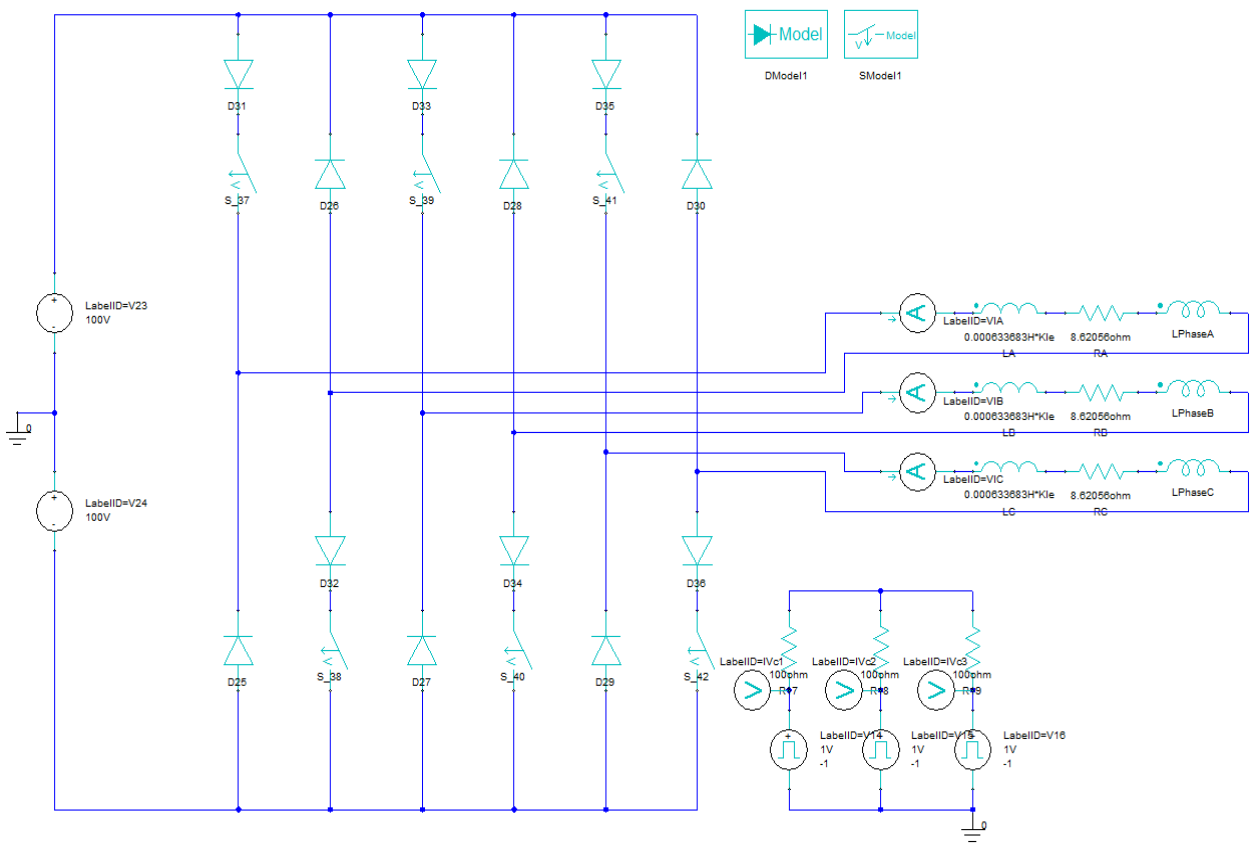

Figure 33: Switching Circuit for SRM [47]

Working principle of the circuit is explained in Switching of phases in Chapter 3.

Stator phases are excited according to rotor position [7]. LPhaseA, LPhaseB and LPhaseC represent three phases of stator which are connected in series with circuit end turn inductance and resistance [47]. Diode in series with voltage-controlled switches represents transistor model while antiparallel diodes are used to provide return path for the current during the motor operation [47]. Sub circuit as shown in bottom right side of the switching circuit includes voltage pulse sources used to controls switches [47]. In DSSRM, both stators are excited by same switching circuit [32]. Phases are turned on and off depending on the rotor position [32].

Extracted 2D model of SRM is shown in the Figure 34 below:

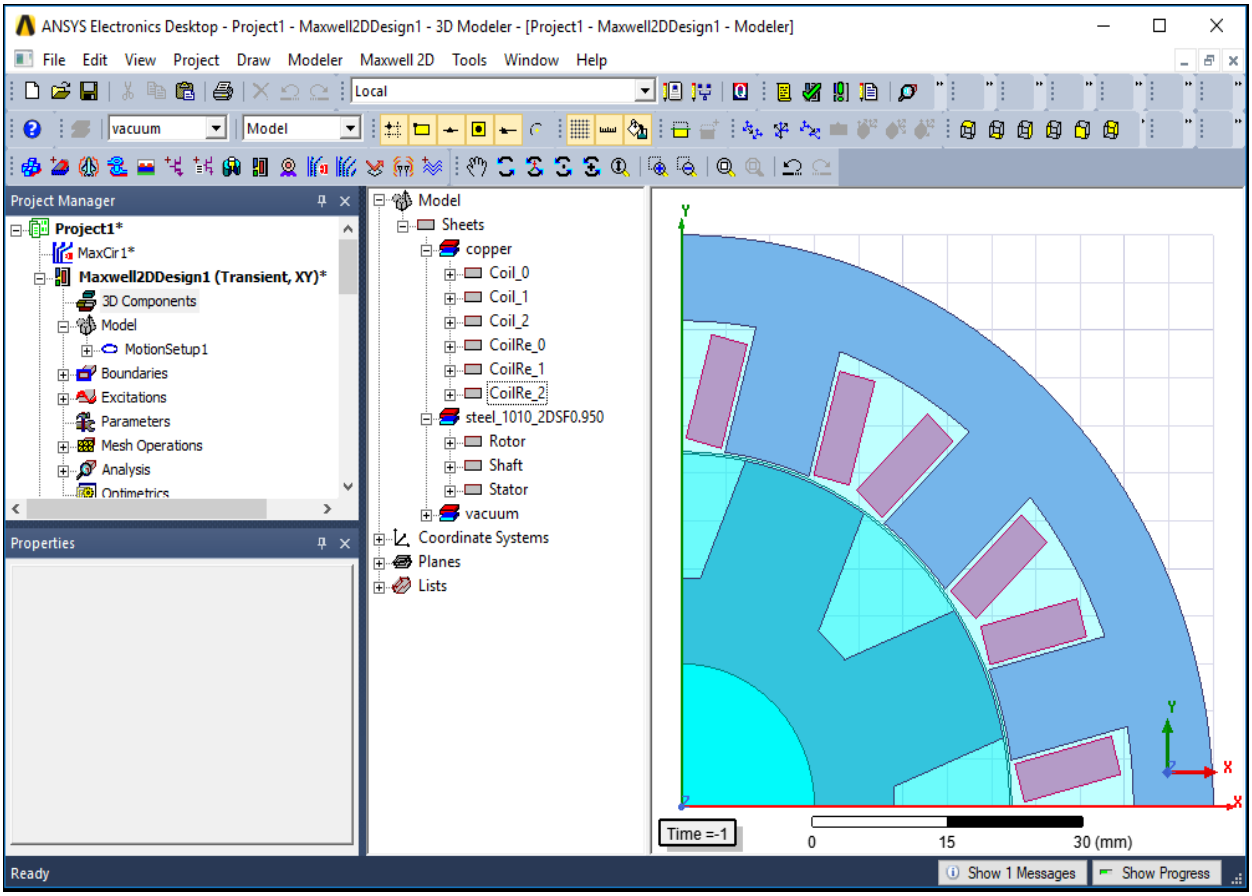

Figure 34: Cross section of extracted 2D model of SRM

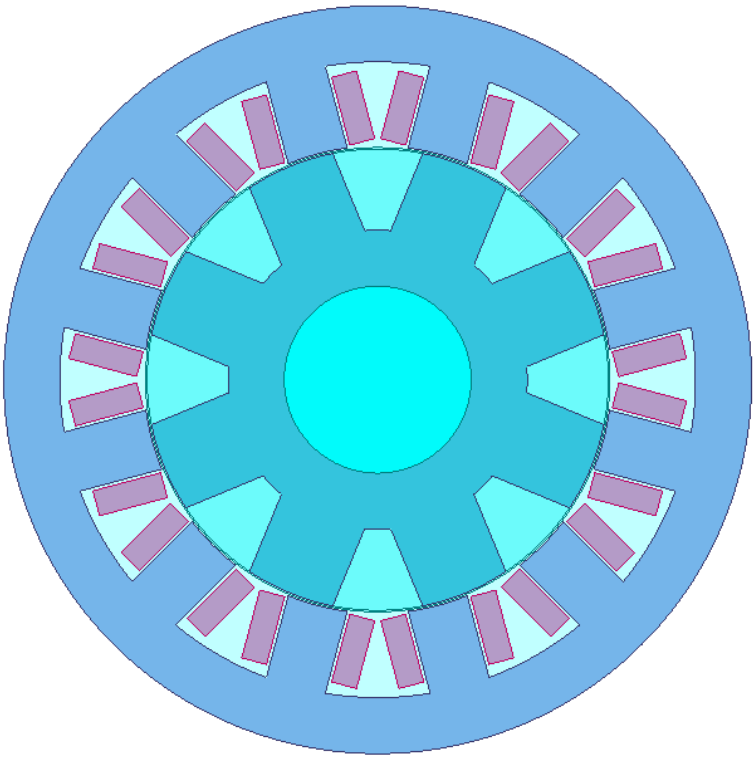

Figure 35: Front view of SRM motor [45]

Chapter 6

2D Design, Simulation and Results

6.1 2D Design of Inner Stator SRM

Inner stator configuration of conventional SRM is designed in Maxwell 2D tool and is shown in figure below.

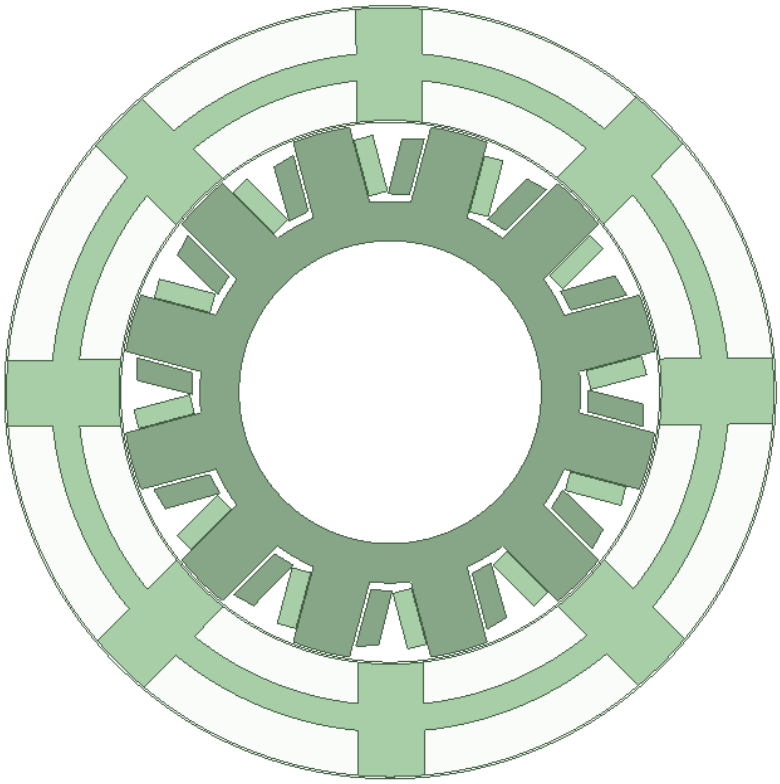

Figure 36: Inner Stator SRM [32]

6.1.1 Magnetostatics Analysis of Inner Stator SRM

Magnetostatics analysis is used to calculate static (DC) magnetic fields [48]. During magnetostatic analysis all objects are stationary [48]. As our motor does not consist permanent magnet so source of static magnetic field is chosen as DC current [48]. Solved magnetic field is used to calculate current density and magnetic flux density [48]. Current density and magnetic flux density is then used to calculate torque, force and inductance [48].

In our research Force in X direction and Y direction is calculated in 60-degree interval from 0 degree to 360-degree. Keeping 150 number of turns, force in X, Y and motional direction is calculated. With 150 number of turns, force in X, Y and motional direction is calculated. Parametric analysis is also performed to study variation of inductance with number of turns. Inductance is calculated by varying number of turns represented by $h. Four values of $h are 1, 51, 101 and 151.

Force in direction of motion and its component in X and Y direction is calculated using magnetostatics analysis. Force is calculated from 0 to 360 degree at each 60 degree interval. Number of turns is kept constant at 150. Then inductance is calculated at 30-degree interval by varying number of turns.

angle (deg)	Force_X (uN)	Force_Y (uN)	Force Mag (uN)
0	262.3510958	100.7387468	281.0273876
60	418.3569277	-94.4973932	428.89658
120	-4.553721136	-1.867528047	4.921792072
180	123.2603446	158.7057766	200.9493371
240	-119.8667038	52.41607908	130.8261137
300	-4.553721136	-1.867528048	4.921792072
360	262.3510975	100.7387474	281.0273894

Table 1: Force in X, Y and Motional direction in Inner Stator SRM

In 0 degree, Force is X-direction is 262.251 uN and Y-direction is 100.7388 uN. Force in direction of motion is 281.02uN or 0.028102 mN.

ang [deg]	Matrix1.L(ICoil0,ICoil0) [uH] - $h='1'	Matrix1.L(ICoil0,ICoil0) [mH] - $h='51'	Matrix1.L(ICoil0,ICoil0) [mH] - $h='101'	Matrix1.L(ICoil0,ICoil0) [mH] - $h='150'
0	22.0086943	57.23999434	224.4894362	495.2086
30	22.13784782	57.57567374	225.8236746	498.1015759
60	22.14016944	57.60476154	225.9469953	498.3198286
90	21.99986334	57.24089961	224.4926028	495.1975014
120	22.13558894	57.574216	225.8035117	498.0915408
150	22.14946309	57.60485576	225.8518685	498.3109194
180	21.99993204	57.23997466	224.5183073	495.1542799
210	22.1285548	57.57459459	225.8287152	498.0590322
240	22.14946127	57.60474228	225.9232973	498.3113051
270	22.00923395	57.23992768	224.4931656	495.197504
300	22.13786275	57.58051164	225.8051428	498.0915408
330	22.14946422	57.60449885	225.946757	498.3097395
360	22.00682724	57.240924	224.4961323	495.1536129
ang [deg]	**Matrix1.L(ICoil0,ICoil1) [uH] - $h='1'**	**Matrix1.L(ICoil0,ICoil1) [mH] - $h='51'**	**Matrix1.L(ICoil0,ICoil1) [mH] - $h='101'**	**Matrix1.L(ICoil0,ICoil1) [mH] - $h='150'**
0	21.43057376	55.73636879	218.592213	482.2023964
30	21.40583522	55.6716683	218.3562126	481.6312924
60	21.10529037	54.91312331	215.3892261	475.0351348
90	21.4218254	55.73741052	218.5954235	482.1880302
120	21.40357204	55.67040517	218.3367792	481.6208909
150	21.1145471	54.91305016	215.2950671	475.0270018
180	21.42183871	55.73635367	218.6208826	482.1497814
210	21.39655187	55.67072487	218.3611984	481.5889393
240	21.11454657	54.91312141	215.3665376	475.0264417
270	21.43109994	55.73632807	218.5953065	482.1880324
300	21.40583443	55.67658527	218.3378384	481.6208909
330	21.11454826	54.91278019	215.3894482	475.0234827
360	21.42886026	55.73743416	218.599524	482.1493559

Table 2: Variation of Inductance with Number of Turns in Inner Stator SRM

Parametric analysis for Inner Stator SRM shows inductance increases with increase in number of turns. Inductance is minimum i.e. 21 uH when number of turns is equal to 1 and maximum i.e. 482.148 mH when number of turns equal to 150.

6.1.2 Transient Analysis of Inner Stator SRM

Transient simulations of SRM is performed to study motion torque, current behavior and flux linkages. Each of the coil consist of 75 number of conductors or turns. Initial position of rotor is adjusted to 358 degrees so that rotor pole and nearby stator pole overlap after activation of corresponding phases. Simulation time is fixed for 60ms with time step 0.5ms. Plots of moving torque, phase currents and flux linkage vs time are shown in figures below:

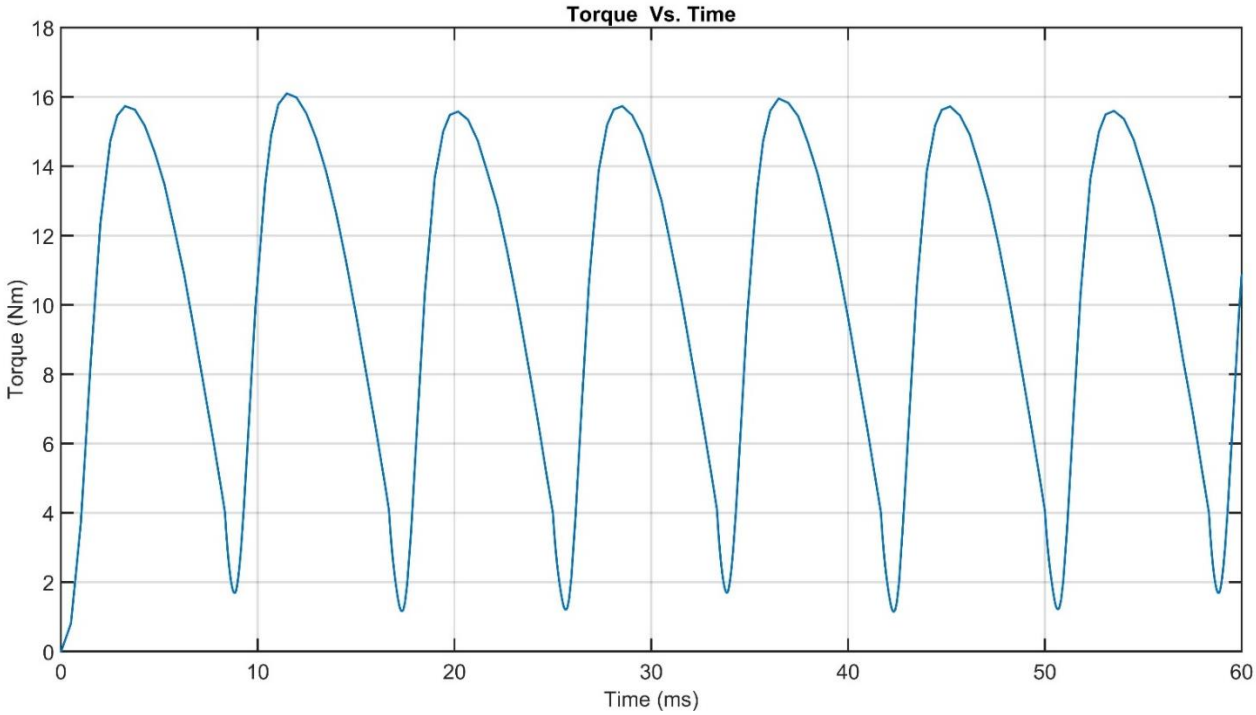

Figure 37: Inner Stator SRM Moving Torque [Nm] vs Time [ms]

Curve Info	Avg	Max
Moving Torque (Transient)	10.1935 Nm	16.0988 Nm

Table 3: Inner Stator SRM Torque Vs Time curve info

Average moving torque and maximum moving torque of motor with inner stator configuration is found to be 10.1935Nm and 16.0988Nm respectively. Torque ripple is calculated using the maximum and minimum values of torque for each pulse using following formula [51]:

$$T_{ripple} = \frac{T_{max} - T_{min}}{T_{max} + T_{min}} \quad (31)$$

Percentage of torque ripple is calculated by computing sum of T_{ripple} of each pulse [51] as follows

$$Sum = \sum_{1}^{NoP} T_{ripple} \tag{32}$$

Where NoP is number of torque pulses considered in calculating Sum.

Percentage of average torque ripple is calculated by [51] using following formula:

$$Avg\ T_{ripple} = \frac{Sum}{NoP} * 100\% \tag{33}$$

In torque ripple calculation of our design we considered 6 number of torque pulses.

Average torque ripple is calculated and found to be 84.30%.

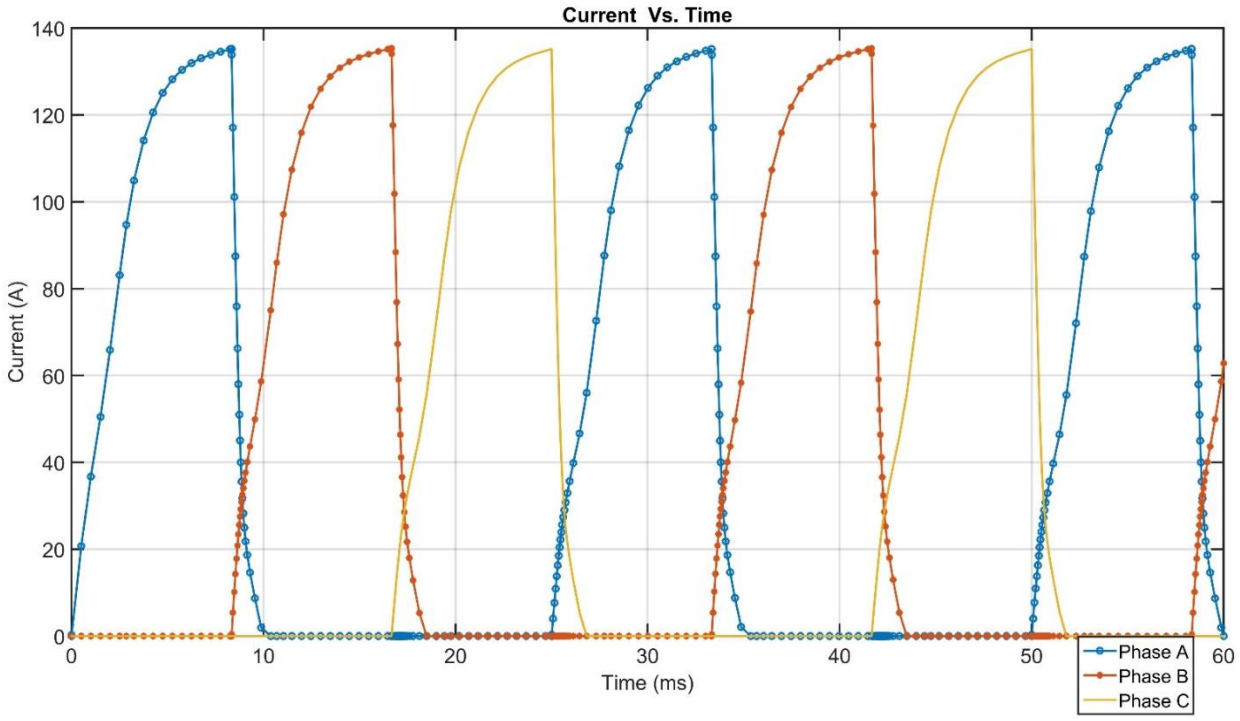

Figure 38: Inner Stator SRM Phase Current [A] vs Time [ms]

Curve Info	Avg	Max
Current(PhaseA) (Transient)	43.8107 A	135.2090 A
Current(PhaseB) (Transient)	31.5602 A	135.3685 A
Current(PhaseC) (Transient)	29.2062 A	135.1883 A

Table 4: Inner Stator SRM Current Vs Time curve info

When Phase A is activated current flows in the coil and continues to increase till it becomes maximum. Maximum current flows when there is perfect alignment between rotor and stator poles. Then current starts decreasing when rotor moves away from stator poles and becomes zero when rotor poles becomes completely misaligned with the stator poles. During this period position of rotor is between two stator poles. Before Phase A current becomes zero, Phase B is activated and current starts rising as seen in Figure 38. Continuous torque is generated during such movement of rotor. On average 43.8107 A, 31.5602 A and 29.2062 A of current flows in Phase A, Phase B and Phase C respectively.

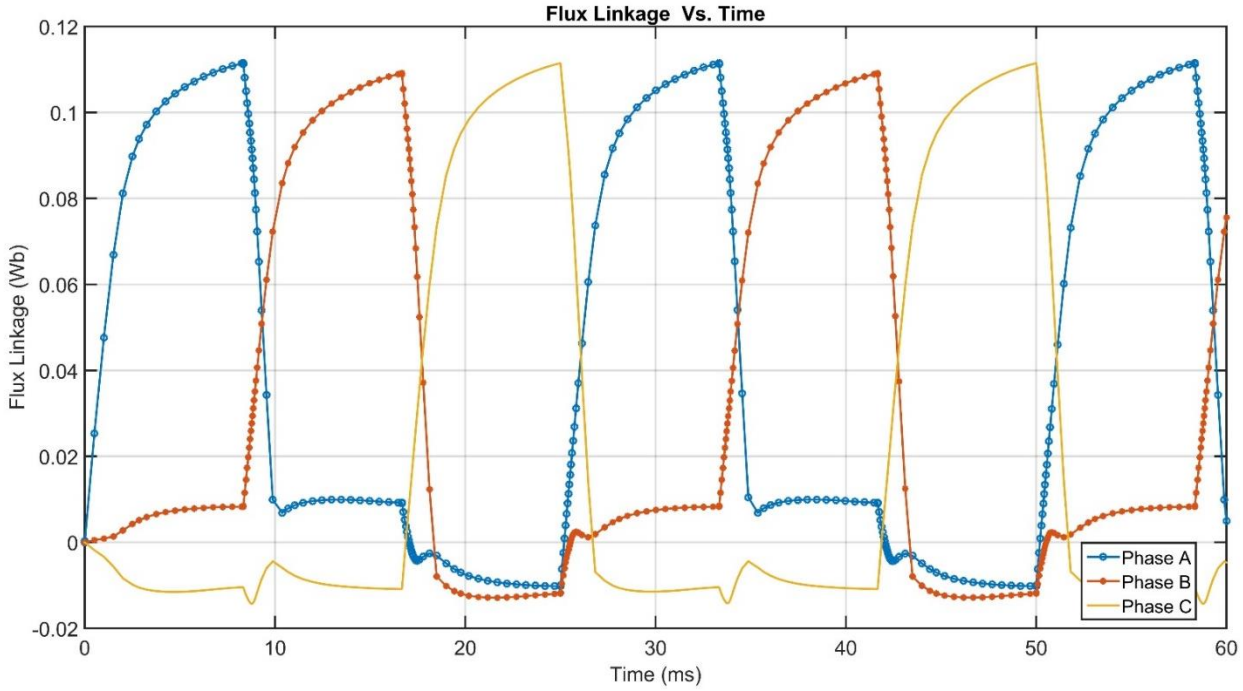

Figure 39: Inner Stator SRM Flux Linkage [Wb] vs Time [ms]

Curve Info	Avg	Max
FluxLinkage(PhaseA) : Transient	0.0419 Wb	0.1115 Wb
FluxLinkage(PhaseB) : Transient	0.0288 Wb	0.1091 Wb
FluxLinkage(PhaseC) : Transient	0.0210 Wb	0.1115 Wb

Table 5: Inner Stator SRM Flux Linkage Vs Time curve info

Flux linkage varies the way current behaves. Average flux linkage for Phase A, Phase B and Phase C is 0.0419 Wb, 0.0288Wb and 0.0210 respectively.

6.2 2D Design of Outer Stator SRM

Outer stator SRM design is shown in figure below.

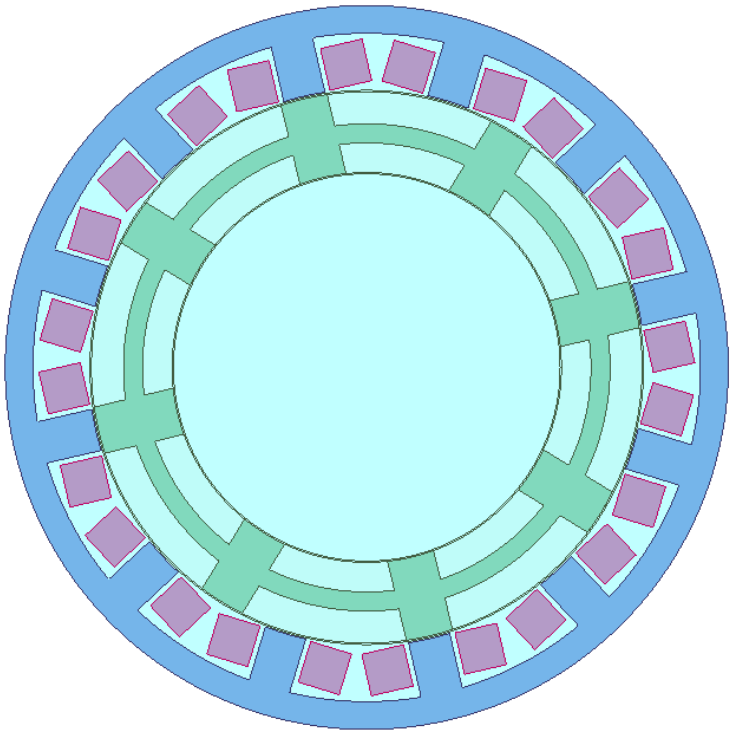

Figure 40: Outer Stator SRM [32]

6.2.1 Magnetostatics Analysis of Outer Stator SRM

angle (deg)	Force_X (mN)	Force_Y (mN)	Force Mag (mN)
0	0.001401	-0.009055	0.009163
60	0.204315	0.024769	0.205811
120	0.093009	-0.055231	0.108172
180	-0.248130	0.012832	0.248462
240	4.171909	-6.094012	7.385243
300	-1.898514	5.350525	5.677366
360	1.121244	-2.297255	2.556280

Table 6: Force in X, Y and Motional direction in Outer Stator SRM

Motional force, and other two components of force in Outer Stator SRM can be observed. For example , At 60 degree rotor angle, force in the direction of motion is 0.2058 mN.

ang [deg]	Matrix1.L(Coil_0, Coil_0) [uH] - $h='1'	Matrix1.L(Coil_0, Coil_0) [mH] - $h='51'	Matrix1.L(Coil_0, Coil_0) [mH] - $h='101'	Matrix1.L(Coil_0, Coil_0) [mH] - $h='150'
0	19.68841745	51.22311972	200.8946843	442.9893926
30	19.88799425	51.72847358	202.8766494	447.4397001
60	19.93772347	51.86016515	203.3855137	448.6235997
90	19.69368299	51.22325275	200.841451	443.1076305
120	19.88267055	51.71502027	202.8238838	447.361767
150	19.93373334	51.8569273	203.3437921	448.6277254
180	19.68841627	51.22312198	200.8415464	443.1077255
210	19.8827452	51.72867985	202.8592169	447.3599428
240	19.93373334	51.86088812	203.3859604	448.5090001
270	19.6936805	51.21908019	200.8831686	443.1078789
300	19.88801771	51.7162574	202.877456	447.3615465
330	19.93882843	51.84742761	203.3977007	448.5073319
360	19.69323632	51.21085402	200.8946729	443.1077227
ang [deg]	**Matrix1.L(Coil_0, Coil_1) [uH] - $h='1'**	**Matrix1.L(Coil_0, Coil_1) [mH] - $h='51'**	**Matrix1.L(Coil_0, Coil_1) [mH] - $h='101'**	**Matrix1.L(Coil_0, Coil_1) [mH] - $h='150'**
0	19.33793731	50.31159291	197.3197217	435.1035894
30	19.26775892	50.11529512	196.5498392	433.4833275
60	19.07410006	49.61354051	194.5739029	429.1884642
90	19.34321087	50.31174235	197.2663879	435.2223754
120	19.26246222	50.10166839	196.4963934	433.4054359
150	19.06992175	49.61001551	194.5324986	429.192088
180	19.33795737	50.31159587	197.2662985	435.2224703
210	19.26246382	50.11544776	196.5317077	433.4051465
240	19.06992175	49.61418647	194.5743487	429.0732393
270	19.34322044	50.30755658	197.308271	435.2221414
300	19.2677294	50.1030091	196.5504354	433.4060109
330	19.07504953	49.60099647	194.5865502	429.0741571
360	19.34280338	50.29930236	197.3197075	435.2226847

Table 7: Variation of Inductance with Number of Turns in Outer Stator SRM

From above data, it can be observed inductance in the coil increases with increase in number of turns. For number of turns = 1 inductance in coil is equal to 19uH (in avg) which increases to 49uH for number of turns equal to 51. For 150 number of turns inductance is maximum and is equal to 432uH (in avg).

6.2.2 Transient Analysis of Outer Stator SRM

Same simulation parameter and setup is used for Outer Stator SRM transient simulation

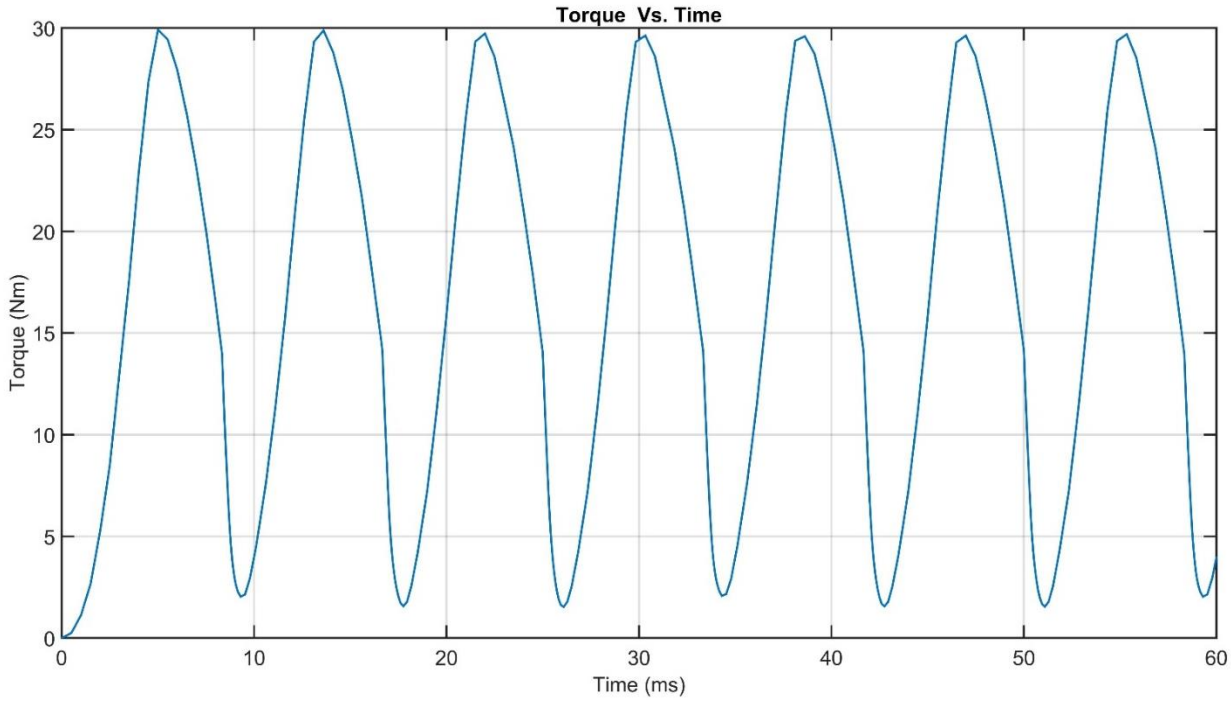

Figure 41: Outer Stator SRM Moving Torque [Nm] Vs Time [ms]

Curve Info	Avg	Max
Moving Torque (Transient)	16.5898 Nm	29.9095 Nm

Table 8: Outer Stator SRM Torque Vs Time curve info

Average moving torque and maximum moving torque of motor with outer stator configuration is found to be 16.5898Nm and 29.9095Nm respectively. Average torque ripple is calculated and found to be 89.09%.

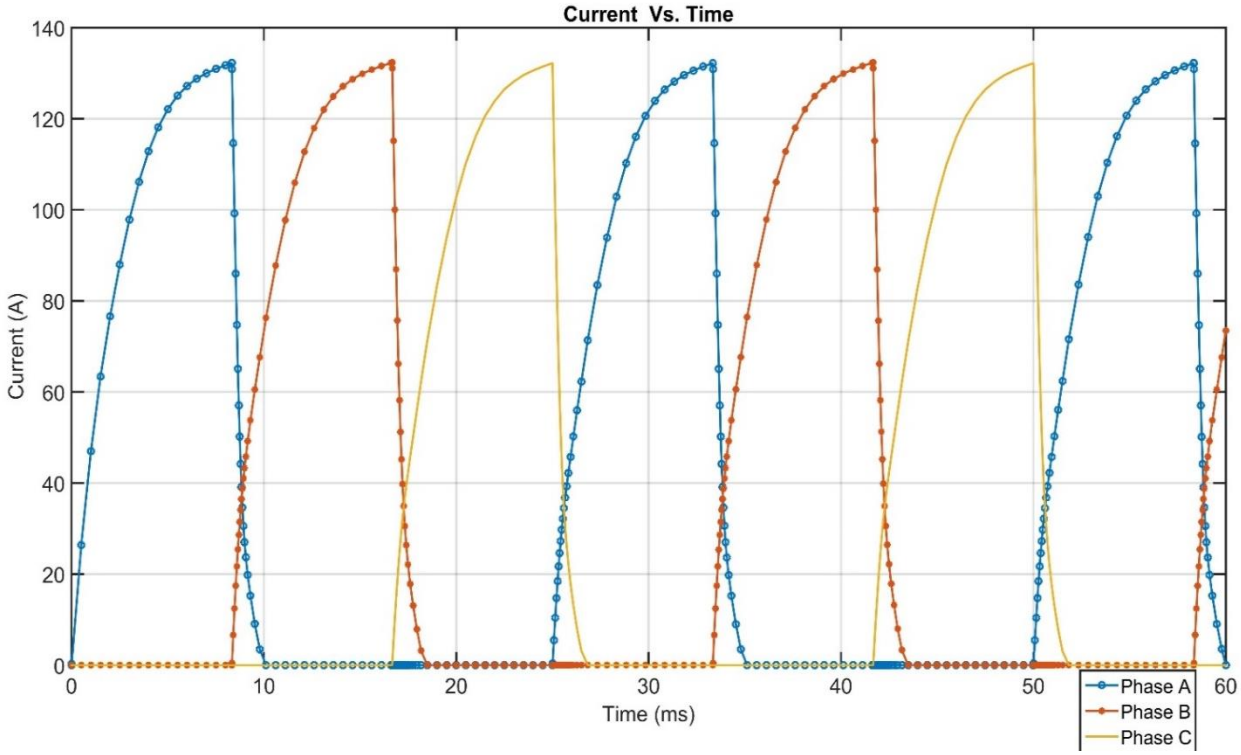

Figure 42: Outer Stator SRM Phase Current [A] vs Time [ms]

Curve Info	Avg	Max
Current(PhaseA) (Transient)	44.1753 A	132.2539 A
Current(PhaseB) (Transient)	31.6613 A	132.3648 A
Current(PhaseC) (Transient)	29.5624 A	132.2126 A

Table 9: Outer Stator SRM Current Vs Time curve info

On average 44.1753 A, 31.6613 A and 29.5624 A of current flows in Phase A, Phase B and Phase C respectively in Outer Stator configuration of conventional SRM.

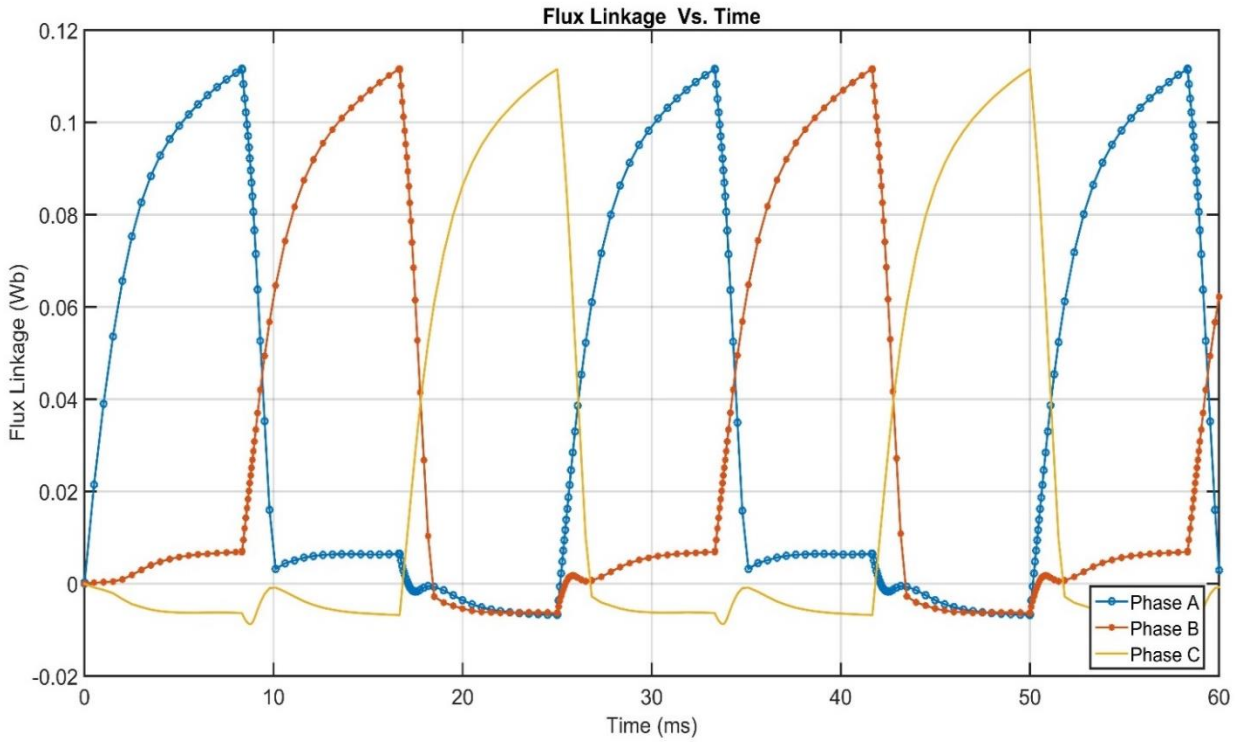

Figure 43: Outer Stator SRM Flux Linkage [Wb] vs Time [ms]

Curve Info	Avg	Max
FluxLinkage(PhaseA) : Transient	0.0393 Wb	0.1116 Wb
FluxLinkage(PhaseB) : Transient	0.0280 Wb	0.1116 Wb
FluxLinkage(PhaseC) : Transient	0.0224 Wb	0.1115 Wb

Table 10: Outer Stator SRM Flux Linkage Vs Time curve info

Average flux linkage for Phase A, Phase B and Phase C is 0.0393 Wb, 0.0280 Wb and 0.0224 respectively.

6.3 2D Design of DSSRM

Conventional motor is then modified in Maxwell 2D tool to design two stators Switched Reluctance Motor as shown in Figure 44. Winding configuration in both the stators are same and poles of both stators are equal in size [32].

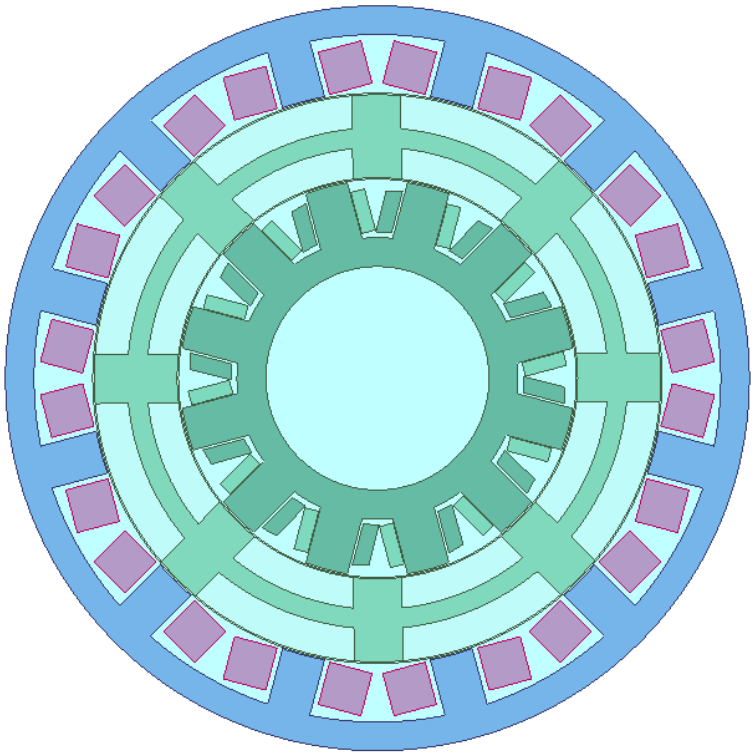

Figure 44: DSSRM [32]

6.3.1 Magnetostatics Analysis of DSSRM

Solution data is presented below.

angle (deg)	Force X (mN)	Force_Y (mN)	Force Mag (mN)
0	-1.387845	0.805675	1.604751
60	0.205904	-1.804931	1.816638
120	1.022587	0.300593	1.065852
180	-8.242127	-5.592148	9.960159
240	-9.651981	0.185904	9.653771
300	0.376358	0.539188	0.657548
360	0.214132	0.437124	0.486754

Table 11: Force in X, Y and Motional direction in DSSRM

Different force components can be studied using above table. For example, in 0 degree movement of rotor, force in X direction, Y-direction and direction of motion is -1.3879 mN, 0.8057 mN and 1.6047 mN.

ang [deg]	Matrix1.L(Coil_0, Coil_0) [uH] - $h='1'	Matrix1.L(Coil_0, Coil_0) [mH] - $h='51'	Matrix1.L(Coil_0, Coil_0) [mH] - $h='101'	Matrix1.L(Coil_0, Coil_0) [mH] - $h='150'
0	19.68984286	51.21569412	200.8752935	443.0440775
30	19.8234419	51.56119409	202.2150558	446.0113386
60	19.93893171	51.8632452	203.3882675	448.626771
90	19.8961511	51.74960748	202.9579066	447.6707476
120	19.79883713	51.50250797	201.9903452	445.5180801
150	19.69054029	51.22130105	200.8831036	443.0751857
180	19.8074785	51.51722054	202.0486742	445.6230246
210	19.93886198	51.86361998	203.4088498	448.6402989
240	19.8997607	51.75765265	203.0105776	447.7453628
270	19.81203243	51.53109497	202.0922964	445.7848347
300	19.69275198	51.22490527	200.8923506	443.1065597
330	19.78885121	51.47080041	201.8453936	445.2475345
360	19.94137987	51.866013	203.4220444	448.6437062
ang [deg]	**Matrix1.L(Coil_0, Coil_1) [uH] - $h='1'**	**Matrix1.L(Coil_0, Coil_1) [mH] - $h='51'**	**Matrix1.L(Coil_0, Coil_1) [mH] - $h='101'**	**Matrix1.L(Coil_0, Coil_1) [mH] - $h='150'**
0	19.33918149	50.30363183	197.2981913	435.1541188
30	19.0825714	49.63417434	194.6575462	429.34087
60	19.07220652	49.6088495	194.5467003	429.1255404
90	19.2210925	49.99376328	196.0714123	432.4815303
120	19.2994618	50.20368498	196.8963723	434.2824437
150	19.34253437	50.31613633	197.333266	435.2454162
180	19.08769985	49.6450789	194.7055482	429.4322019
210	19.07115713	49.60672743	194.5579681	429.1178582
240	19.20793447	49.95813168	195.9528557	432.1784093
270	19.29417923	50.18415884	196.8094073	434.1328435
300	19.34578223	50.32245156	197.3529585	435.2998531
330	19.09919441	49.67700311	194.810758	429.7301196
360	19.07228685	49.60554124	194.5563826	429.0905261

Table 12: Variation of Inductance with Number of Turns in DSSRM

From above table, it can be observed that inductance in the coil increases with increase in number of turns. For number of turns equal to 1, inductance in coil is equal to 19uH (in avg) which

increases to 49uH for number of turns equal to 51. For 150 number of turns inductance is maximum and is equal to 432uH(in avg).

6.3.2 Transient Analysis of DSSRM

With same simulation and setup parameter transient simulation is performed for DSSRM.

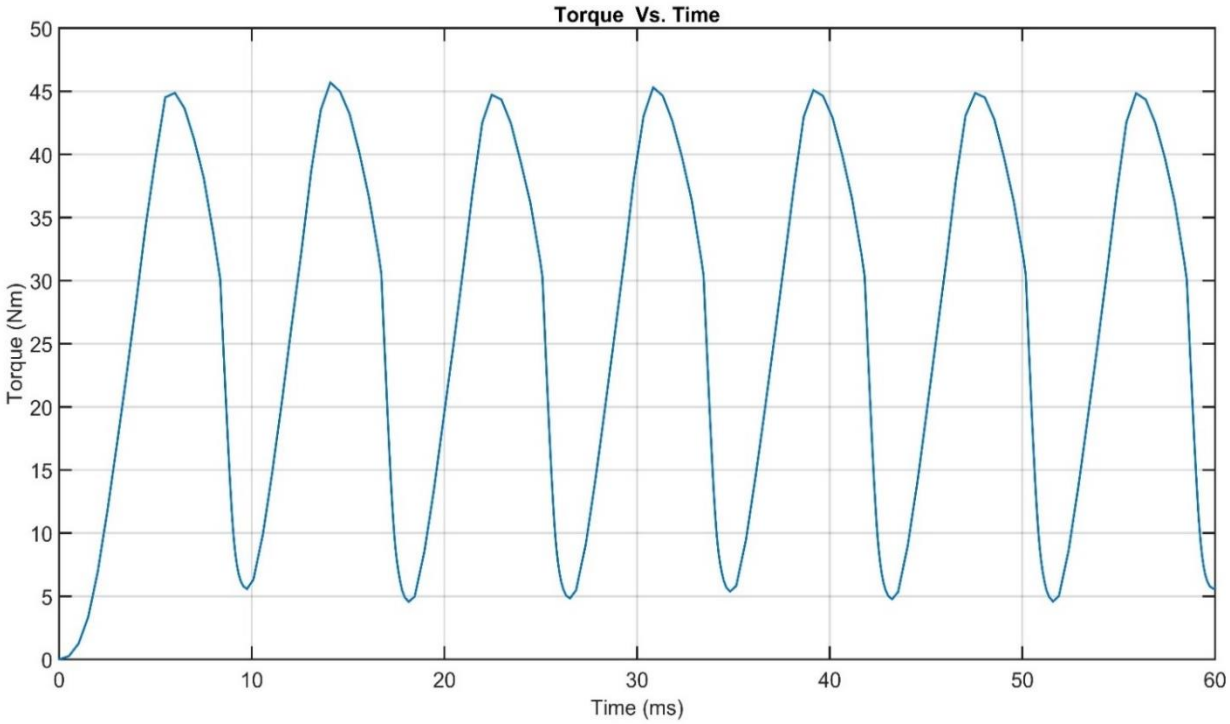

Figure 45: DSSRM's Moving Torque [Nm] vs Time [ms]

Curve Info	Avg	Max
Moving Torque (Transient)	26.5352 Nm	45.6867 Nm

Table 13: DSSRM Stator SRM Torque Vs Time curve info

Moving Torque of DSSRM is found to be 26.5352 Nm in average and maximum torque of motor is calculated as 45.6867 Nm . Average torque ripple is calculated and found to be 80.23%.

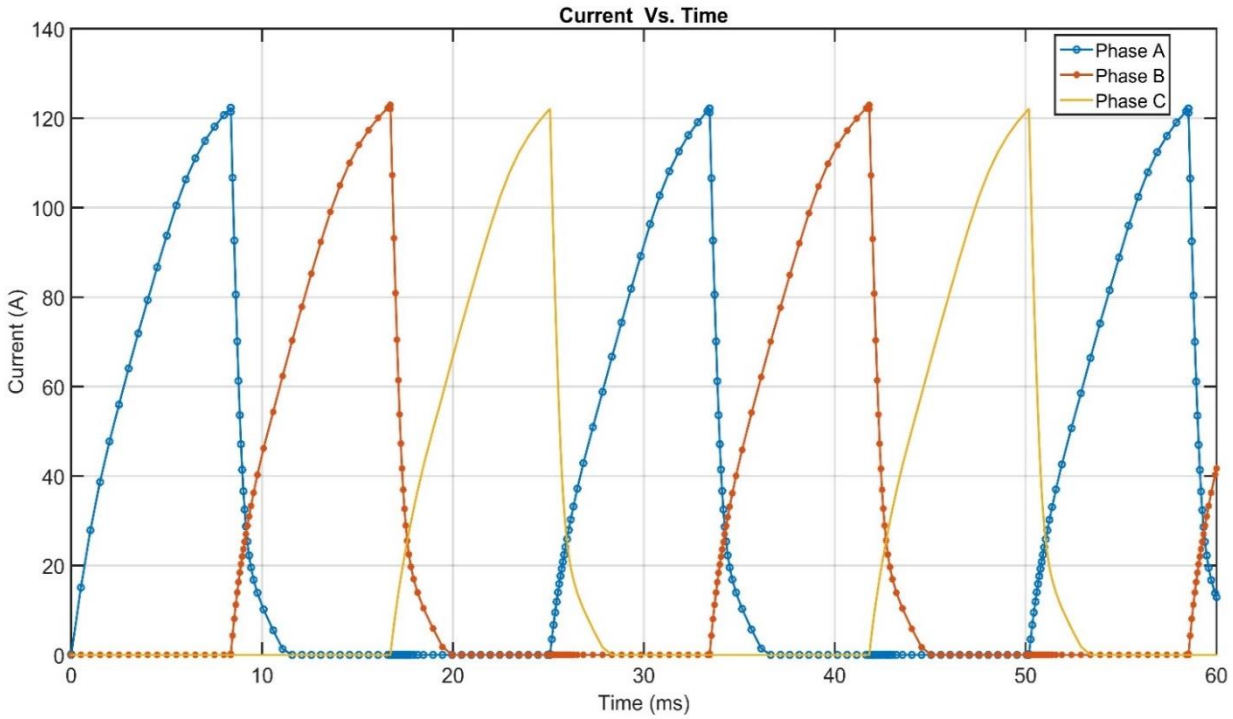

Figure 46: DSSRM's Phase Current [A] vs Time [ms]

Curve Info	Avg	Max
Current(PhaseA) (Transient)	35.4280 A	122.3566 A
Current(PhaseB) (Transient)	25.1488 A	122.9684 A
Current(PhaseC) (Transient)	23.6693 A	122.1569 A

Table 14: DSSRM Current Vs Time curve info

On average 35.4280 A, 25.1488 A and 23.6693 A of current flows in Phase A, Phase B and Phase C respectively in Double Stator configuration of SRM.

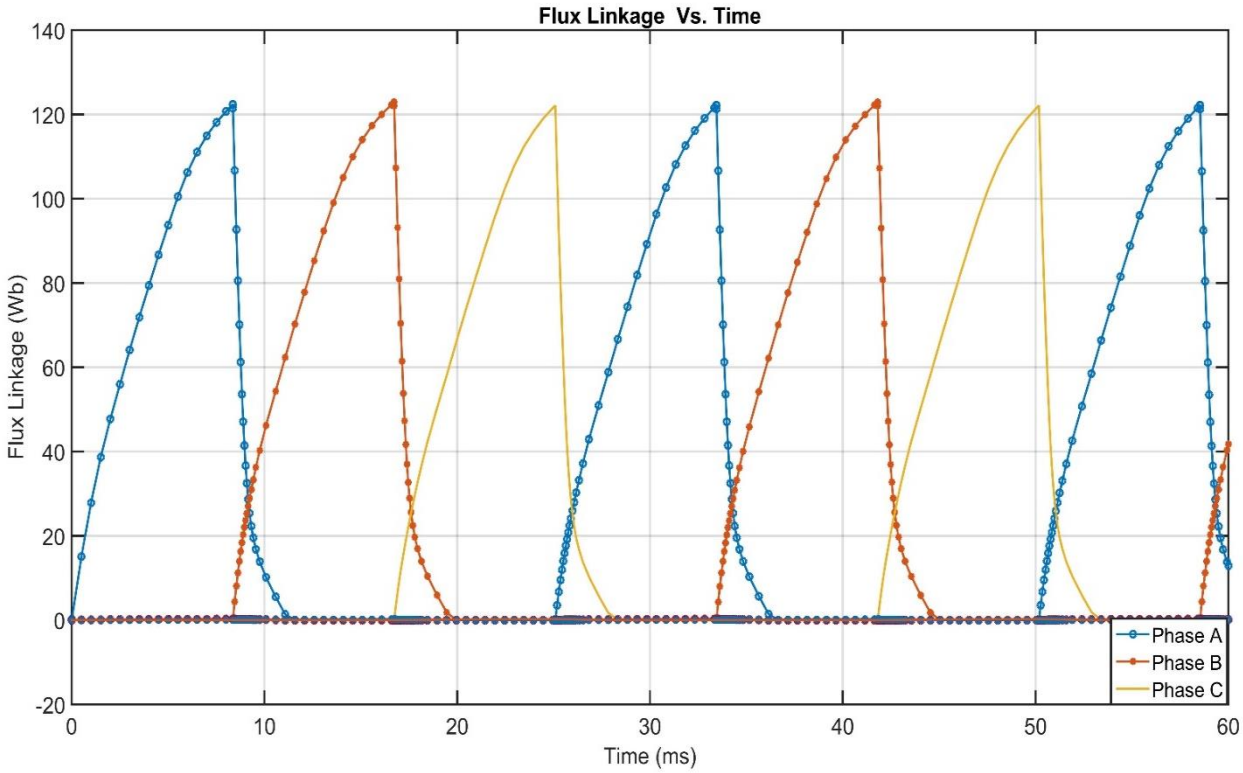

Figure 47: DSSRM's Flux Linkage [Wb] vs Time [ms]

Curve Info	Avg	Max
FluxLinkage(PhaseA) : Transient	0.0779 Wb	0.2252 Wb
FluxLinkage(PhaseB) : Transient	0.0535 Wb	0.2230 Wb
FluxLinkage(PhaseC) : Transient	0.0486 Wb	0.2250 Wb

Table 15: DSSRM Stator SRM Flux Linkage Vs Time curve info

Average flux linkage for Phase A, Phase B and Phase C is 0.0779 Wb, 0.0535 Wb and 0.0486 respectively.

6.4 Comparison of Inner Stator SRM, Outer Stator SRM and DSSRM

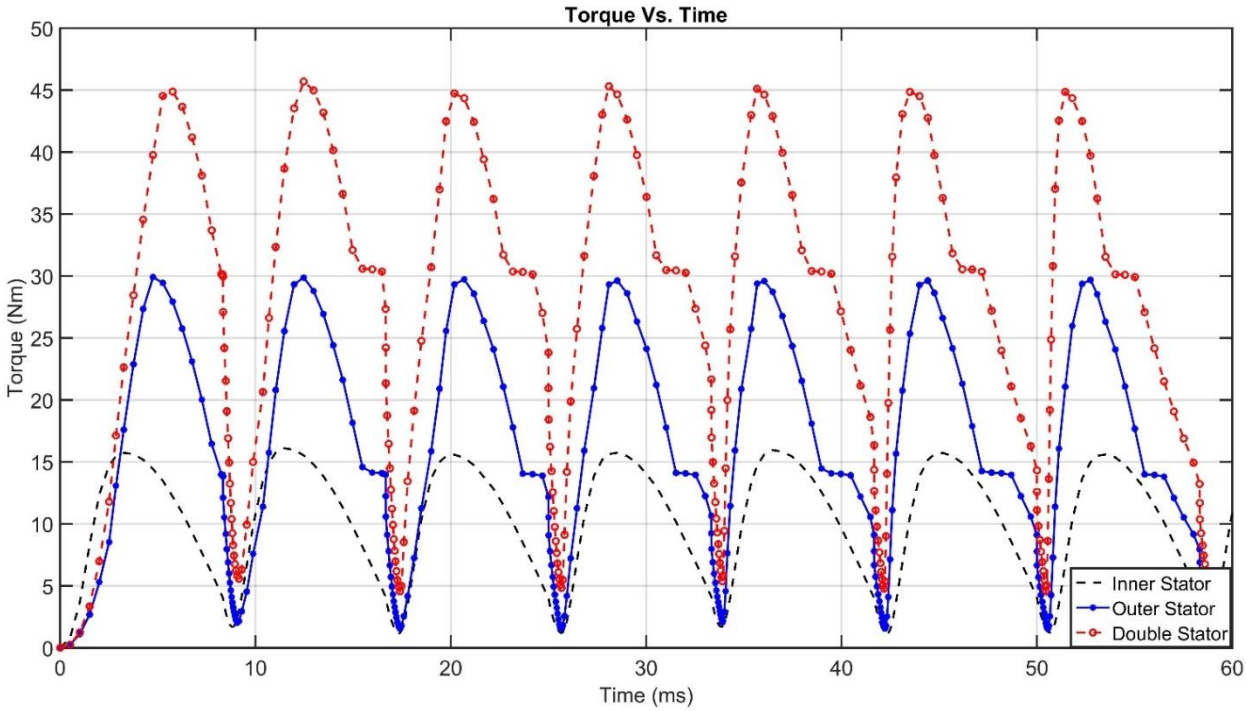

Figure 48: Moving Torque of Inner Stator, Outer Stator and DSSRM

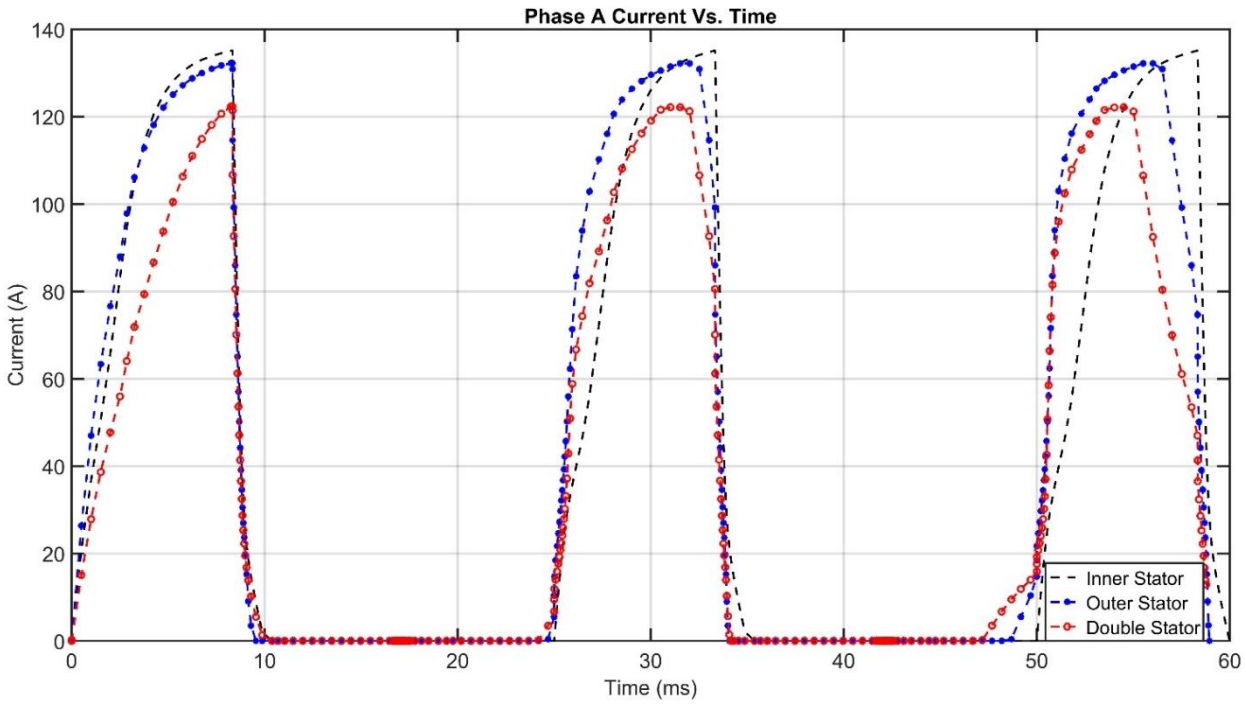

Figure 49: Phase A current of Inner Stator, Outer Stator and DSSRM

Comparing force data from magnetostatic analysis, force in the direction of motion is found to be maximum in DSSRM. At 240 degree, motional force in DSSRM, Outer Stator and Inner Stator is 9.053mNewton, 7.38mNewton and 1.30mNewton respectively. Inductance of the coil is maximum when number of turns is maximum. For 1 number of turns, minimum inductance is observed in all three motors while for 150 number of turns maximum inductance is obtained.

From transient analysis data, motional torque is highest i.e. 26.5352 Nm in Double Stator SRM, and lowest i.e. 10.1935 Nm in Inner Stator SRM. DSSRM give rise to minimum torque ripple i.e. 80.23% among all three motors. Torque ripple is found to be maximum i.e. 89.09% in Outer Stator SRM. Maximum current of 135 A flows in inner stator SRM while minimum current of 122 A flows in Double Stator SRM.

6.5 Design Modification

Outer Stator SRM, Inner Stator SRM and DSSRM is modified by chamfering the edges of stator and rotor. Chamfering is done on different edges of stator and rotor and effect on motor performance with different chamfer radius is studied. Best result of chamfering for each of the motor is presented below.

6.5.1 Design modification of Inner Stator SRM

Chamfering on motoring side of stator and rotor is done as shown in figure below.

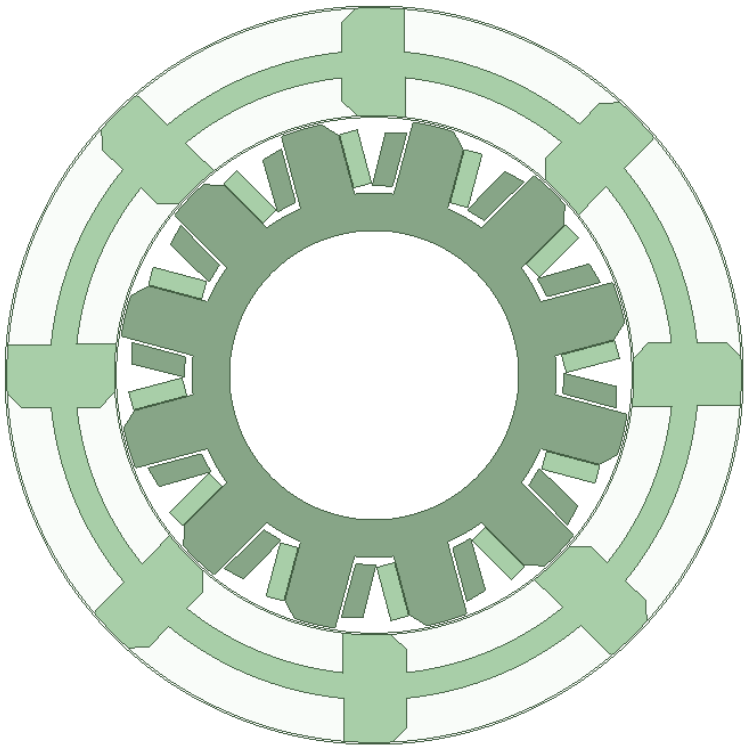

Figure 50: Chamfer Design of Inner Stator SRM

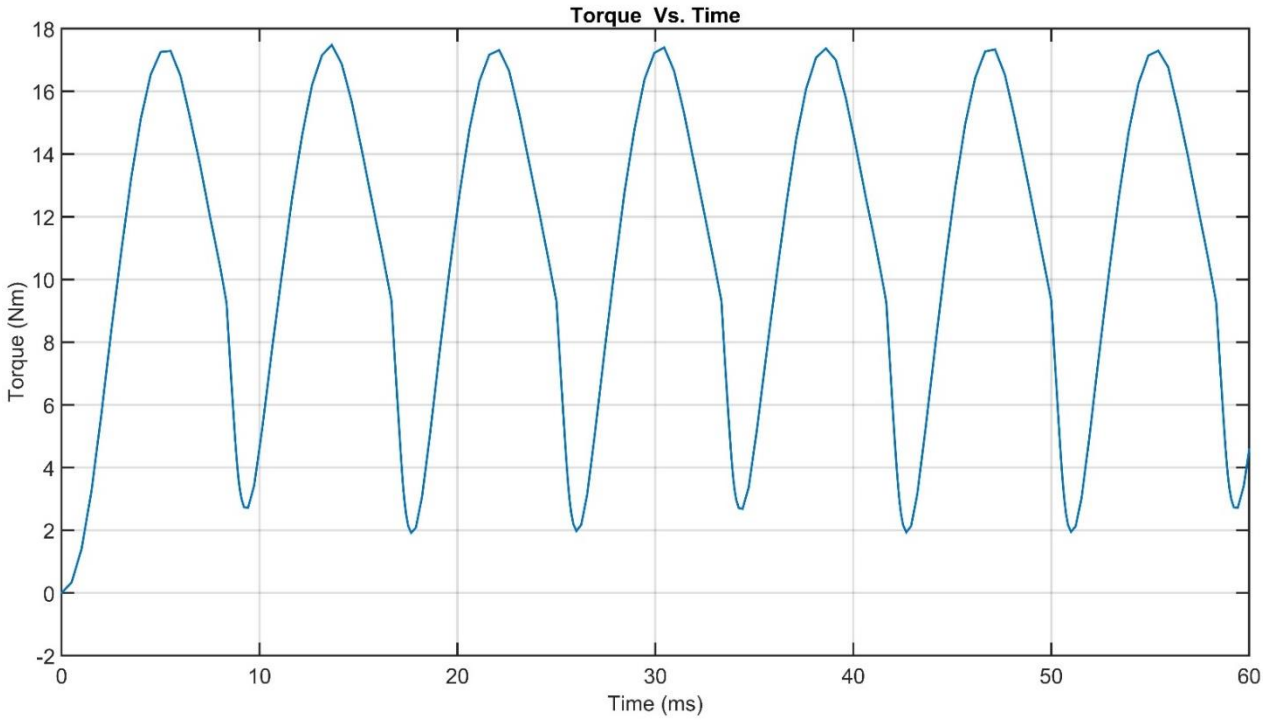

Figure 51: Torque Vs Time Plot of Inner Stator SRM with Chamfer

Curve Info	Avg	Max
Moving Torque (Transient)	10.9479 Nm	17.4826 Nm

Table 16: Chamfered Inner Stator SRM Torque Vs Time curve info

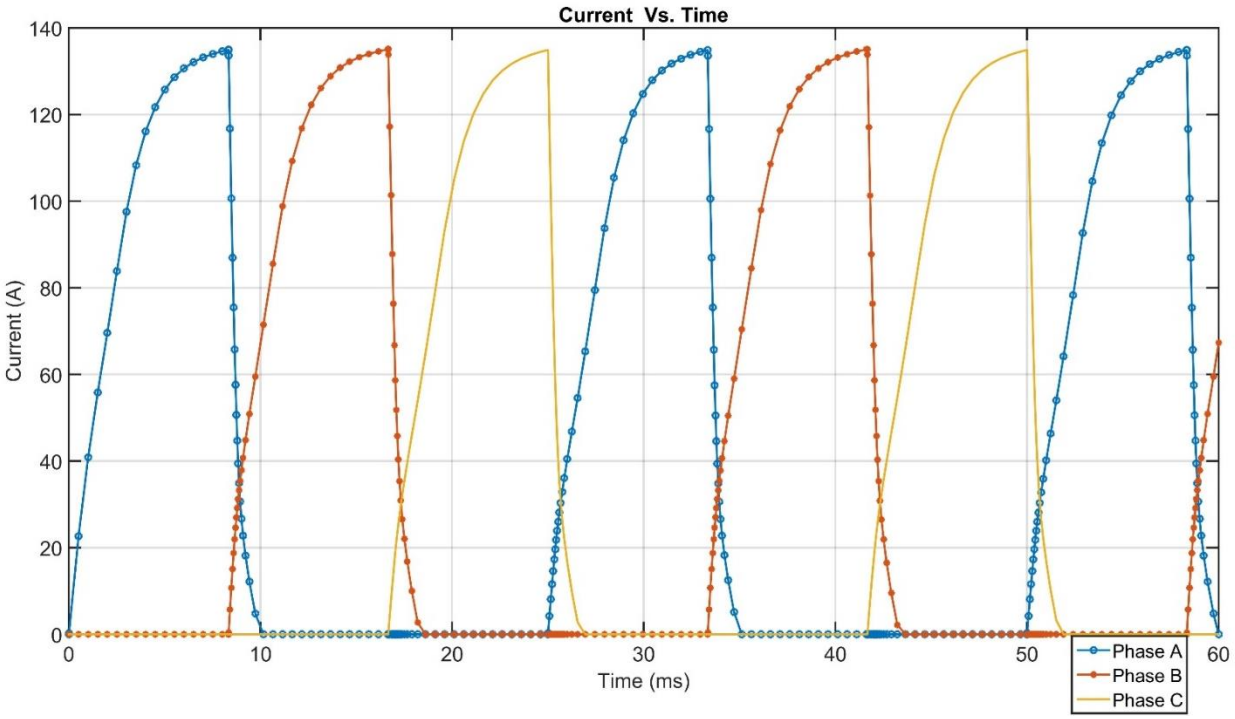

Figure 52: Current Vs Time Plot of Inner Stator SRM

Curve Info	Avg	Max
Current(PhaseA) (Transient)	44.078 A	134.9683 A
Current(PhaseB) (Transient)	31.7308 A	135.1023 A
Current(PhaseC) (Transient)	29.3972 A	134.9324 A

Table 17: Chamfered Inner Stator SRM Current Vs Time curve info

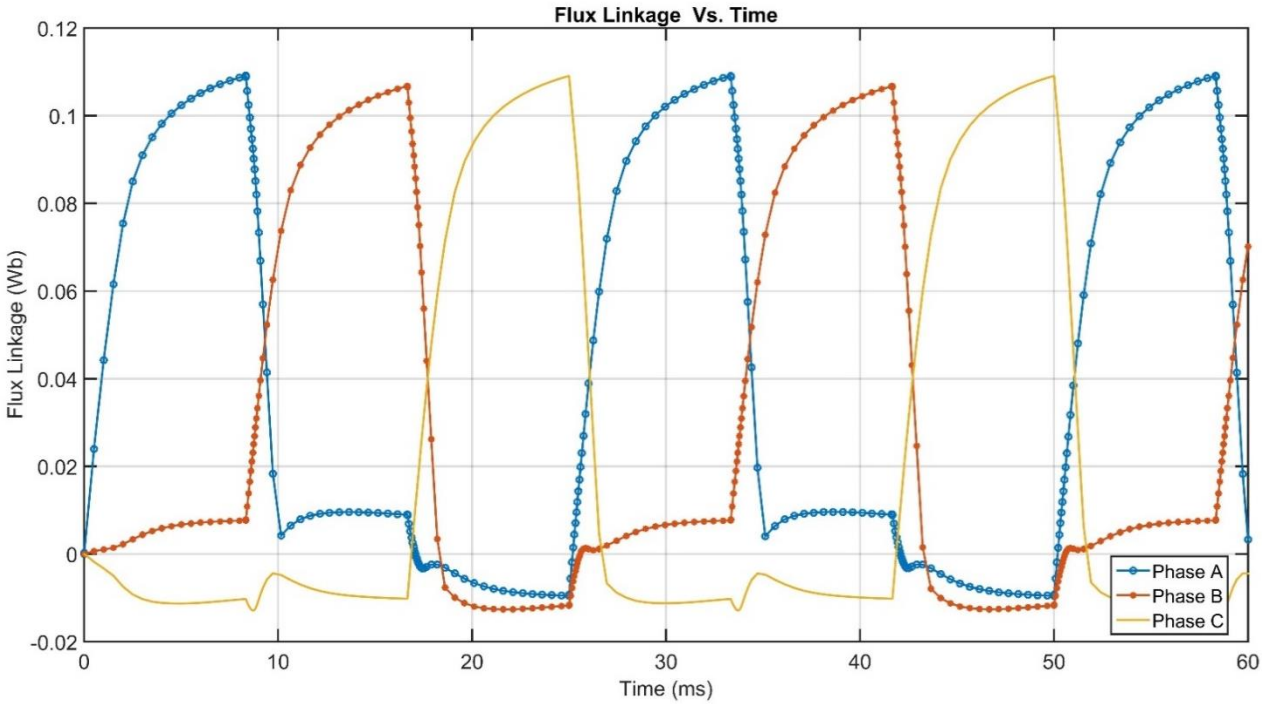

Figure 53: Flux Linkage Vs Time Plot of Inner Stator SRM

Curve Info	Avg	Max
FluxLinkage(PhaseA) : Transient	0.0406 Wb	0.1091 Wb
FluxLinkage(PhaseB) : Transient	0.0275 Wb	0.1068 Wb
FluxLinkage(PhaseC) : Transient	0.0205 Wb	0.1091 Wb

Table 18: Chamfered Inner Stator SRM Flux Linkage Vs Time curve info

Comparison of Chamfered Inner stator and Original Inner Stator SRM

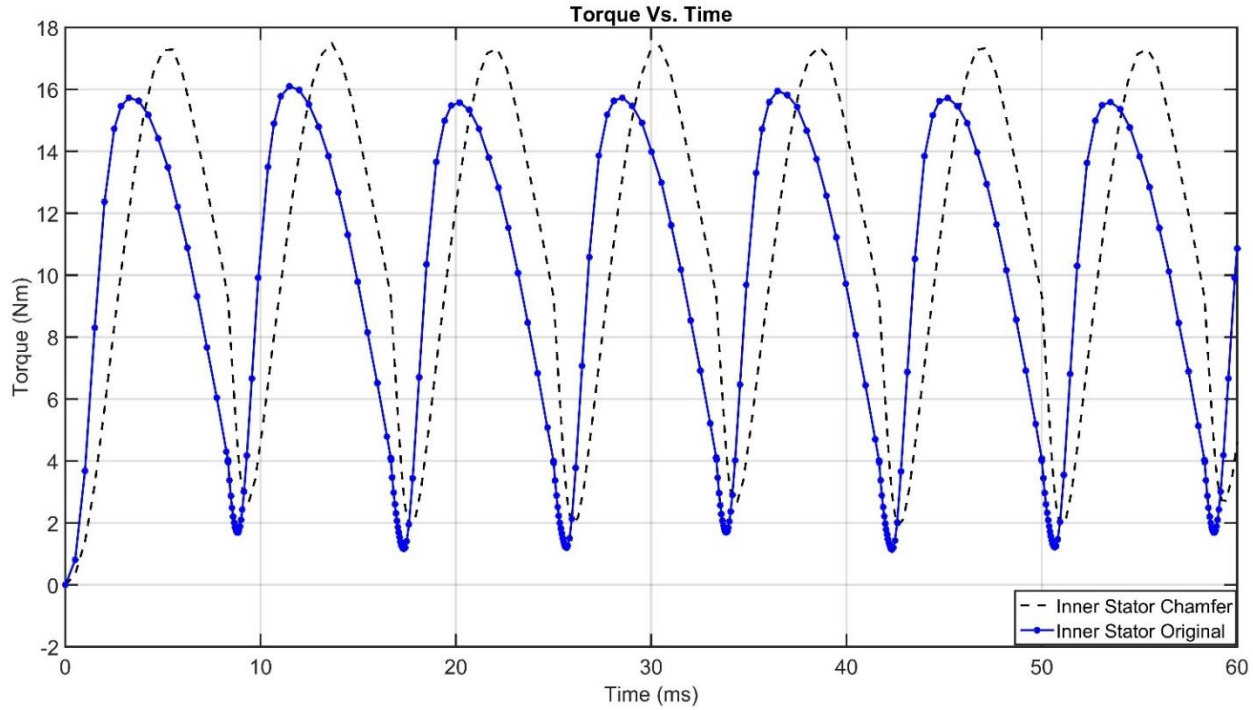

Figure 54: Moving Torque of Chamfered Inner Stator and Original Inner Stator SRM

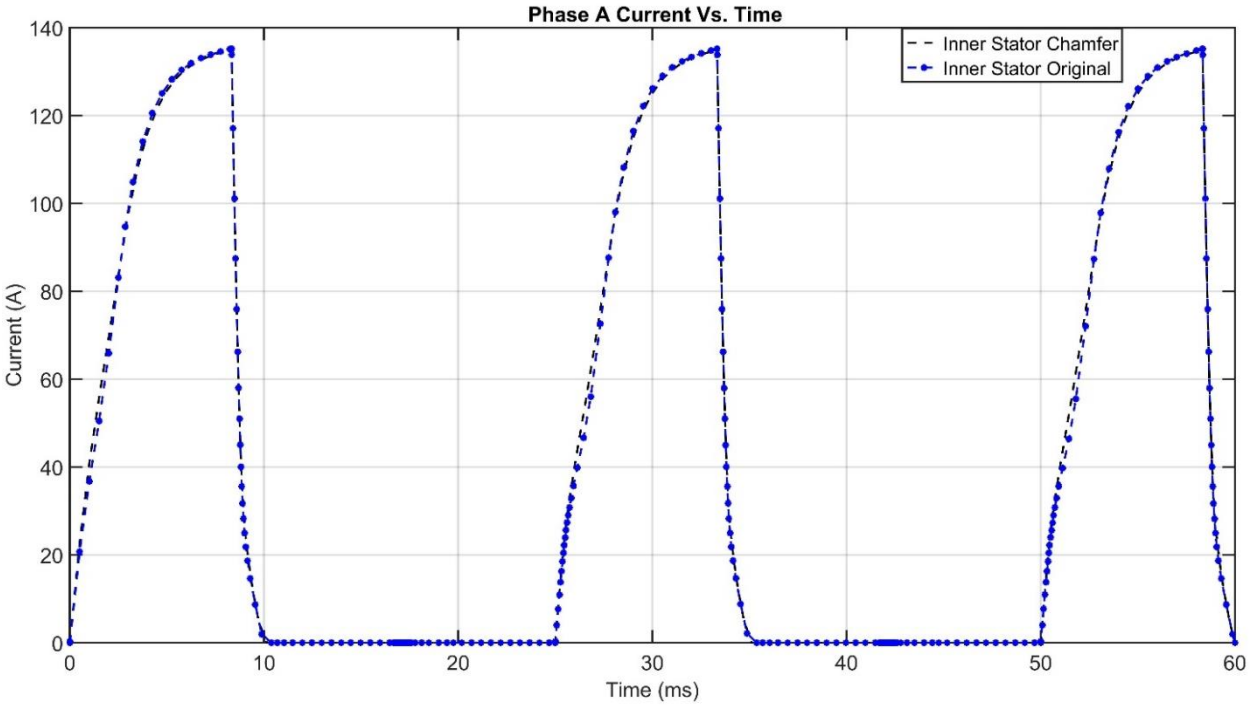

Figure 55: Phase A Current of Chamfered Inner Stator and Original Inner Stator SRM

Chamfering of radius 4mm is done on motoring edge of both stator and rotor. Average moving torque is found to be 10.9479 Nm after chamfering while conventional inner stator SRM has average torque of 10.1935 Nm. Torque ripple is calculated and found to be 77.614%, which is smaller than that of conventional inner stator SRM (Torque ripple of conventional inner stator is 84.30%). Chamfering of radius 4mm on both stator and rotor increases moving torque with simultaneous decrease in torque ripple of inner stator SRM.

6.5.2 Design modification of Outer Stator SRM

Chamfering is done on motoring edge of outer stator and rotor as shown in figure below.

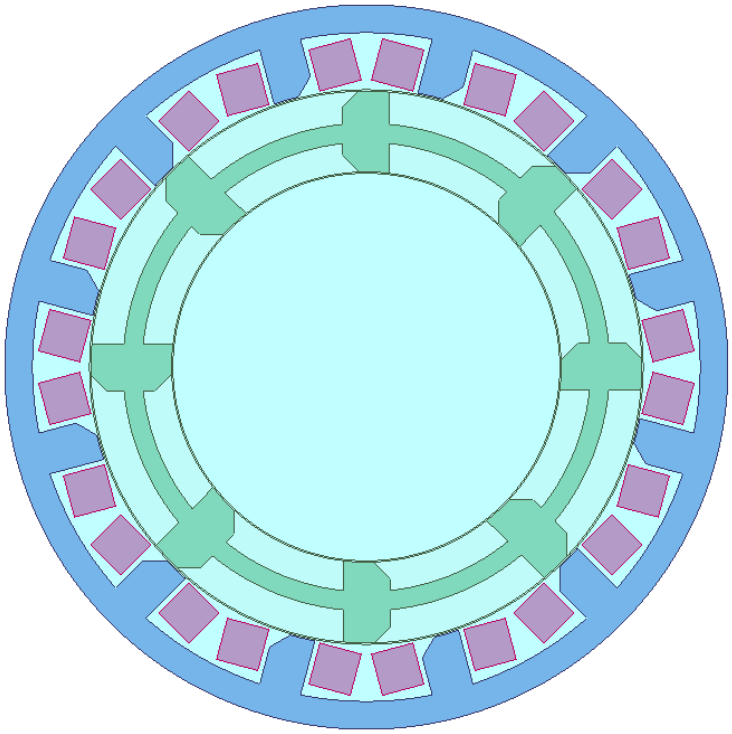

Figure 56: Chamfer Design of Outer Stator SRM

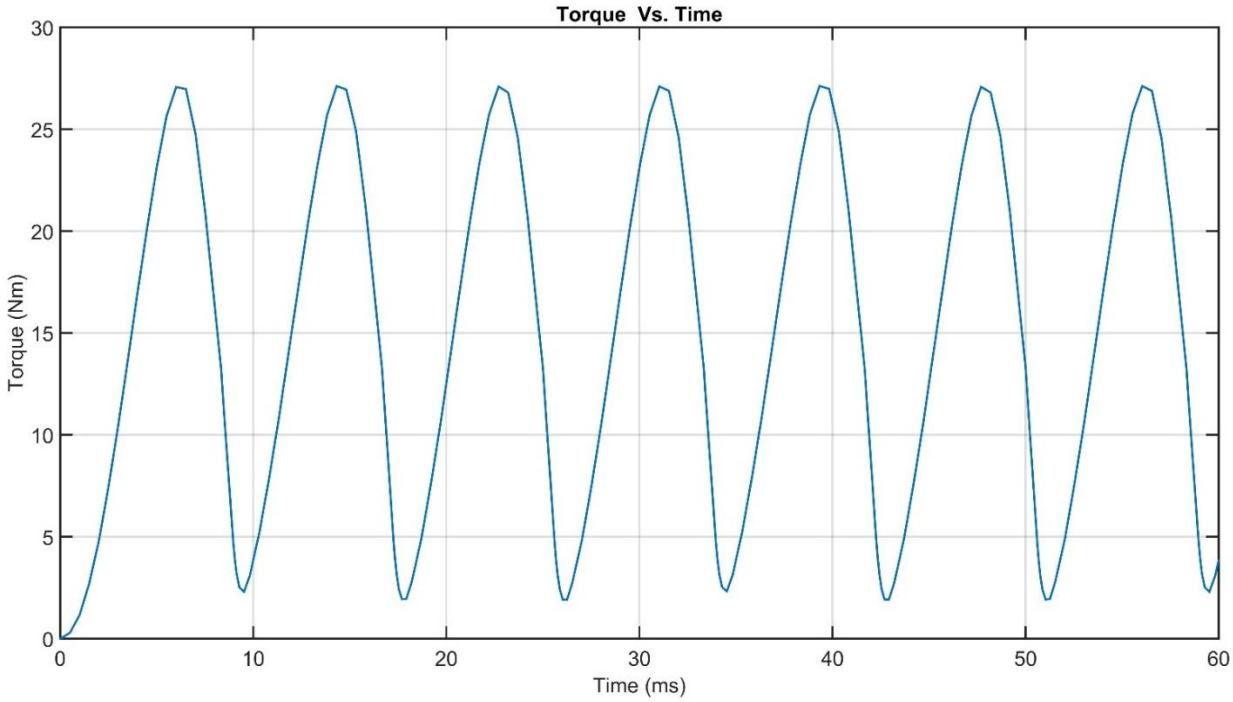

Figure 57: Torque Vs Time Plot of Outer Stator SRM

Curve Info	Avg	Max
Moving Torque (Transient)	15.0746 Nm	27.122 Nm

Table 19: Chamfered Outer Stator SRM Torque Vs Time curve info

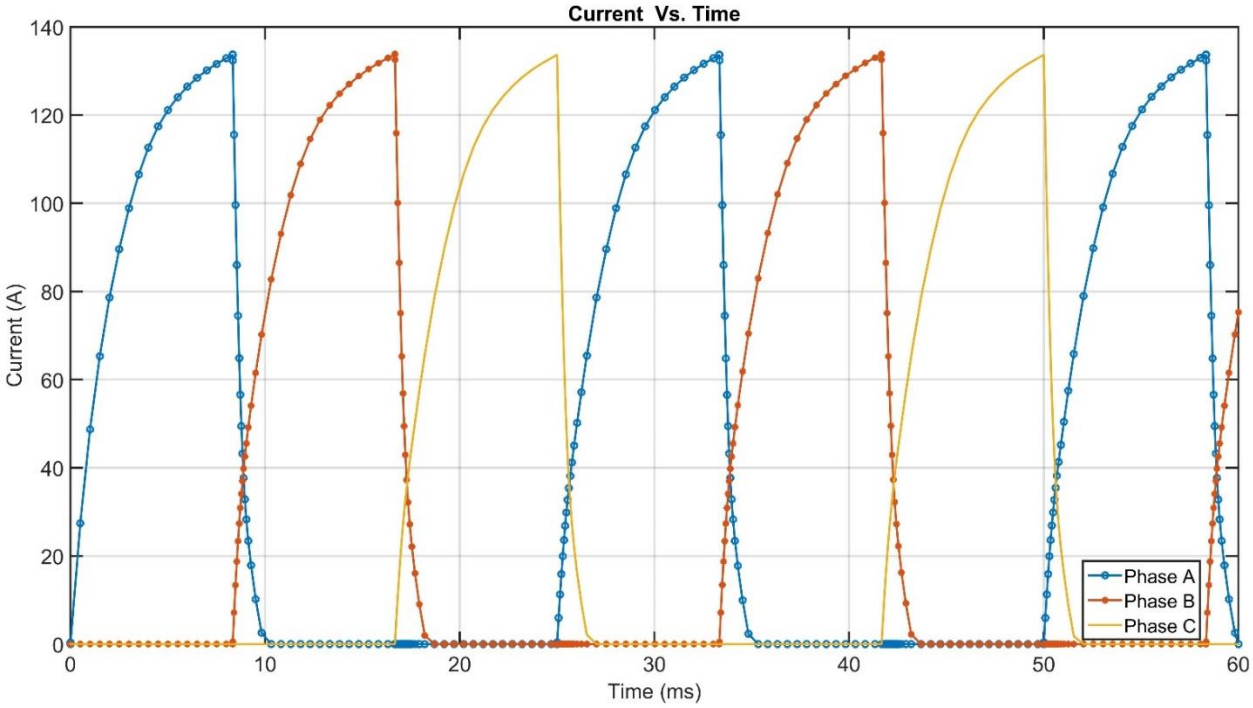

Figure 58: Current Vs Time Plot of Outer Stator SRM

Curve Info	Avg	Max
Current(PhaseA) (Transient)	44.5695 A	133.6928 A
Current(PhaseB) (Transient)	31.8405 A	133.8049 A
Current(PhaseC) (Transient)	29.8199 A	133.6782 A

Table 20: Chamfered Outer Stator SRM Current Vs Time curve info

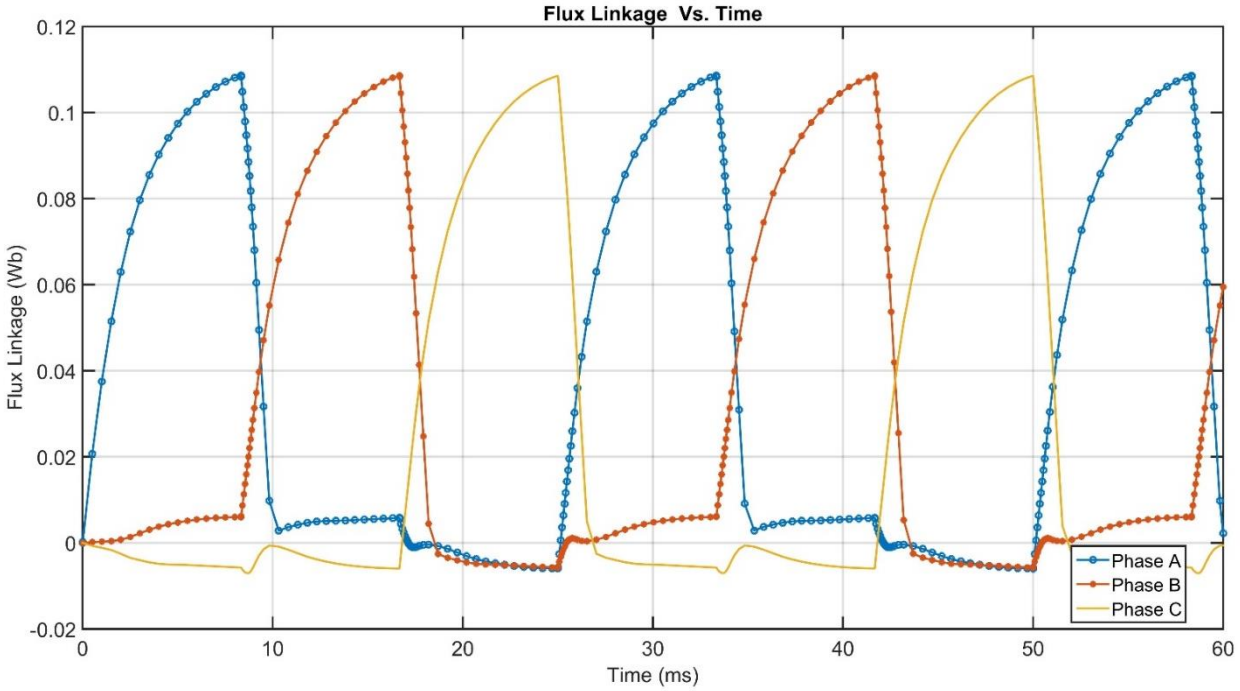

Figure 59: Flux Linkage Vs Time Plot of Outer Stator SRM

Curve Info	Avg	Max
FluxLinkage(PhaseA) : Transient	0.0382 Wb	0.1086 Wb
FluxLinkage(PhaseB) : Transient	0.0271 Wb	0.1086 Wb
FluxLinkage(PhaseC) : Transient	0.0223 Wb	0.1086 Wb

Table 21: Chamfered Outer Stator SRM Flux Linkage Vs Time curve info

Comparison of Chamfered Outer stator and Original Outer Stator SRM

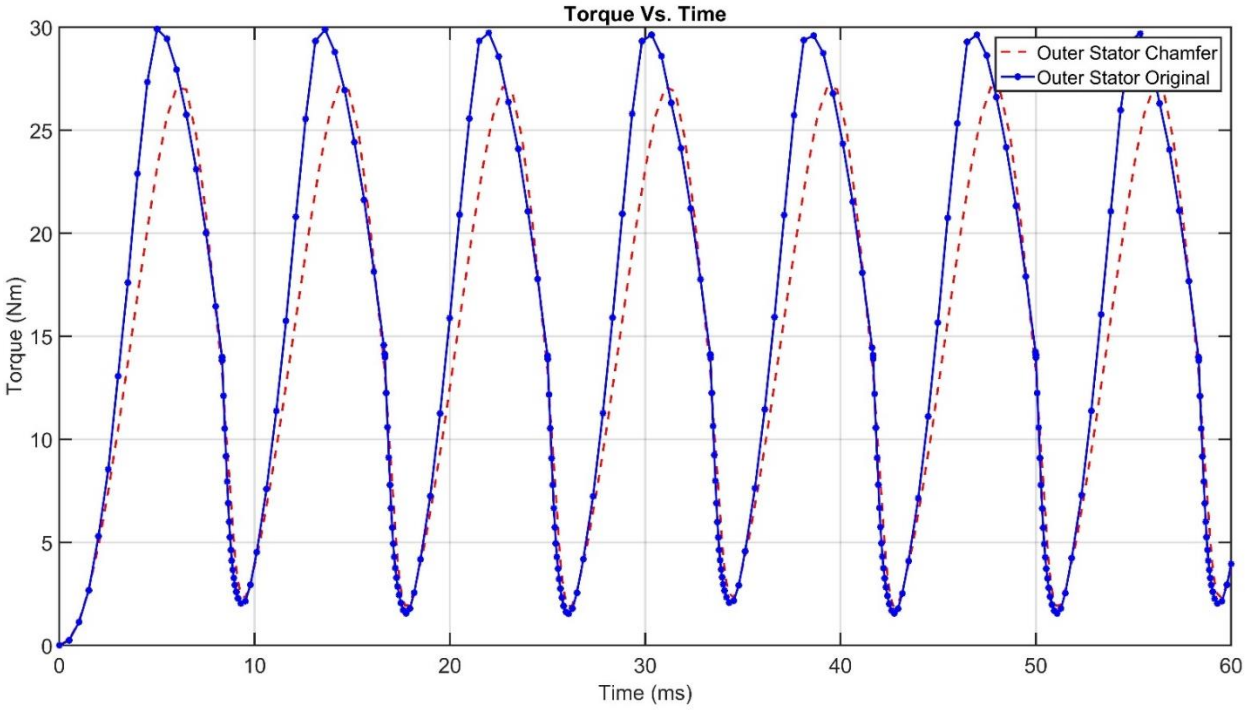

Figure 60: Moving Torque of Chamfered Outer Stator and Original Outer Stator SRM

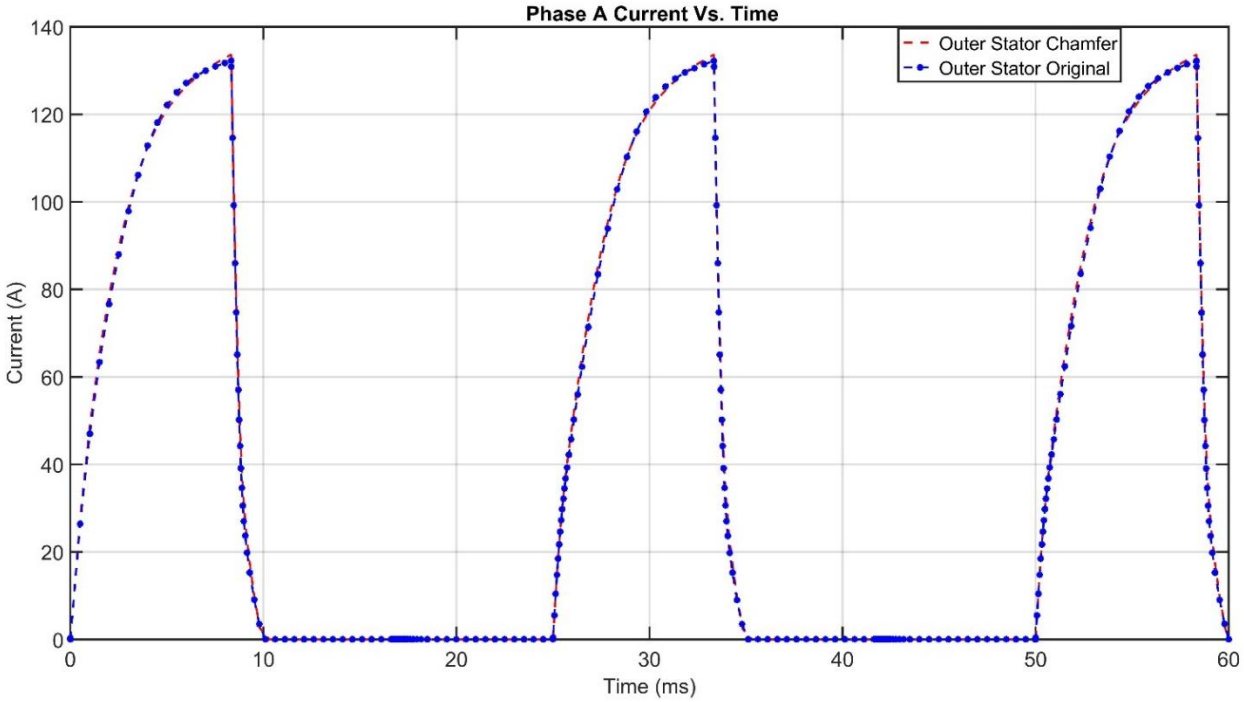

Figure 61: Phase A Current of Chamfered Outer Stator and Original Outer Stator SRM

Chamfering the motoring edges of outer stator SRM results decrease in torque ripple from 89.09% to 85.89%. But chamfering effect lowered moving torque of outer stator SRM. With chamfering the motoring edges, moving torque is 15.0746 Nm while before chamfering moving torque was 16.5898 Nm.

6.5.3 Design Modification of DSSRM

Chamfering is done on both inner & outer stators and rotor of DSSRM as shown in figure below.

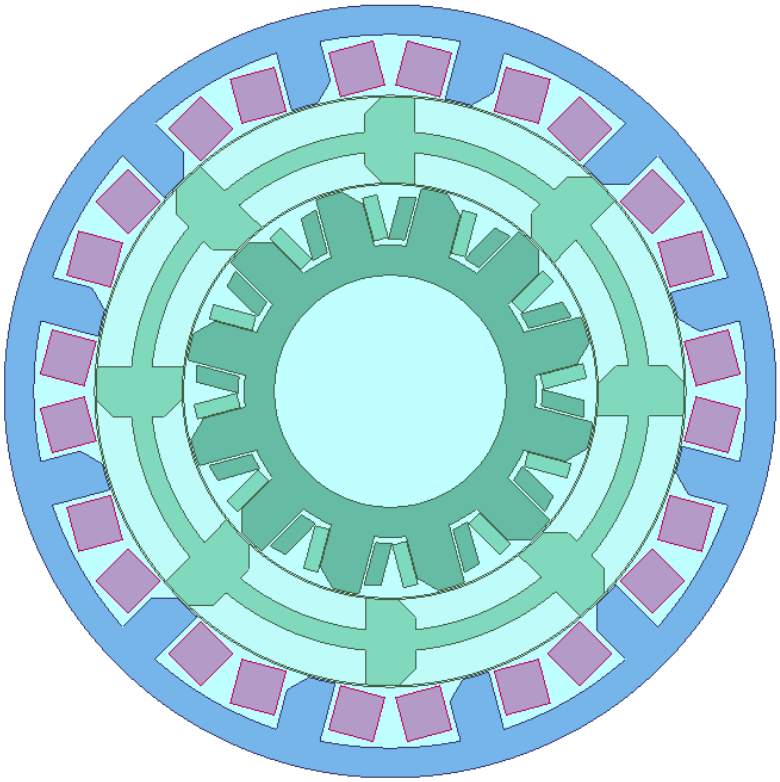

Figure 62: Chamfer Design of DSSRM

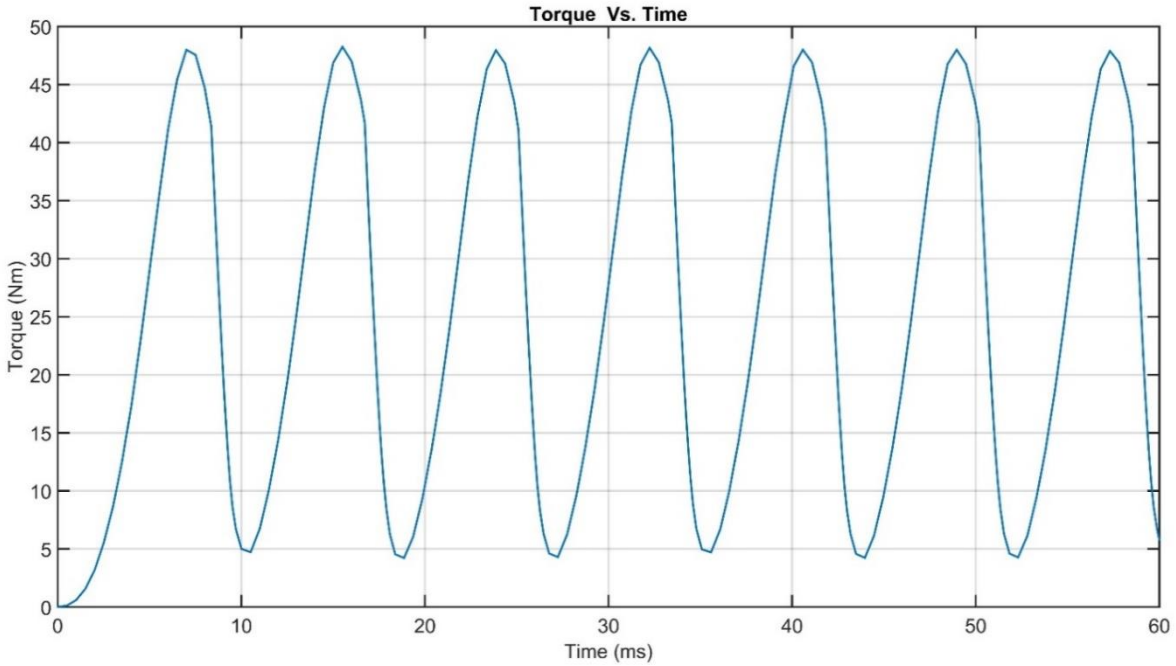

Figure 63: Torque Vs Time Plot of DSSRM

Curve Info	Avg	Max
Moving Torque (Transient)	25.1911 Nm	48.2557 Nm

Table 22: Chamfered DSSRM Torque Vs Time curve info

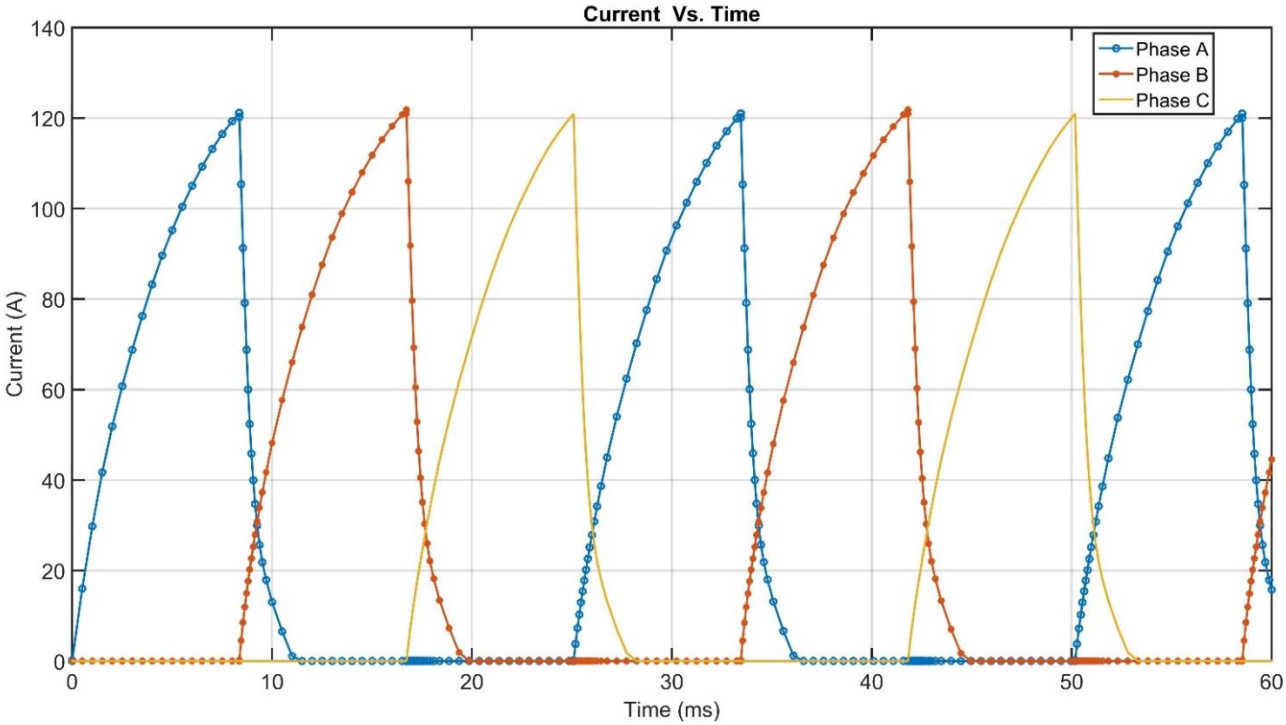

Figure 64: Current Vs Time Plot of DSSRM

Curve Info	Avg	Max
Current(PhaseA) (Transient)	36.3443 A	121.1281 A
Current(PhaseB) (Transient)	25.7543 A	121.8516 A
Current(PhaseC) (Transient)	24.3052 A	133.6782 A

Table 23: Chamfered DSSRM Current Vs Time curve info

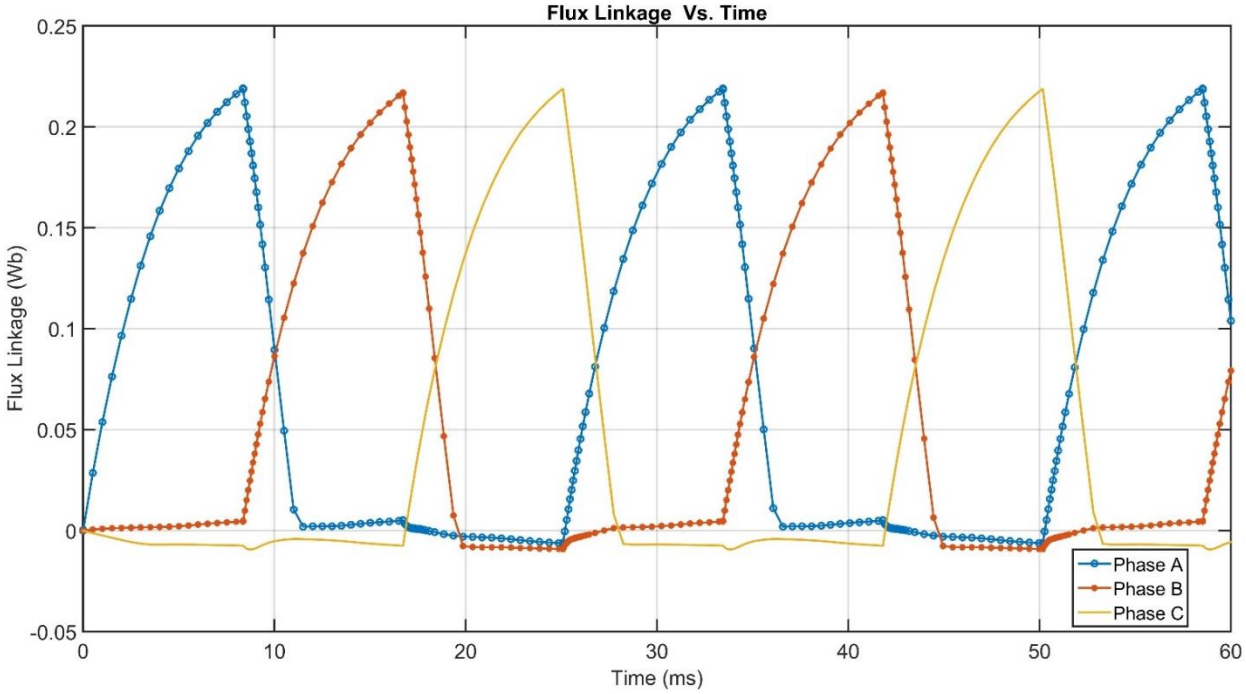

Figure 65: Flux Linkage Vs Time Plot of DSSRM

Curve Info	Avg	Max
FluxLinkage(PhaseA) : Transient	0.0742 Wb	0.219 Wb
FluxLinkage(PhaseB) : Transient	0.0509 Wb	0.2169 Wb
FluxLinkage(PhaseC) : Transient	0.0462 Wb	0.2189 Wb

Table 24: Chamfered DSSRM Flux Linkage Vs Time curve info

Comparison of Chamfered DSSRM and Original DSSRM

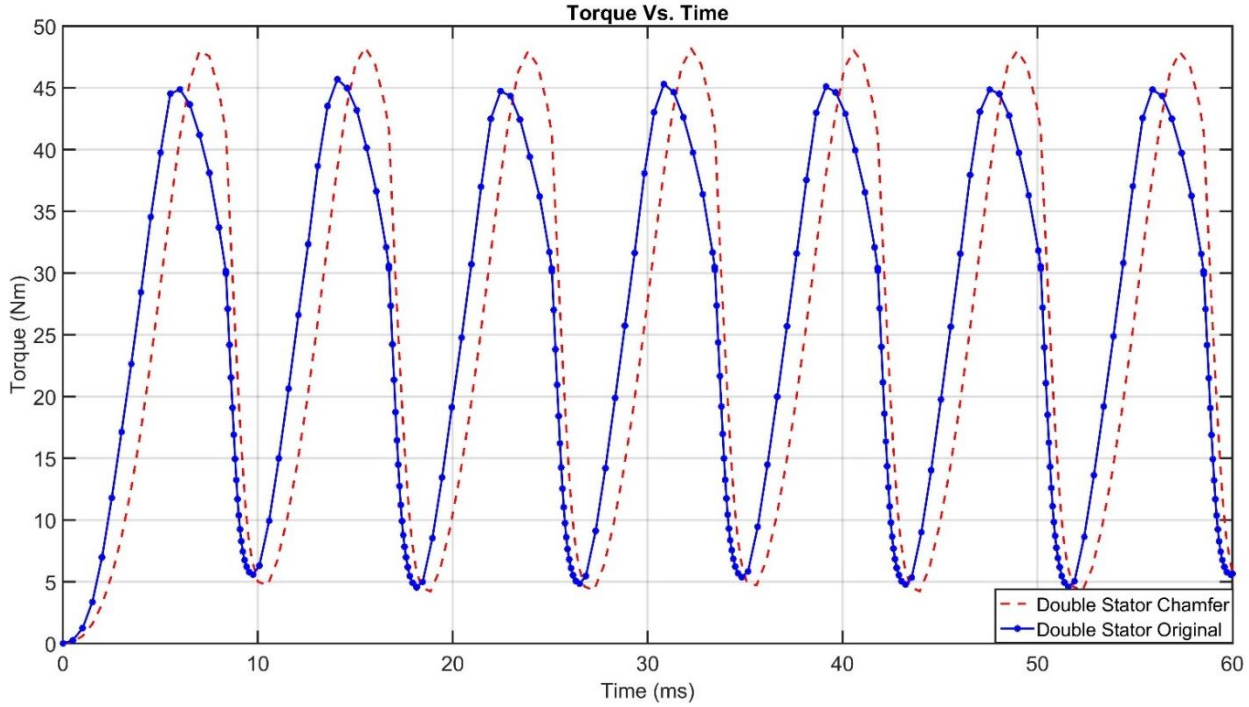

Figure 66: Moving Torque of Chamfered DSSRM and Original DSSRM

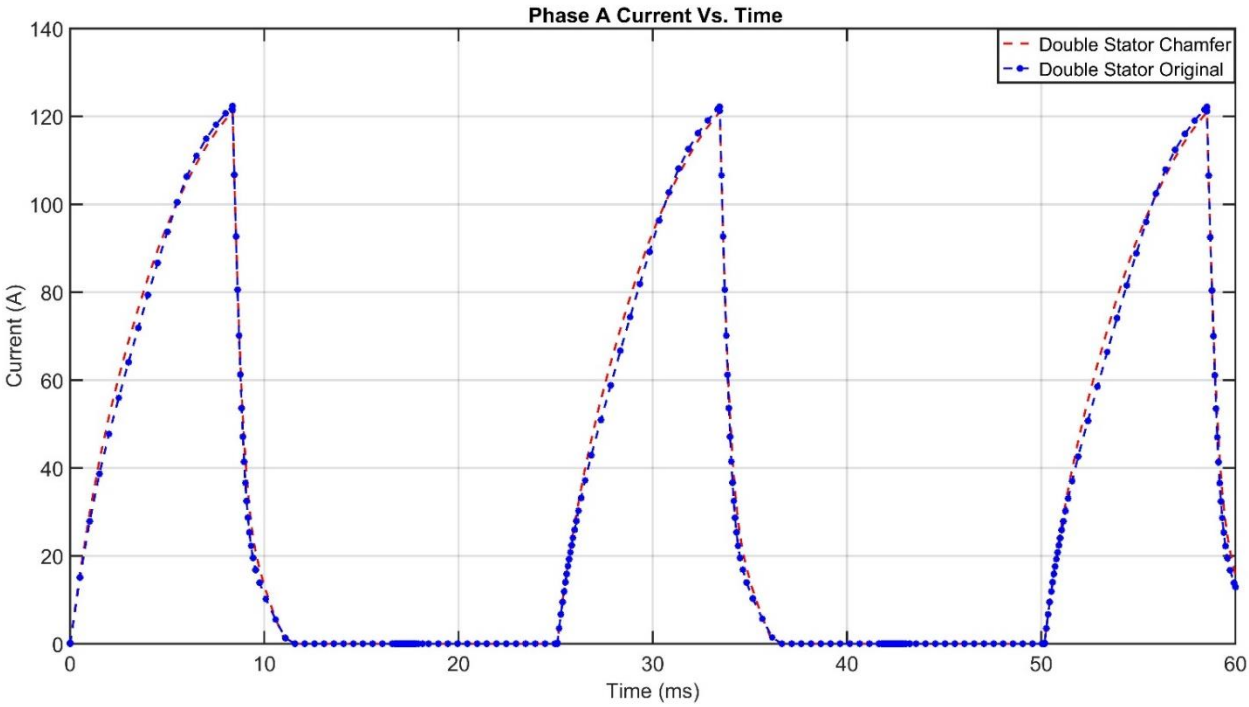

Figure 67: Phase A Current of Chamfered DSSRM and Original DSSRM

Chamfering in DSSRM is found to degrade motor performance. Chamfering increased torque ripple from 80.23% to 82.49% and decreased moving torque from 26.5352 Nm to 25.1911 Nm.

6.6 Rotor Modification of DSSRM

Rotor of DSSRM is modified as shown in figure with the aim to increase motor performance. Excitation is changed to adapt with modification. Diametrically opposite stators poles are not excited at a same time.

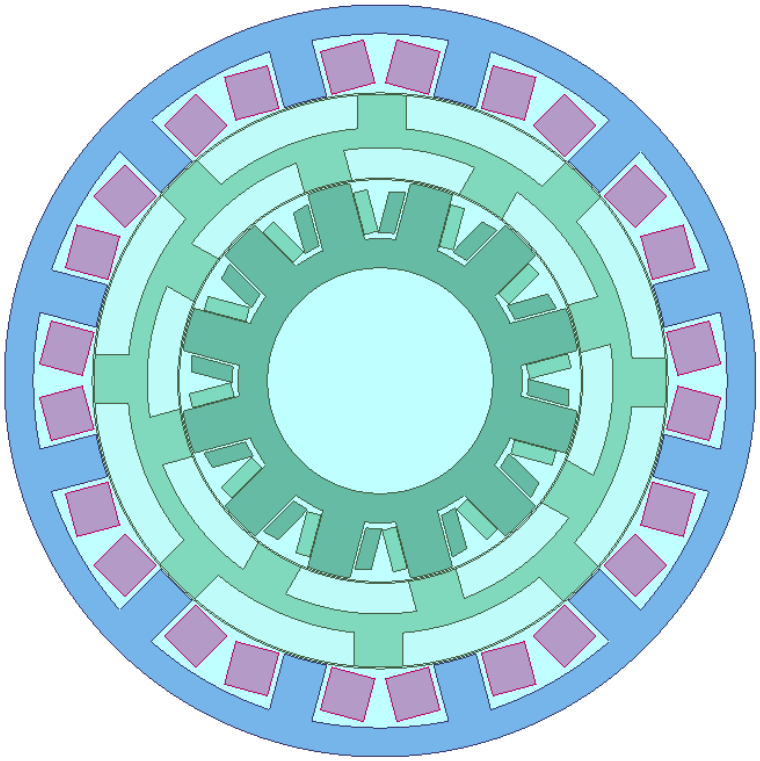

Figure 68: Rotor Modification of DSSRM

Transient analysis result is shown in following plots.

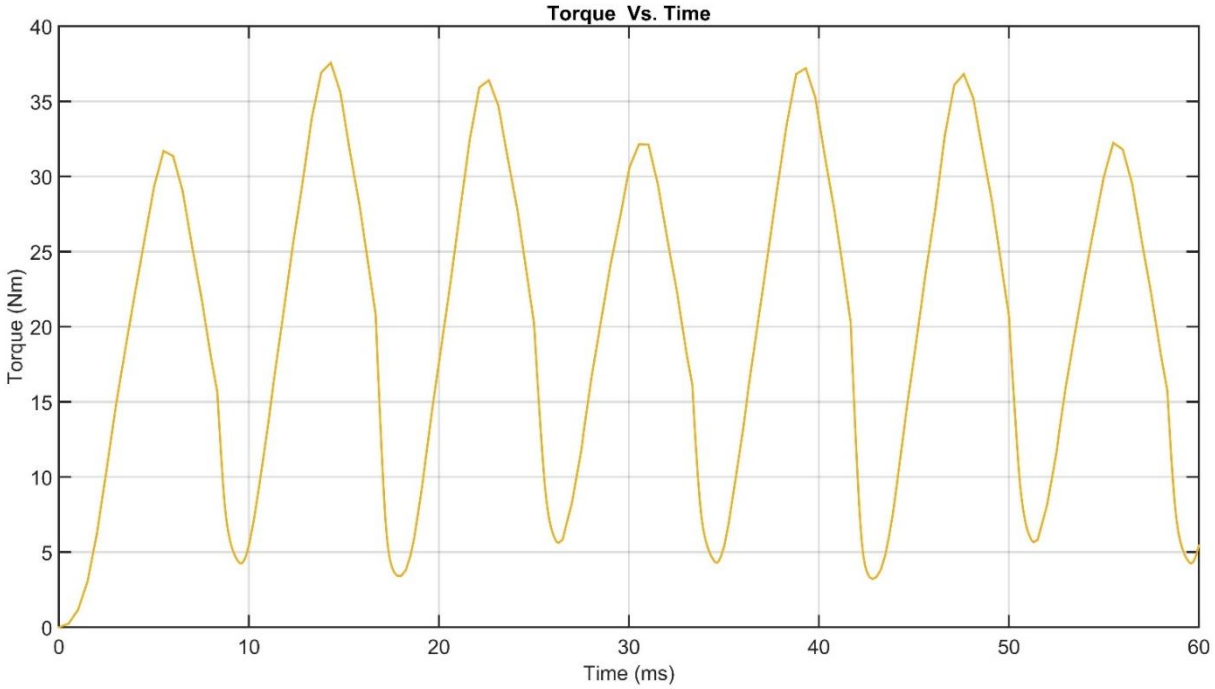

Figure 69: Torque Vs Time Plot of modified rotor DSSRM

Curve Info	Avg	Max
Moving Torque (Transient)	20.0424 Nm	37.5621 Nm

Table 25: Torque Vs Time curve info of Modified Rotor DSSRM

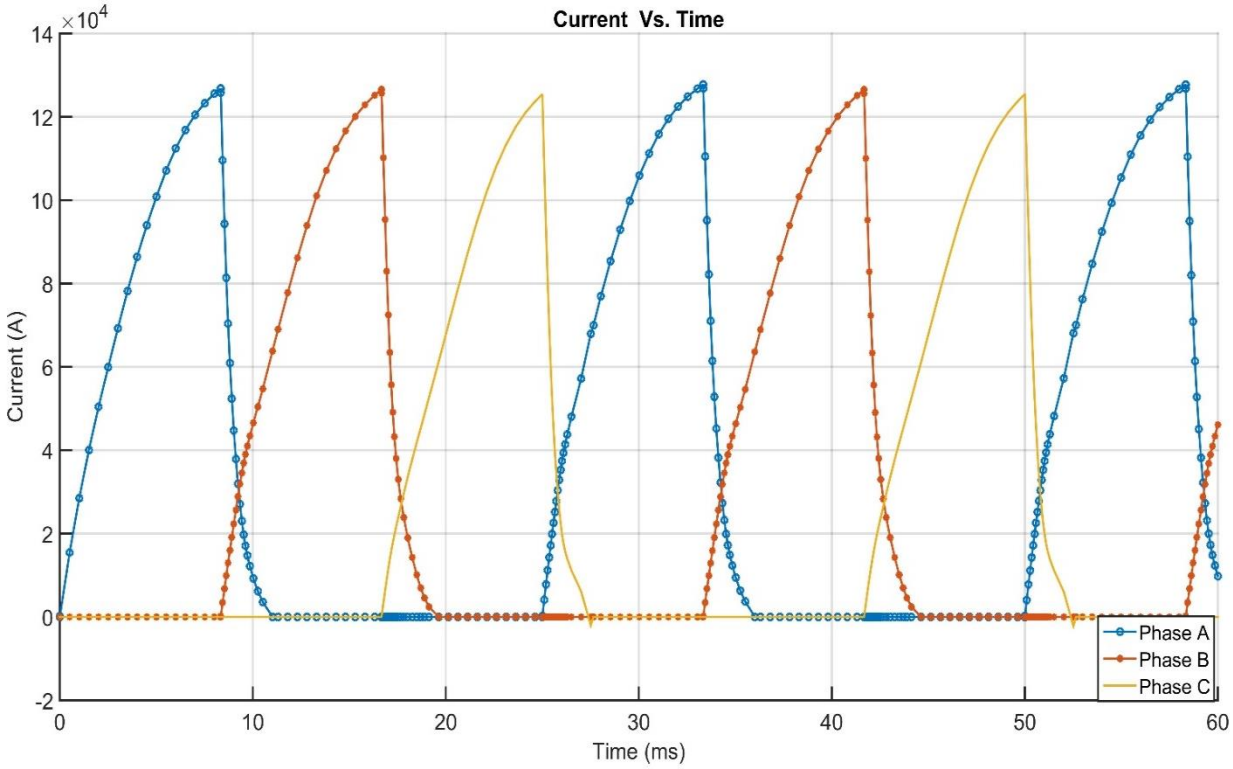

Figure 70: Current Vs Time Plot of modified rotor DSSRM

Curve Info	Avg	Max
Current(PhaseA) (Transient)	39.0449 A	127.757 A
Current(PhaseB) (Transient)	26.1648 A	126.572 A
Current(PhaseC) (Transient)	23.7945 A	125.467 A

Table 26: Current Vs Time curve info of modified rotor DSSRM

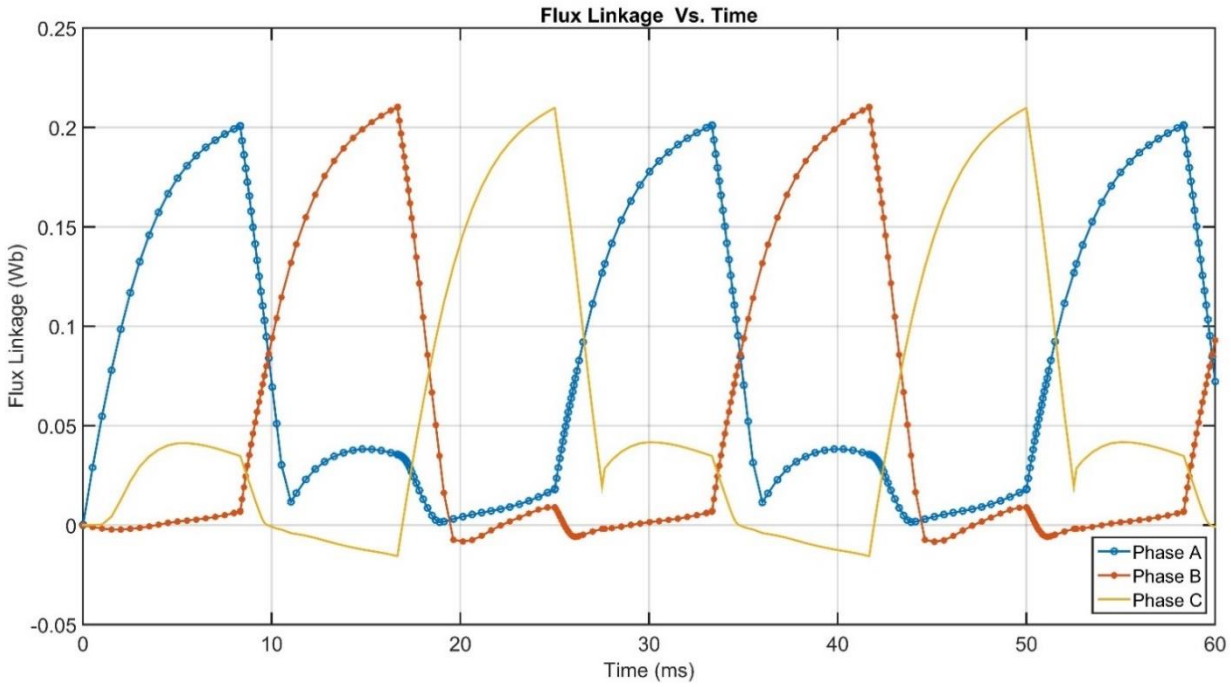

Figure 71: Flux Linkage Vs Time Plot of DSSRM

Curve Info	Avg	Max
FluxLinkage(PhaseA) : Transient	0.0821 Wb	0.2012 Wb
FluxLinkage(PhaseB) : Transient	0.0527 Wb	0.2104 Wb
FluxLinkage(PhaseC) : Transient	0.0592 Wb	0.2099 Wb

Table 27: Flux Linkage Vs Time info of modified rotor DSSRM

Comparison of Rotor Modified DSSRM and Original DSSRM

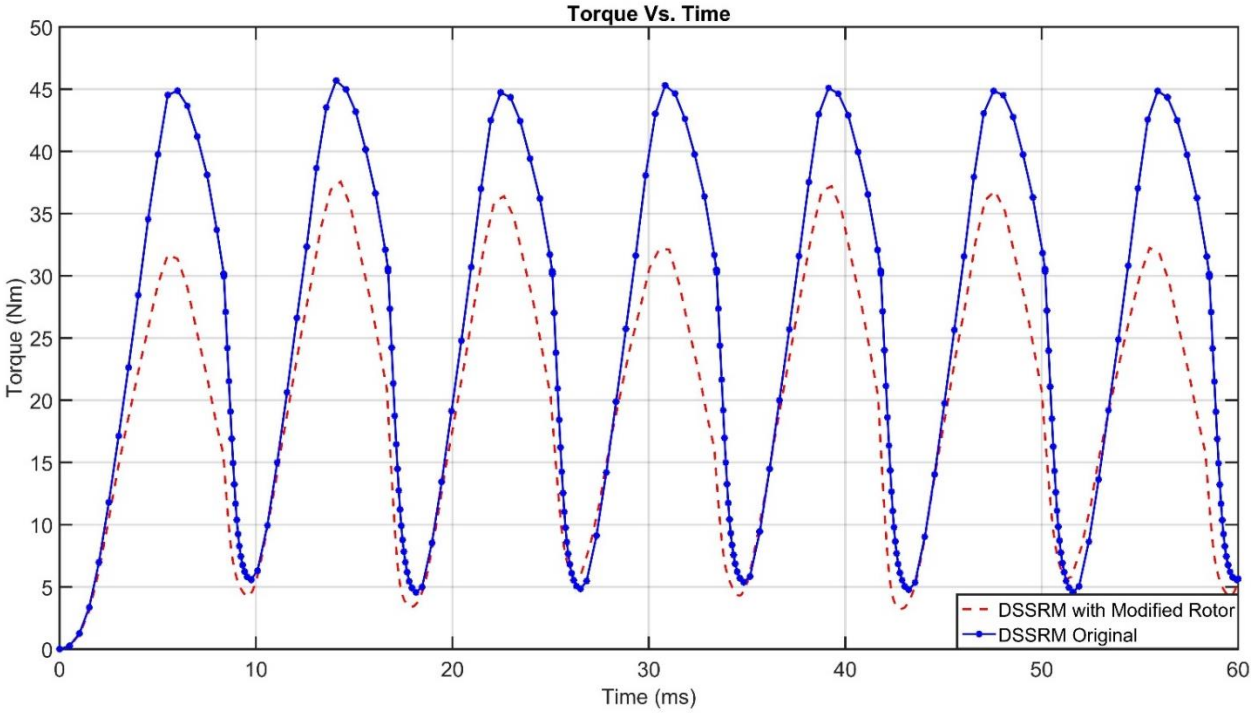

Figure 72: Moving Torque of Rotor Modified DSSRM and Original DSSRM

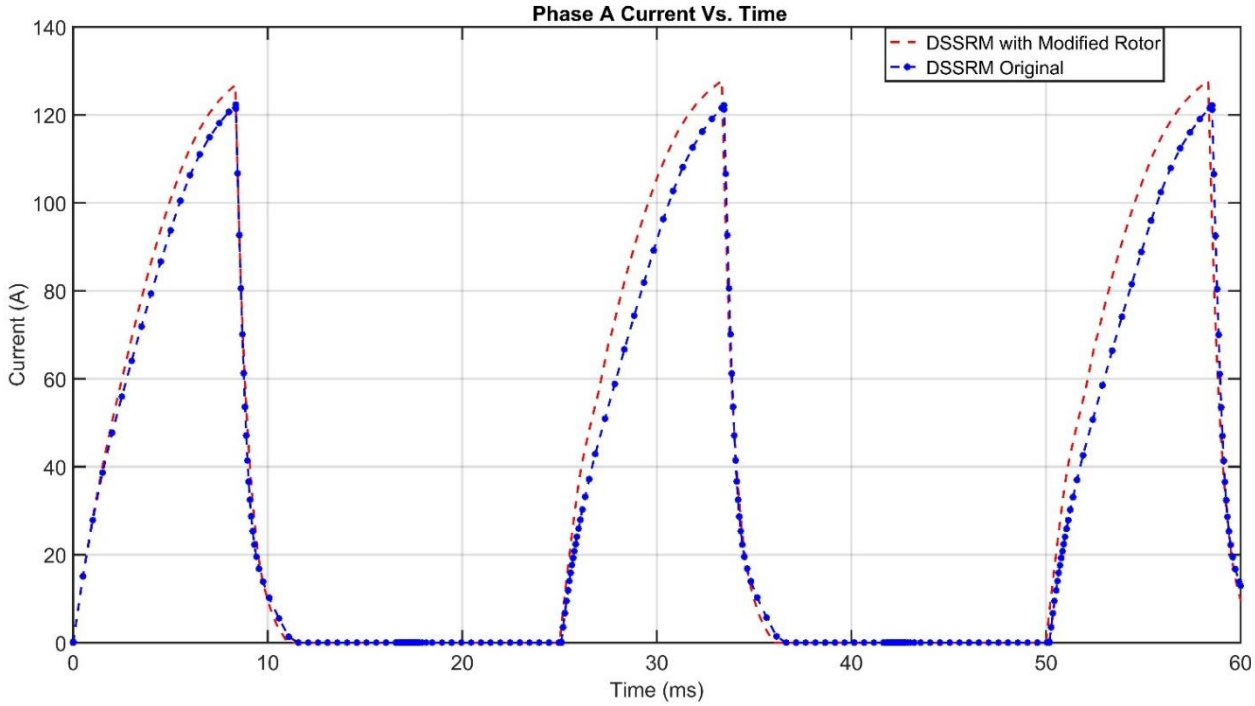

Figure 73: Phase A Current of Rotor Modified DSSRM and Original DSSRM

Rotor modification did not improve Double Stator Switched Reluctance Motor as expected. Torque ripple decreased from 80.23% (Without Rotor Modification) to 77.715% (From transient analysis, but it is observed moving torque decreased to 20.0424 Nm as compared to moving torque 26.5352 Nm of designed DSSRM.

Conclusions

This thesis research presents 2D Design and Finite Element Analysis of Double Stator Switched Reluctance Motor and conventional SRM motors. DSSRM is then compared with two SRM viz. Outer Stator and Inner Stator SRM. Transient analysis is performed to study torque behavior, current and flux linkage. From data and plots related to transient analysis, it is observed that moving torque in DSSRM is found to be higher than conventional SRM. Moving torque is higher in DSSRM than Outer stator SRM by 59.95% and Inner stator SRM by 160.31%. Similarly, torque ripple decreases in DSSRM by 9.94% than Outer Stator SRM and 4.83% than Inner Stator SRM. To conclude, increase in motional torque with simultaneous decrease in torque ripple is found in DSSRM by using transient analysis.

Magnetostatic analysis is performed to study force behavior in DSSRM and Conventional SRM. From the data obtained from the simulation, motional force in DSSRM is higher than Outer Stator and Inner Stator SRM. Parametric analysis is performed to study variation of inductance with the change in number of turns. Highest inductance is observed when number of turns is equal to 150 and lowest when number of turns is 1 in all three motors. Such improvement in performance of DSSRM will be advantageous in Electric Vehicle applications.

Expected improvement is not obtained after modifying motor design. Though chamfering improved both moving torque and torque ripple in inner stator SRM, positive result is not obtained in case of DSSRM. Chamfering the motoring edges of stators and rotors decreased motional torque by 5.07% and increased torque ripple by 2.74%.

Modifying rotor of DSSRM decreased moving torque by 24.47% as compared to original design. However, improvement in torque ripple is observed after modifying rotor. Torque ripple decreased by a percentage of 3.13 as compared to original design.

Bibliography

[1] Martin Eberhard and Marc Tarpenning, “The 21st Century Electric Car”, Tesla Motors Inc. 6 October 2006, *https://web.stanford.edu/group/greendorm/participate/cee124/TeslaReading.pdf*

[2] B. Poudel, E. Amiri, and P. Rastgoufard “Design and Analysis of Line Start Synchronous Reluctance Motor with Dual Saliency” *IEEE Transportation Electrification Conference and Expo (ITEC)*, Long Beach, California, June 2018.

[3] F. Ghoroghchian, A. Damaki Aliabad, E. Amiri and B. Poudel, "Line start permanent magnet synchronous motor with dual magnetic polarity," *2017 IEEE International Electric Machines and Drives Conference (IEMDC)*, Miami, FL, 2017, pp. 1-6.

[4] B. Poudel, E. Amiri, A. Damaki Aliabad and F. Ghoroghchian, "Line start synchronous motor for multi-speed applications," *2017 IEEE International Electric Machines and Drives Conference (IEMDC)*, Miami, FL, 2017, pp. 1-6.

[5] E. Bostanci, M. Moallem, A. Parsapour and B. Fahimi, "Opportunities and Challenges of Switched Reluctance Motor Drives for Electric Propulsion: A Comparative Study," in *IEEE Transactions on Transportation Electrification*, vol. 3, no. 1, pp. 58-75, March 2017.

[6] D. G. Dorrell, A. M. Knight, M. Popescu, L. Evans and D. A. Staton, "Comparison of different motor design drives for hybrid electric vehicles," *2010 IEEE Energy Conversion Congress and Exposition*, Atlanta, GA, 2010, pp. 3352-3359.

[7] R. Krishnan, “Switched Reluctance Motors Drives: Modeling Simulation,Analysis, Design, and Applications”. Boca Raton, FL: CRC Press,2001.

[8] P. J. Lawrenson, "Development and application of reluctance motors," in *Electronics and Power*, vol. 11, no. 6, pp. 195-198, June 1965.

[9] J. Rizk, M. H. Nagrial and A. Hellany, "Design and performance of switched reluctance motors," *Sixth International Conference on Electrical Machines and Systems, 2003. ICEMS 2003.*, Beijing, China, 2003, pp. 211-216 vol.1.

[10] P. J. Lawrenson, J. M. Stephenson, P. T. Blenkinsop, J. Corda and N. N. Fulton, "Variable-speed switched reluctance motors," in *IEE Proceedings B - Electric Power Applications*, vol. 127, no. 4, pp. 253-265, July 1980.

[11] I. Sengor, A. Polat and L. T. Ergene, "Design and analysis of switched reluctance motors," 2013 8th International Conference on Electrical and Electronics Engineering (ELECO), Bursa, 2013, pp. 586-590.

[12] M. Besharati, J. Widmer, G. Atkinson, V. Pickert and J. Washington, "Super-high-speed switched reluctance motor for automotive traction," *2015 IEEE Energy Conversion Congress and Exposition (ECCE)*, Montreal, QC, 2015, pp. 5241-5248.

[13] T. J. E. Miller, "Optimal design of switched reluctance motors," in *IEEE Transactions on Industrial Electronics*, vol. 49, no. 1, pp. 15-27, Feb 2002.

[14] D. S. Schramm, B. W. Williams and T. C. Green, ”Torque ripple reduction of switched reluctance motors by phase current optimal profiling,” Power Electronics Specialists Conference, 1992. PESC ’92 Record., 23rd Annual IEEE, Toledo, 1992, pp. 857-860 vol.2.

[15] K. Park, X. Liu and Z. Chen, "A non-unity torque sharing function for torque ripple minimization of switched reluctance generators," *2013 15th European Conference on Power Electronics and Applications (EPE)*, Lille, 2013, pp. 1-10.

[16] Jin Woo Lee, Hong Seok Kim, Byung Il Kwon and Byung Taek Kim, "New rotor shape design for minimum torque ripple of SRM using FEM," in *IEEE Transactions on Magnetics*, vol. 40, no. 2, pp. 754-757, March 2004.

[17] Y. Li and D. C. Aliprantis, "Optimum stator tooth shapes for torque ripple reduction in switched reluctance motors," *2013 International Electric Machines & Drives Conference*, Chicago, IL, 2013, pp. 1037-1044.

[18] Y. Ozoglu, M. Garip and E. Mese, "New pole tip shapes mitigating torque ripple in short pitched and fully pitched switched reluctance motors," *Conference Record of the 2002 IEEE Industry Applications Conference. 37th IAS Annual Meeting (Cat. No.02CH37344)*, Pittsburgh, PA, USA, 2002, pp. 43-50 vol.1.

[19] L. Du, B. Gu, J. S. J. Lai and E. Swint, "Control of pseudo-sinusoidal switched reluctance motor with zero torque ripple and reduced input current ripple," *2013 IEEE Energy Conversion Congress and Exposition*, Denver, CO, 2013, pp. 3770-3775.

[20] T. Kusumi, T. Hara, K. Umetani and E. Hiraki, "Simple control technique to eliminate source current ripple and torque ripple of switched reluctance motors for electric vehicle propulsion," *IECON 2016 - 42nd Annual Conference of the IEEE Industrial Electronics Society*, Florence, 2016, pp. 1876-1881.

[21] W. Ye, Q. Ma and J. Hu, "Torque ripple minimization of switched reluctance motors by controlling the phase currents during commutation," *2014 17th International Conference on Electrical Machines and Systems (ICEMS)*, Hangzhou, 2014, pp. 1866-1870.

[22] M. Ilić-Spong, T. J. E. Miller, S. R. MacMinn and J. S. Thorp, "Instantaneous torque control of electric motor drives," *1985 IEEE Power Electronics Specialists Conference*, Toulouse, France, 1985, pp. 42-48.

[23] I. Husain and M. Ehsani, "Torque ripple minimization in switched reluctance motor drives by PWM current control," in *IEEE Transactions on Power Electronics*, vol. 11, no. 1, pp. 83-88, Jan 1996.

[24] A. C. Pop, V. Petrus, C. S. Martis, V. Iancu and J. Gyselinck, "Comparative study of different torque sharing functions for losses minimization in Switched Reluctance Motors used in electric vehicles propulsion," *2012 13th International Conference on Optimization of Electrical and Electronic Equipment (OPTIM)*, Brasov, 2012, pp. 356-365.

[25] Hye-Ung Shin; Kiwoo Park and Kyo-Beum Lee, A Non-Unity Torque Sharing Function for Torque Ripple Minimization of Switched Reluctance Generators in Wind Power Systems, *Energies*, 8, (10), 2015, 1-17.

[26] E. Gouda, M. Hamouda and A. R. A. Amin, "Artificial intelligence based torque ripple minimization of Switched Reluctance Motor drives," *2016 Eighteenth International Middle East Power Systems Conference (MEPCON)*, Cairo, 2016, pp. 943-948.

[27] W. Qin, X. Shi, H. Chi and J. Wu, "Nonlinear Neural Network-based Modeling of Switched Reluctance Motor," *2010 Asia-Pacific Power and Energy Engineering Conference*, Chengdu, 2010, pp. 1-4.

[28] X. Yao, R. Qi, Z. Deng and J. Cai, "High-Performance Torque Control for Switched Reluctance Motor Based on Online Fuzzy Neural Network Modeling," *2010 International Conference on Intelligent System Design and Engineering Application*, Changsha, 2010, pp. 817-822.

[29] C. H. Lin and S. J. Chiang, "Torque-ripple reduction in switched reluctance motor drive using SHRFNN control," *2006 37th IEEE Power Electronics Specialists Conference*, Jeju, 2006, pp. 1-6.

[30] E. Swint and J. Lai, "Switched reluctance motor without torque ripple or electrolytic capacitors," *2011 IEEE Energy Conversion Congress and Exposition*, Phoenix, AZ, 2011, pp. 1657-1663.

[31] G. Vakil, P. Upadhyay, N. Sheth, A. Patel, A. Tiwari and D. Miller, "Torque ripple reduction in the flux reversal motor by rotor pole shaping and stator excitation," *2008 International Conference on Electrical Machines and Systems*, Wuhan, 2008, pp. 2980-2985.

[32] M. Abbasian, M. Moallem and B. Fahimi, "Double-Stator Switched Reluctance Machines (DSSRM): Fundamentals and Magnetic Force Analysis," in *IEEE Transactions on Energy Conversion*, vol. 25, no. 3, pp. 589-597, Sept. 2010.

[33] A. H. Isfahani and B. Fahimi, "Comparison of Mechanical Vibration Between a Double-Stator Switched Reluctance Machine and a Conventional Switched Reluctance Machine," in *IEEE Transactions on Magnetics*, vol. 50, no. 2, pp. 293-296, Feb. 2014.

[34] A. H. Isfahani and B. Fahimi, "Multi-physics analysis of double stator switched reluctance machines," *2013 IEEE Energy Conversion Congress and Exposition*, Denver, CO, 2013, pp. 2827-2833.

[35] N. Arbab, W. Wang, C. Lin, J. Hearron and B. Fahimi, "Thermal Modeling and Analysis of a Double-Stator Switched Reluctance Motor," in *IEEE Transactions on Energy Conversion*, vol. 30, no. 3, pp. 1209-1217, Sept. 2015.

[36] E. Bostanci, L. Gu, E. Cosoroaba, M. Moallem and B. Fahimi, "Performance improvement and comparison of concentrated winding segmental rotor and double stator switched reluctance machines," *2016 IEEE Conference on Electromagnetic Field Computation (CEFC)*, Miami, FL, 2016, pp. 1-1.

[37] M. Abbasian and H. Jalali, "Temperature distribution analysis of Double Stator Switched Reluctance Machine using finite element method," *2015 Intl Aegean Conference on Electrical Machines & Power Electronics (ACEMP), 2015 Intl Conference on Optimization of Electrical & Electronic Equipment (OPTIM) & 2015 Intl Symposium on Advanced Electromechanical Motion Systems (ELECTROMOTION)*, Side, 2015, pp. 232-236.

[38] M. A. Tavakkoli and M. Moallem, "Torque ripple mitigation of double stator switched reluctance motor (DSSRM) using a novel rotor shape optimization," *2012 IEEE Energy Conversion Congress and Exposition (ECCE)*, Raleigh, NC, 2012, pp. 848-852.

[39] Miller T.J.E., “Switched Reluctance Motors and Their Control”, Oxford, UK,: Magna Physics Publishing/Oxford Science,1993

[40] Srinivas Pratapgiri , “Switched Reluctance Motor : Concept, Control And Applications-Direct Instantaneous Torque Controlled Switched Reluctance Motor Drive for fan Type Load and Constant Torque Load ”, 2017 Edited by Ahmed Tahour and Abdel Ghani Aissaoui, IntechOpen, DOI: 10.5772/intechopen.69149.

[41] JIn-Woo Ahn (February 10th 2011). Switched Reluctance Motor, Torque Control Moulay Tahar Lamchich, IntechOpen, DOI: 10.5772/10520. Available from: *https://www.intechopen.com/books/torque-control/switched-reluctance-motor*

[42] Michael T. DiRenzo, “ Switched Reluctance Motor Control –Basic operation and example using the TMS320F240”, February 2000, Texas Instrument. Available from: *http://d1.amobbs.com/bbs_upload782111/files_9/ourdev_262731.pdf*

[43] Patent: Byrne, John (Dalkey, EI), Lacy, James C. (Dublin, EI) 1976,“Electrodynamic system comprising a variable reluctance machine”, United States

[44] Z. Q. Zhu and D. Howe, "Electrical Machines and Drives for Electric, Hybrid, and Fuel Cell Vehicles," in *Proceedings of the IEEE*, vol. 95, no. 4, pp. 746-765, April 2007.

[45] S. Mir "Classification of SRM converter topologies for automotive applications" *SAE 2000 World Congr.* 2000-Mar.-69.

[46] L. Chang, "Development of switched reluctance motor drives and the applications in automobiles," *Proceedings 1995 Canadian Conference on Electrical and Computer Engineering*, Montreal, Que., 1995, pp.

[47] ANSYS RMxprt 2017, ANSYS, Inc.

[48] ANSYS Maxwell 2D 2017, ANSYS, Inc.

[49] D.J. Griffiths, “Introduction to Electrodynamics, 2nd Ed.”, Prentice Hall, 1989

[50] Maxwell’s Equations. Available from: *http://www.maxwells-equations.com/*

[51] BEYOGLU, Nurdan GUZE. "Effect of stator and rotor pole shapes on the torque ripple in a Switched Reluctance Motor.”(1999)

Vita

Nirdesh Neupane was born in Dang, Nepal. He obtained his undergraduate degree in Electronics and Communication Engineering from Dehradun Institute of Technology, India in 2014. He joined University of New Orleans in Fall 2016 to pursue Master of Science in Electrical Engineering. His research interest includes Power System, Electric Motors and Renewable Energy.